MARTIN MARIETTA ENERGY SYSTEMS LIBRARIES
3 4456 0285495 3

123
CENTRAL RESEARCH LIBRARY
DOCUMENT COLLECTION

ORNL-2911
UC-34 - Physics and Mathematics

HEAT TRANSFER, BURNOUT, AND PRESSURE DROP FOR WATER IN SWIRL FLOW THROUGH TUBES WITH INTERNAL TWISTED TAPES

W. R. Gambill
R. D. Bundy
R. W. Wansbrough

CENTRAL RESEARCH LIBRARY
DOCUMENT COLLECTION
LIBRARY LOAN COPY
DO NOT TRANSFER TO ANOTHER PERSON
If you wish someone else to see this document, send in name with document and the library will arrange a loan.

OAK RIDGE NATIONAL LABORATORY
operated by
UNION CARBIDE CORPORATION
for the
U.S. ATOMIC ENERGY COMMISSION

Printed in USA. Price $2.50. Available from the

Office of Technical Services
Department of Commerce
Washington 25, D.C.

LEGAL NOTICE

This report was prepared as an account of Government sponsored work. Neither the United States, nor the Commission, nor any person acting on behalf of the Commission:

A. Makes any warranty or representation, expressed or implied, with respect to the accuracy, completeness, or usefulness of the information contained in this report, or that the use of any information, apparatus, method, or process disclosed in this report may not infringe privately owned rights; or

B. Assumes any liabilities with respect to the use of, or for damages resulting from the use of any information, apparatus, method, or process disclosed in this report.

As used in the above, "person acting on behalf of the Commission" includes any employee or contractor of the Commission, or employee of such contractor, to the extent that such employee or contractor of the Commission, or employee of such contractor prepares, disseminates, or provides access to, any information pursuant to his employment or contract with the Commission, or his employment with such contractor.

Ey 123

ERRATA FOR ORNL-2911

page 4: In some copies, the word anneal (line 8) is smeared.

page 9: In line 2, interst should read interest.

In line 14, replace g by a_t.

In Eq. 9, replace g_i by $(a_t)_i$.

Continue line 19 with "when g in Eq. 8 is replaced by a_t."

page 25: In lines 7 – 9, replace 10%, 20% and 15% by 2%, 16%, and 10%, respectively.

page 34: In Eqs. 31 and 32, replace g by a_t/g.

page 40: In Eq. 35, replace g by a_t/g.

In Eq. 36, replace $g = V_t^2/g_c R_i$ by $a_t/g = V_t^2/g R_i$.

page 48: In line 5, tree should read three.

page 58: Add to figure legend: "$\Delta P_e = P_1 - P_3$ of Fig. 24-a."

page 59: In some copies, the sign $\approx$ (following G_a in line 10) is smeared.

page 65: In Eq. 62, L should be L_h.

page 82: In line 4, 3.6 Mw/ft^3 should read 316 Mw/ft^3.

page 91: ΔP_{a-b} in Eq. 99 should read $\overline{\Delta P}_{a-b}$.

page 98: In line 10, immediately following Eq. 116, Eq. 114 should read Eq. 115.

ORNL-2911

Contract No. W-7405-eng-26

REACTOR EXPERIMENTAL ENGINEERING DIVISION

HEAT TRANSFER, BURNOUT, AND PRESSURE DROP FOR WATER IN SWIRL FLOW THROUGH TUBES WITH INTERNAL TWISTED TAPES

W. R. Gambill
R. D. Bundy
R. W. Wansbrough

DATE ISSUED

MAR 28 1960

OAK RIDGE NATIONAL LABORATORY
Oak Ridge, Tennessee
Operated by
UNION CARBIDE CORPORATION
For the
U. S. ATOMIC ENERGY COMMISSION

MARTIN MARIETTA ENERGY SYSTEMS LIBRARIES

3 4456 0285495 3

SUMMARY

Experimental determinations of heat-transfer coefficients, burnout heat fluxes, and friction factors have been made for swirl flow of low- and moderate-pressure water through electrically heated aluminum, nickel, and copper tubes containing full-length Inconel twisted tapes.

Swirl-flow heat-transfer coefficients for nonboiling conditions were successfully correlated with both Froude number and the modulus group $\left[\text{Grashof No.}/(\text{Reynolds No.})^2\right]$, which is a measure of the ratio of buoyant to inertial forces in the presence of a temperature gradient. Swirl-flow heat-transfer coefficients are larger than equivalent straight-flow coefficients on the basis of equal coolant velocity, of equal frictional pressure drop, or of equal frictional pumping power. The advantage exhibited by swirl flow appears to be significantly dependent on surface roughness.

Swirl-flow burnout heat fluxes are shown to be independent of both degree of subcooling and of pressure, and to be as much as five-fold larger than straight-flow burnout fluxes when coolant temperature, pressure, and velocity are held constant. At low pressure, swirl-flow burnout heat fluxes are approximately two-fold larger than for straight flow through the same tube at equal pumping power.

Friction factors for swirl flow are larger than for axial flow; and for the tubes used in this investigation, are dependent on tube diameter and tape twist ratio, but independent of Reynolds number.

Six other recent studies of swirl-flow heat transfer are reviewed and the results outlined. Equations for various swirl-flow parameters are derived for a rotating slug-flow model. Earlier burnout heat flux

data for tubes with inlet swirl generators are reassessed from a new viewpoint, and recommendations are made for further studies.

The applicability of vortex-tube fuel elements to nuclear reactor cores is discussed. Relative to practical plate-element matrices, vortex-tube elements have several advantages — large heat-transfer area per unit volume (if both surfaces are cooled), increased fuel element rigidity, larger heat-transfer rates at and below burnout, and the possibility of lower operating pressure levels; these combine to indicate a promising potential for vortex-tube fuel elements.

CONTENTS

PAGE

I. General Description of Experimental System and Test Sections ... 1

II. Heat-Transfer Coefficients 4

A. Measurements and Calculation Procedure 4

B. Nonboiling Forced-Convection Heat-Transfer Coefficients 8

C. Local-Boiling Heat-Transfer Coefficients 16

III. Burnout Data and Correlations 16

A. Data Tabulation and General Comments 16

B. Straight-Flow Burnout Tests 25

C. Swirl-Flow Burnout Tests 29

Pumping Power Dependence 29

Subcooling Dependence 31

Comparison with Calculated Straight-Flow Burnout Values .. 34

Correlation of Vortex-Flow Burnout Heat Fluxes 38

Burnout Test of Oval Twisted Tube 46

IV. Friction Factors 46

A. Isothermal and Nonboiling Data 47

B. Local Boiling Data 51

C. Inlet Pressure Loss 54

V. Other Recent Swirl-Flow Heat-Transfer Studies 57

A. Boiling Water 57

B. Boiling Freon 62

C. Heating Air 63

D. Heating Santowax Liquid 68

E. Boiling Mercury 69

F. Heating Air and Water 71

CONTENTS (continued)

PAGE

VI. General Discussion 71

A. Relation of Heat Transfer to Friction in Swirl Flow 71

B. Swirl-Flow Advantages and Potential Applications 78

C. Recommendations for Further Investigation 82

ACKNOWLEDGEMENTS 83

LITERATURE CITED 84

APPENDIX 1 — Derivation of Twisted-Tape Vortex-Flow Equations 87

A. Equivalent Diameter 87

B. Swirl-Flow Path Length at Inner Tube Wall 87

C. Resultant Fluid Velocity at Inner Tube Wall 88

D. Rotation Rate of Fluid 88

E. Centrifugal Intensity (gees) at Inner Tube Wall 89

F. Radial Pressure Gradient 89

G. Inlet Pressure Loss due to Swirl Formation 90

H. "True" Equivalent Diameter 91

APPENDIX 2 — Further Evaluation of Inlet-Swirl-Generator Burnout Data. 95

NOTATION 100

HEAT TRANSFER, BURNOUT, AND PRESSURE DROP FOR WATER IN SWIRL FLOW THROUGH TUBES WITH INTERNAL TWISTED TAPES

W. R. Gambill, R. D. Bundy, and R. W. Wansbrough*

An earlier study[1] of boiling burnout with water in vortex flow through test sections with inlet swirl generators gave promising results which prompted an extended investigation of full-length twisted-tape swirl generators. The results of the extended program, which was completed in mid-August, 1959, are given in this report, and include information on nonboiling and boiling heat-transfer coefficients and friction factors as well as burnout heat fluxes.

I. General Description of Experimental System and Test Sections

The experimental system is shown schematically in Fig. 1; only minor changes were made to the apparatus originally used. Heat fluxes were calculated from water flow rate, temperature rise, and internal test-section surface area. Thirty-gage Chromel-Alumel thermocouples were brazed or discharge welded onto the outside tube surface at nominal 2-in. intervals and externally insulated with asbestos tape secured by woven-glass ribbon. All instrumentation – rotameters, pressure gages, and recording instruments – were calibrated prior to use. Heise pressure gages which had been checked on a dead-weight tester and which were electrically isolated with Nylon Swagelok fittings were used for measurement of inlet and exit pressure levels in vortex tests 19 to 40.** Calibrated pressure gages of somewhat lower precision were used in all earlier tests. The pressure gage installation

*Summer employee.

**Test numbers in the text refer to the numbers in Tables 1 and 2.

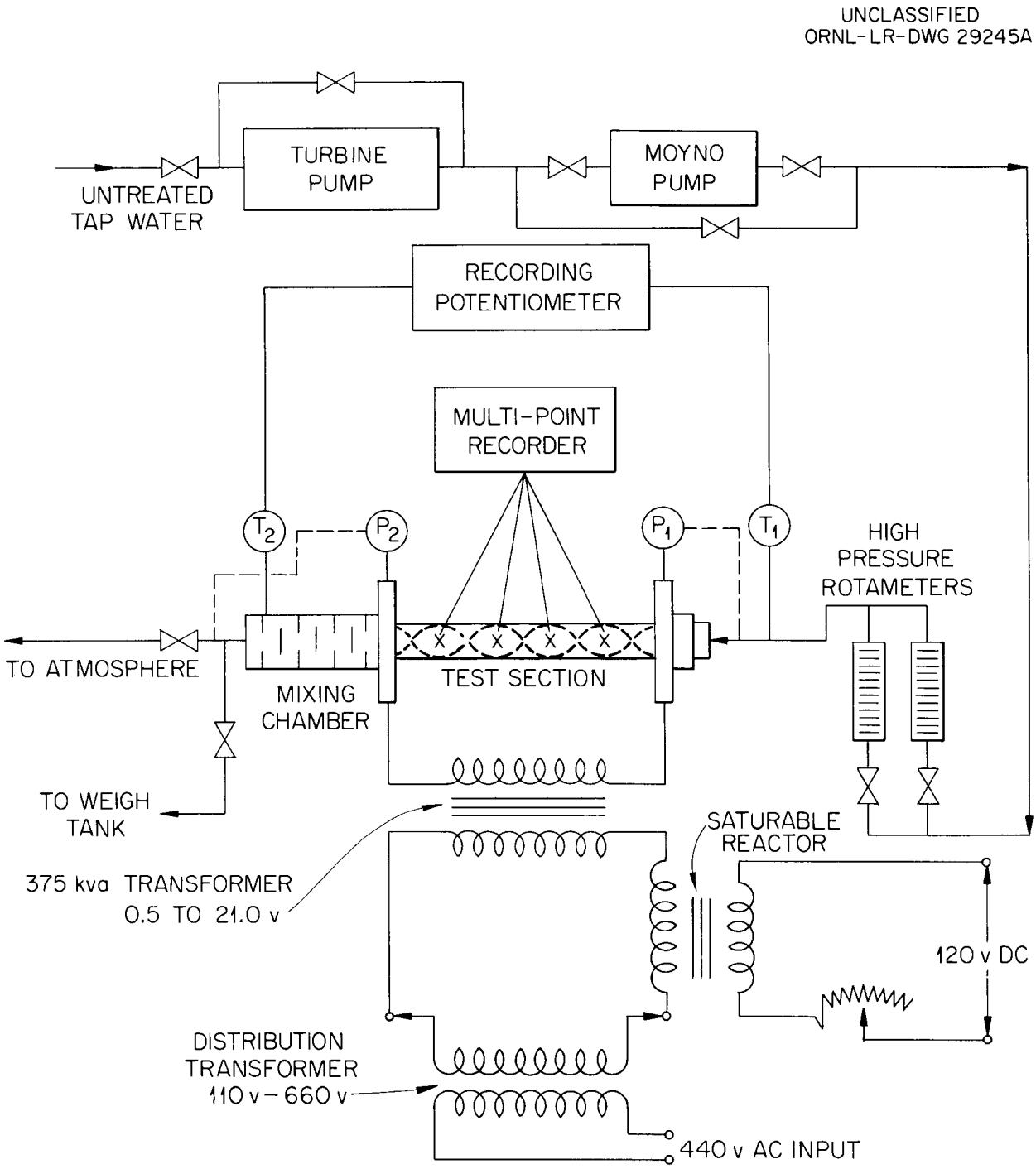

Fig. 1. Experimental Heat-Transfer Apparatus.

denoted by solid lines in Fig. 1 was made by drilling 1/32-in. holes through the electrodes and the tube wall; the inner wall surface was then deburred and the pressure gage attached to a fitting on the outer surface of the electrode.

For most of the tests, the copper tubes were brazed into the electrodes with high-temperature silver solder; the aluminum tubes were joined with a relatively low-melting eutectic compound. For vortex tests 36 – 40, the ends of the tubes were clamped into split electrodes; this method was particularly convenient for the aluminum tubes since there was then no danger of melting the tube wall during a joining operation.

For the straight-flow tests, water flow was developed and stabilized before heating began with either a smooth convergent cone upstream of the inlet electrode or an unheated length about 40 tube diameters long. Burnout never occurred at the tube inlet, and the entry regions described were considered adequate for flow development. For the twisted-tape tests, the water flowed directly from a 1-in.-dia stainless steel pipe into the test section, and no special entry region was used.

Several difficulties were encountered in early efforts to fit twisted tapes into the tubes. If the twisted tape was slightly too large in diameter, it would tend to stretch and straighten out; if too loose, it would have to be tack-welded or otherwise secured at the tube ends to prevent its rotation. Another problem encountered with insufficiently tightly twisted tapes was lateral vibration accompanied by an apparent arc erosion phenomenon, whereby the tape would emerge from the tube after a test with a tapered diameter which decreased toward the exit. A better fit was obtained in some tests by screwing the tape into double grooves which had been cut into the inner tube wall. This procedure was fairly satisfactory, but X rays revealed a mismatch

of tape edges and grooves in some of the test sections, and this technique in general gave excessive trouble.

The most satisfactory method of fitting the twisted tapes to the copper tubes involved first drawing the original tubing on a mandrel to an ID slightly larger than the tape diameter, followed by insertion of the tape and drawing of the tube on the tape until the tube ID was 0.002 in. to 0.003 in. less than the tape OD. The same procedure was followed with the aluminum tubes, but three draws were made, with a 550°C anneal between the second and third draws. This procedure caused the tape to penetrate the tube wall about a mil; subsequent X rays showed that the spiral pattern was quite uniform and undistorted.

The tapes were made of 0.015-in.-thick Inconel for all the tests. It was found that no heat treatment was required for twisting down to a twist ratio y of about 2.0 diameters/180-deg twist. The first tapes were twisted on a bench rig consisting of a vise and fixed C-clamp. Later tapes were made by the more satisfactory method of suspending the sheared strip vertically with a dead weight of 40 – 80 lb attached to the bottom; the weight was then twisted and the tape yielded uniformly in torsion to produce the desired twist ratio. It was necessary to adjust the sheared width of the original strip in order to compensate for the reduction experienced during the spiralling operation.

II. Heat-Transfer Coefficients

A. Measurements and Calculation Procedure

Data suitable for calculation of heat-transfer coefficients were gathered during a series of equilibrations preceding most of the test-section

burnouts. Copper tubes of 0.136-in., 0.189-in., and 0.249-in. ID, as well as 0.249-in.-ID aluminum tubes, were fitted with twisted tapes for which $2.3 < y < 12.0$. The L_h/D_i range was 45 to 70; ϕ was varied from 0.8×10^6 to 8.0×10^6 Btu/hr·ft^2 in the nonboiling runs and from 2.3×10^6 Btu/hr·ft^2 to 9.3×10^6 Btu/hr·ft^2 in the local boiling tests. Test-section pressure during the local boiling runs varied from 30 to 220 psia. $(Re)_a$ was varied from 5,000 to 427,000.

Heat flux was based on coolant heat absorption rate and total internal surface area, uncorrected for the small area covered by the edges of the twisted tapes. Neglecting the tape-covered area gives h values ~ 5% smaller than would result from use of the net surface area. Calculated heat generation in the tapes never exceeded 0.3% of the total heat generation, assuming perfect tape-wall contact; this correction was therefore not included. The axial voltage gradient along the test section was measured and used to obtain the wall temperature drop from a plot based on the complete Kreith-Summerfield series solution[2] for the case of internal heat generation in a tube wall with variable thermal and electrical properties:

$$t_i = t_o - \frac{m(R_o - R_i)^2}{(1 + \beta' t_o)(1 + \alpha t_o)} - \frac{m(R_o - R_i)^3}{3 R_o(1 + \beta' t_o)(1 + \alpha t_o)} - \left[\frac{m^2}{6} \frac{(3\alpha + 4\alpha\beta' t_o + \beta')}{(1 + \alpha t_o)^3 (1 + \beta' t_o)^3} \frac{m}{4 R_o^2 (1 + \beta' t_o)(1 + \alpha t_o)} \right] (R_o - R_i)^4 + \ldots \tag{1}$$

where $$m = \frac{3.413\ (dE/dx)^2}{2\ \rho_o\ k_o} \quad (°F/ft^2), \tag{1-b}$$

and where α and β' are defined by:

$$k = k_o\ (1 + \alpha t)\ , \tag{1-c}$$

$$\rho = \rho_o\ (1 + \beta' t)\ . \tag{1-d}$$

Electrical resistivity data from ref 3 were used, and thermal conductivity data for copper* and aluminum were taken from Eckert and Drake.[4]

Exit bulk water temperatures were measured with a recording potentiometer and a thermocouple located immediately downstream of the outlet disk-and-doughnut mixing chamber. The inlet bulk water temperature for a test with heating was taken as the exit water temperature of the preceding isothermal equilibration. The small temperature rise of the coolant due to frictional heating in high-velocity tests did not have to be subtracted from the total temperature rise in a heating test when this procedure was followed. Local film temperature drop was computed as the difference between the calculated inside wall temperature and the local bulk water temperature (t_b was assumed to vary linearly with heated length). Wall saturation temperatures were taken from steam tables to correspond to the measured terminal wall pressures. At each thermocouple location, heat-transfer coefficients based on Δt_f (nonboiling tests) or on Δt_{sat} (boiling runs) were calculated. The resulting curve was graphically integrated by planimetry to obtain an average h for the test section. A typical plot of pertinent temperatures and the derived heat-transfer coefficient is shown as Fig. 2 for a nonboiling test. A graph of this type was prepared for each of the 60 heat-transfer coefficient determinations.

Some difficulties were encountered with the middle three thermocouples, which tended to separate from the tube surface after several cycles of switching power off and on for transformer tap adjustment. In some of the earlier tests, the same thermocouples gave readings that varied peculiarly in level

---

*Values of k for pure copper were reduced by 11% to account for average impurities in the grade of copper used.

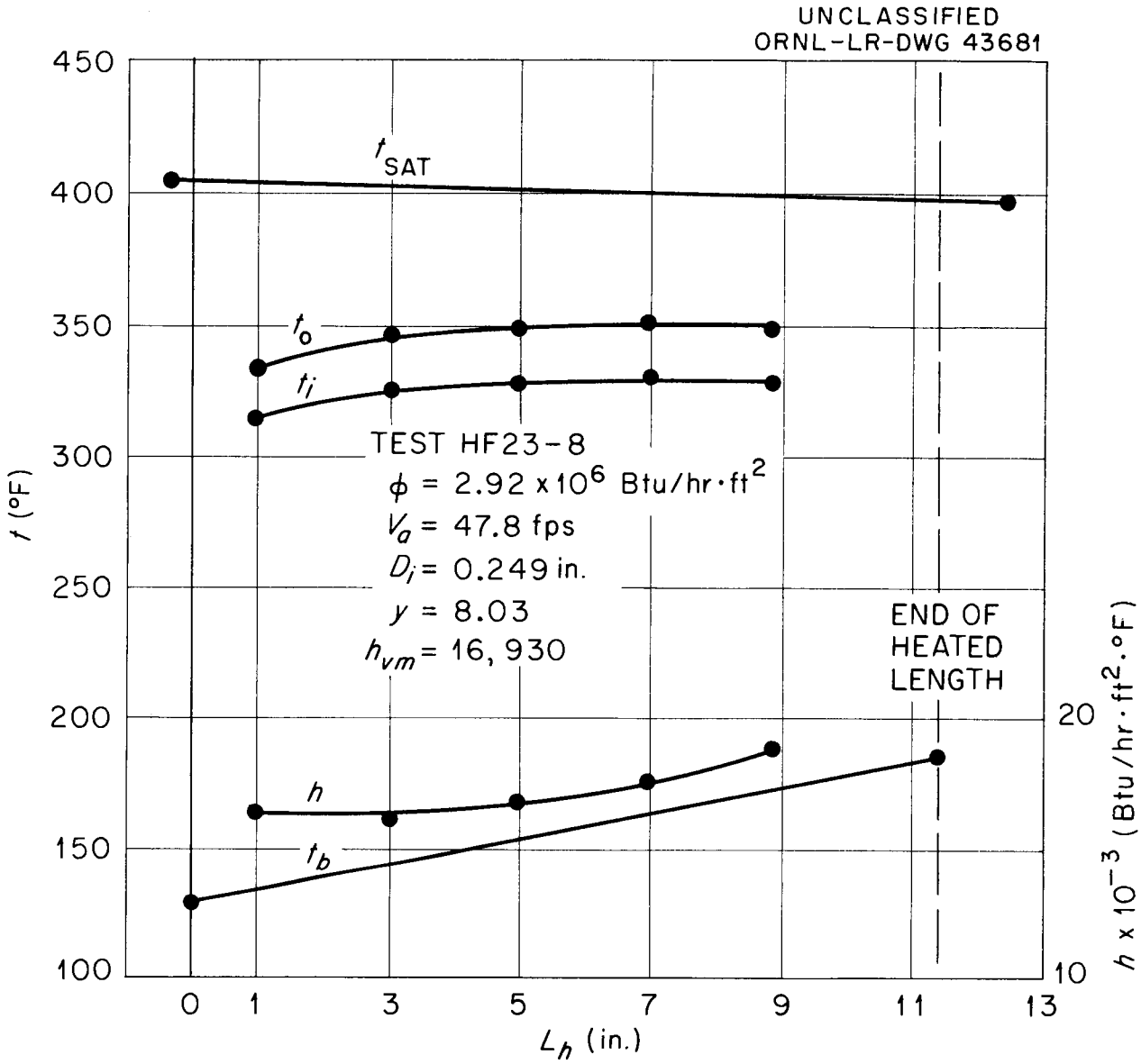

Fig. 2. Typical Plot of Variation of t_b, t_i, t_o, t_{SAT} AND h with Heated Length.

from test to test. This problem was largely solved by positioning the thermocouple beads, with the aid of X rays, so that none was directly over a tape edge; the measured temperature distributions were considerably more consistent and uniform after this procedure was adopted. Because of the quite large radial and axial variations of t_b, no attempt was made to correlate local h, which generally increased slightly with length, probably because of the favorable physical property variation. All values of calculated average h have been included in the correlations discussed below. Since the coolant was untreated tap water, the heat-transfer coefficients determined may be somewhat smaller than they would be had high-purity water been used, because of scale formation. If scale did form, it apparently did so in a uniform fashion, since the data do not show an extreme scatter in the correlations discussed below.

B. Nonboiling Forced-Convection Heat-Transfer Coefficients

Several correlations of the nonboiling data were made which were based on the intuitive concept that vortex heat-transfer coefficients could be characterized by the product of the axial-flow h from the Colburn equation:

$$St = \frac{0.023\left[1 + (D_i/L_h)^{0.7}\right]}{Pr^{2/3}\,Re^{0.2}} \tag{2}$$

and an additional group representing the effect of radial acceleration and enhanced buoyancy force on heat-transfer rate.

For axial forced convection, the Froude number:

$$Fr = \frac{V_a^{\,2}}{g\,D_i} \tag{3}$$

represents the ratio of inertial forces to gravity forces:

$$Fr = \frac{F_I}{F_G} \tag{4}$$

and is therefore of potential interest.

In free-convection flow, the Grashof number:

$$Gr = \frac{D_i^{\,3}\, \rho^2\, g\, \beta_f (\Delta t)_f}{\mu^2} \tag{5}$$

possesses a similar importance. Where neither forced- nor free-convection can be neglected, as in the present instance, the ratio Gr/Re^2 is particularly suitable, since it may be regarded as the ratio of buoyancy forces to inertial forces:

$$Gr/(Re)_a^{\,2} = \frac{F_B}{F_I} \quad , \tag{6}$$

where

$$(Re)_a = \frac{D_i\, \rho_b V_a}{\mu_b} \quad . \tag{7}$$

Combination of Eqs. 5 and 7 reduces Eq. 6 to:

$$Gr/(Re)_a^{\,2} = \frac{g\, \beta_f (\Delta t)_f\, D_i}{V_a^{\,2}} \quad . \tag{8}$$

Furthermore, * a_t/g (at the wall) for twisted-tape swirl flow can be related to D_i, V_a, and y as follows (see Appendix 1 for derivations of swirl-flow equations):

$$* \quad (a_t)_i = \frac{b}{D_i} \left(\frac{V_a}{y} \right)^2 \quad , \tag{9}$$

where b is a numerical constant.

Combination of Eqs. 8 and 9 gives; when g in Eq. 8 is replaced by a_t.

$$Gr/(Re)_a^{\,2} \propto \frac{\beta_f (\Delta t)_f}{y^2} \quad . \tag{10}$$

* See inset

Eq. 3 may similarly be reduced to its simplest form for twisted-tape vortex flow by combining it with Eq. 9, which gives:

$$Fr \propto y^2 \quad . \tag{11}$$

Theoretical bases for the use of the modulus ratio $Gr/(Re)^2$ may be found in the texts of Eckert and Drake[5] and of Bird et al.,[6] as well as in recent papers by Acrivos[7] and Ostrach and Braun.[8]

The ratios of the experimental mean vortex heat-transfer coefficients (h_{vm}) to the equivalent mean axial-flow coefficients (h_{am}), evaluated at equal bulk coolant temperature and weight flow rate with Eq. 2, were accordingly plotted versus the groups of Eqs. 10 and 11. This is equivalent to plotting the Nusselt number ratio $(Nu)_{vm}/(Nu)_{am}$ versus the indicated groups, since D_i was used in calculating h_{am} from Eq. 2. The plots are shown as Figs. 3 and 4. The best correlation equations are:

$$\frac{h_{vm}}{h_{am}} = 2.18\ y^{-0.090} \tag{12}$$

and

$$\frac{h_{vm}}{h_{am}} = 1.65 \left(\frac{10^2\ \beta_f^{1/2}\ \Delta t_f^{1/2}}{y} \right)^{0.084} . \tag{13}$$

Each correlation exhibits an average deviation of 10.1% with respect to the 47 data points. Though Eq. 13 probably better accounts for the effect of heat flux variation, Eq. 12 correlates the data as well and is considerably simpler. Since Δt_f appears in Eq. 13, numerical solution for h_{vm} must be made by iteration; and if calculations are made with Eq. 13, it is suggested that Eq. 12 be used to obtain a first approximation to Δt_f. Eqs. 12 and 13 may be combined with Eq. 2 to give the following generalized correlations

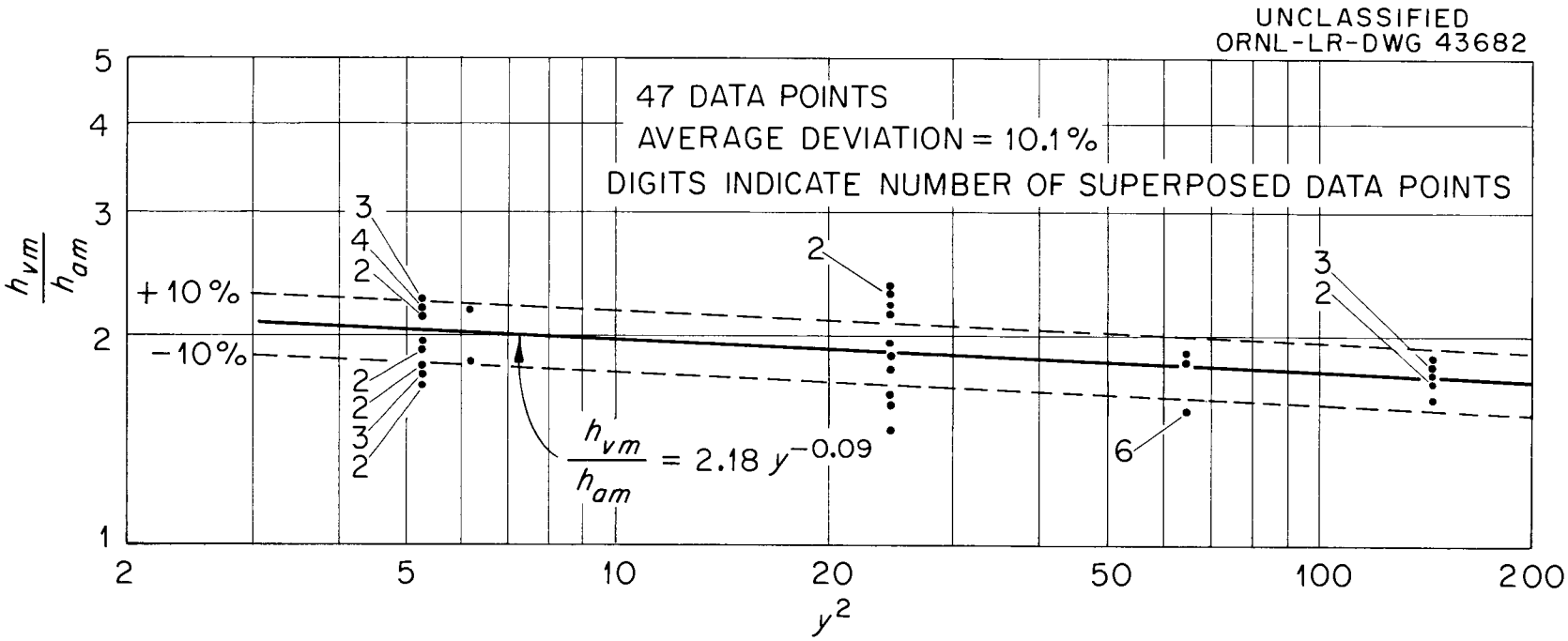

Fig. 3. Correlation of Heat-Transfer-Coefficient Ratio with Froude Number for Non-Boiling Water.

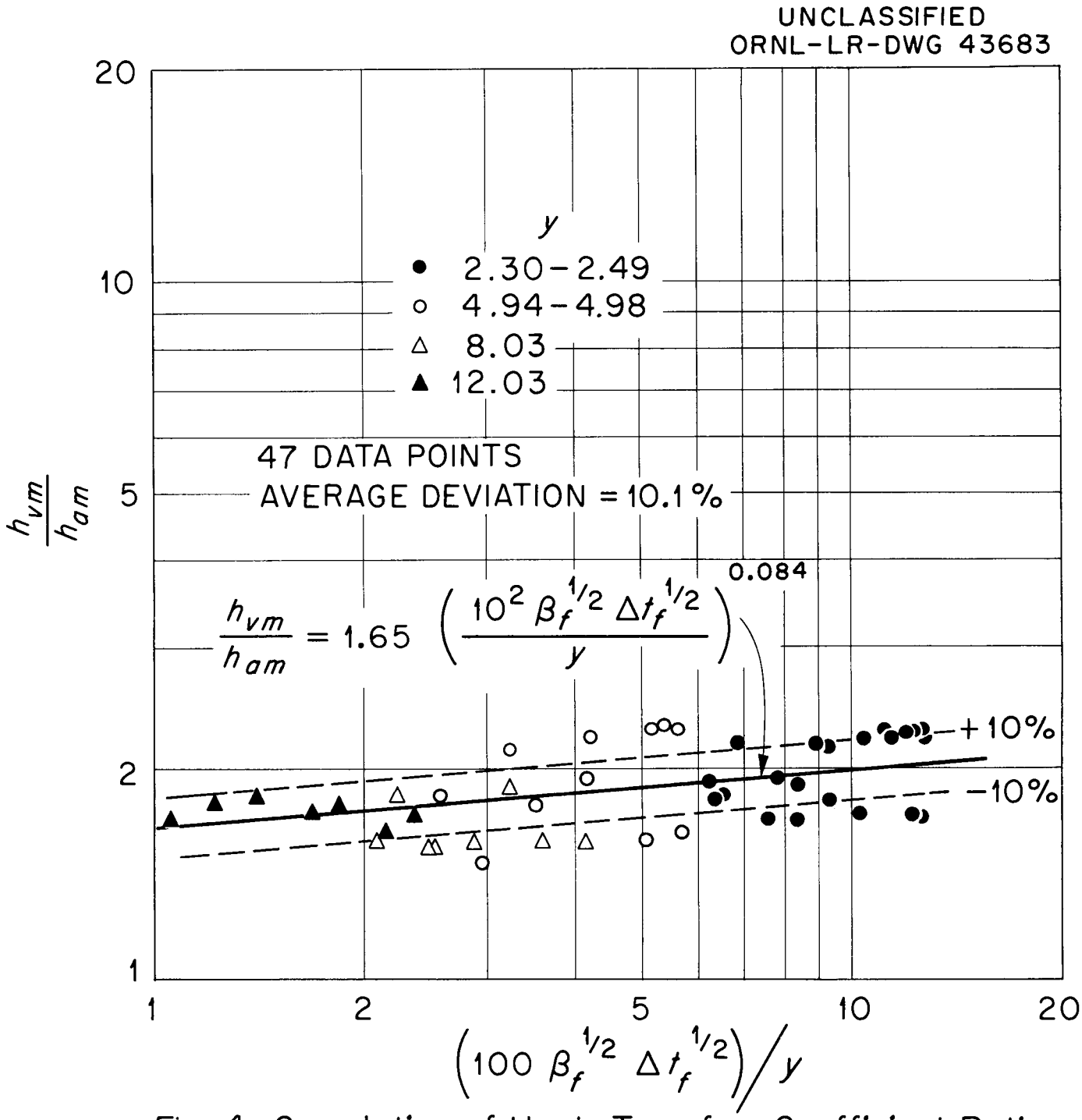

Fig. 4. Correlation of Heat-Transfer-Coefficient Ratio With the Modulus Ratio $Gr/(Re)_a^2$ for Nonboiling Water.

for average twisted-tape vortex-flow heat-transfer coefficients:

$$\left(\frac{h_{vm}}{C_{Pb}\,G_a}\right)\left(\frac{y^{0.09}}{2.18}\right) = \frac{0.023\left[1 + (D_i/L_h)^{0.7}\right]}{(Pr)_b^{2/3}\,(Re)_b^{0.2}}\ , \qquad (\underline{\underline{14}})^*$$

$$\left(\frac{h_{vm}}{C_{Pb}\,G_a}\right)\left[\frac{y^{0.084}}{2.43\,(\beta_f\,\Delta t_f)^{0.042}}\right] = \frac{0.023\left[1 + (D_i/L_h)^{0.7}\right]}{(Pr)_b^{2/3}\,(Re)_b^{0.2}}\ . \qquad (15)$$

In each equation, Re is calculated with D_i and V_a (or D_i and G_a). In reducing the data, values of β which had been calculated from the accurate density data for water given by Dorsey[9] were used; this β,t relation is given as Fig. 5.

Two additional correlations of h_{vm} were made, identical to those described above except that the mean film coolant temperatures of the vortex tests were used in calculating the equivalent values of h_{am}. Since the deviations (~ 12-1/2 %) of these correlations based on film temperature were greater than those of Eqs. 12 and 13, they offer no advantage and are not given here.

A check to see whether the Re dependency of h_{vm} is the same as for axial flow was made by plotting the ratio of h_{vm}/h_{am} to the correlation of Eq. 12 versus axial Reynolds number. As shown by Fig. 6, no significant drift of the ordinate group with $(Re)_a$ is evident. We may therefore conclude that, as in axial flow,

$$h_{vm} \propto (Re)_a^{0.8}\ . \qquad (16)$$

---

*Equation numbers of recommended correlations are doubly underlined throughout the text.

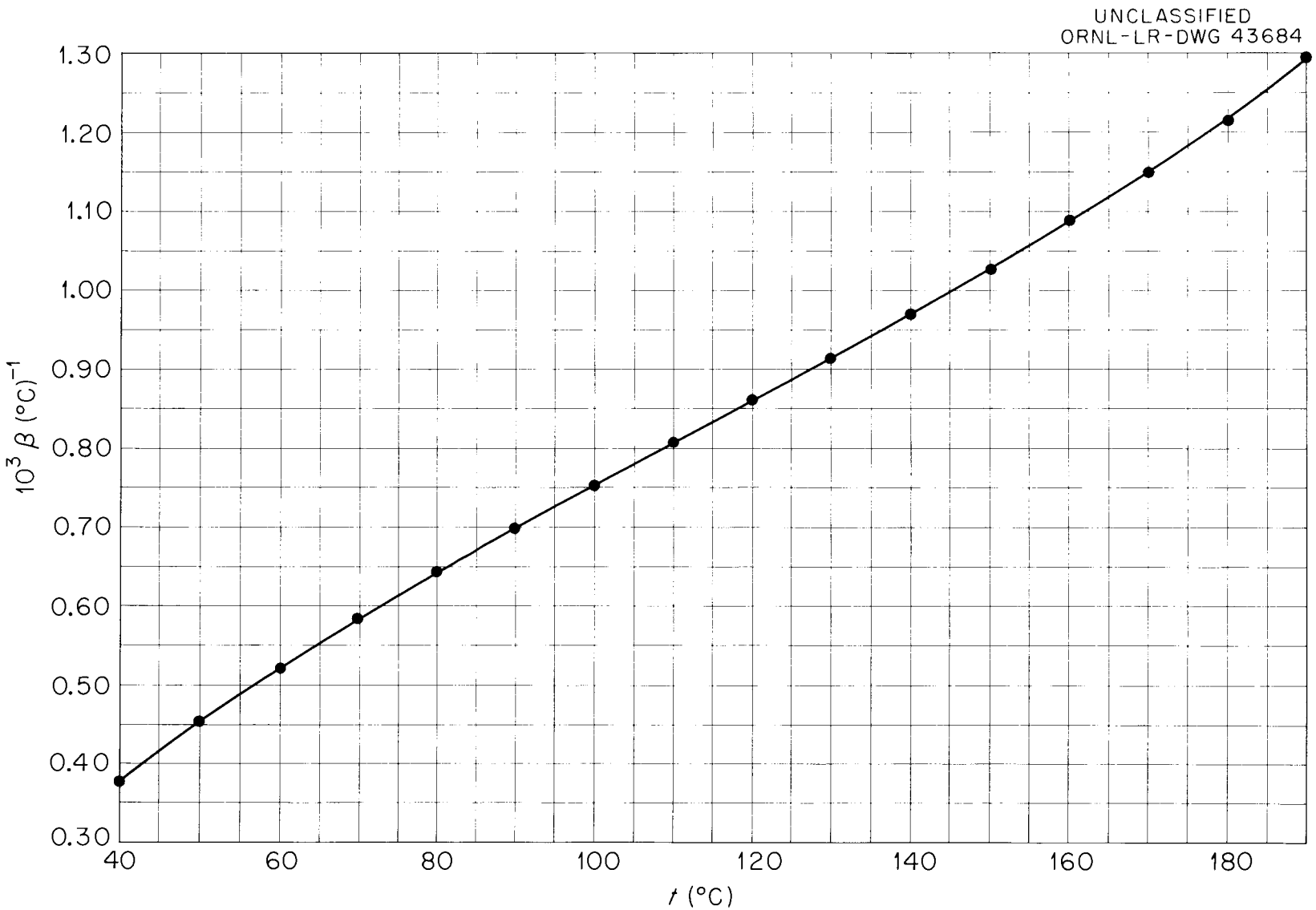

Fig. 5. Volumetric Coefficient of Thermal Expansion for Liquid Water vs. Temperature.

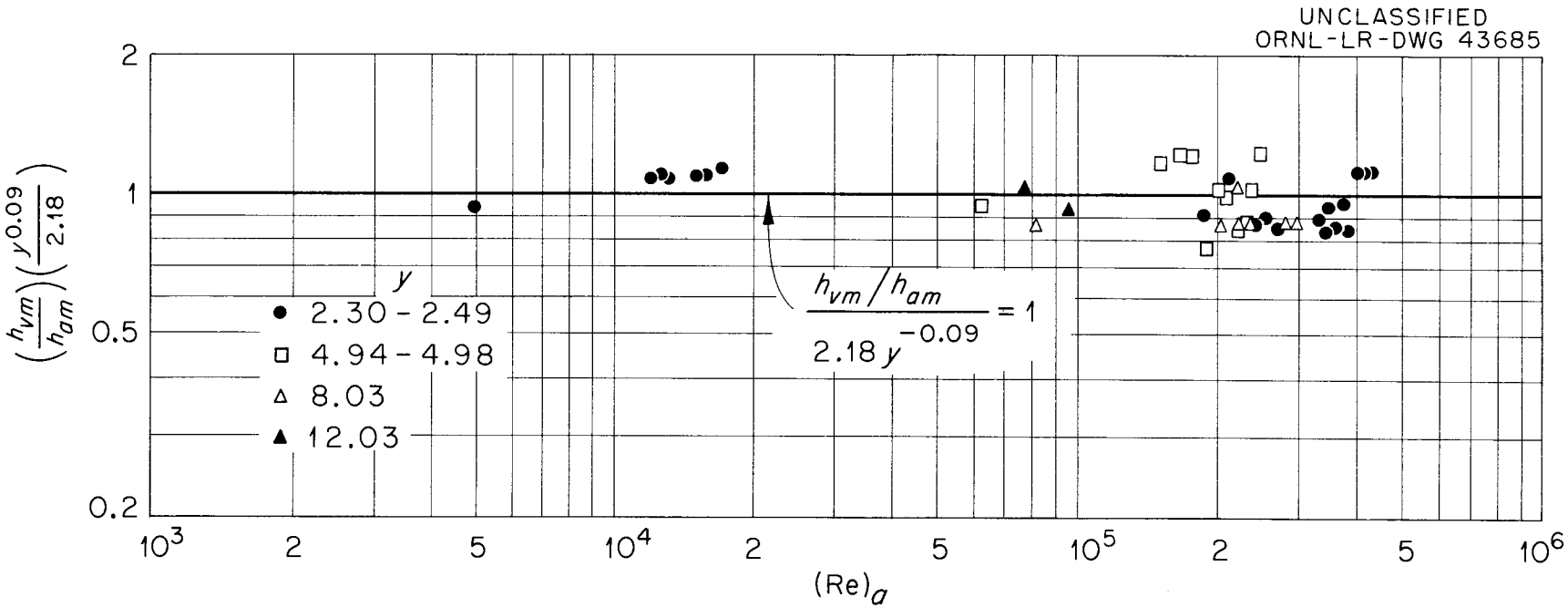

Fig. 6. Drift Plot of Correlated Mean Vortex Heat-Transfer Coefficient vs. Axial Reynolds Number.

C. Local-Boiling Heat-Transfer Coefficients

In Fig. 7, the few local-boiling data (below burnout) have been plotted as ϕ versus Δt and y. The curves, which separate reasonably clearly according to tape twist ratio, were empirically superposed, with the exception of one point, by introducing $y^{0.6}$ in the ordinate, as shown in Fig. 8. Within an average deviation of 14.8%, the liquid-film superheat, Δt_{sat}, is correlated by:

$$\Delta t_{sat} = \frac{y^{0.81}\,\phi^{1.35}}{0.34} \quad . \tag{17}$$

Slightly better correlation was obtained when a pressure correction factor of the Jens and Lottes type[10] was included. Since only 13 data points were available, however, the validity of the pressure correction could not be verified and was not pursued further.

III. Burnout Data and Correlations

A. Data Tabulation and General Comments

Burnout heat flux data for the twisted-tape vortex-flow tests are tabulated in Table 1; comparative straight-flow burnout data are summarized in Table 2. Ranges of test conditions for all the burnout data are given in Table 3.

The heat flux at burnout was calculated from the water heat absorption rate and the total internal surface area of the tube:

$$q_{bo} = W\, C_P\, (t_{b_2} - t_{b_1})_{bo} \;, \tag{18}$$

$$A_h = \pi\, D_i\, L_h \;, \tag{19}$$

$$\phi_{bo} = q_{bo}/A_h \quad . \tag{20}$$

A schematic of the equipment arrangement is given in Fig. 1. The tests were

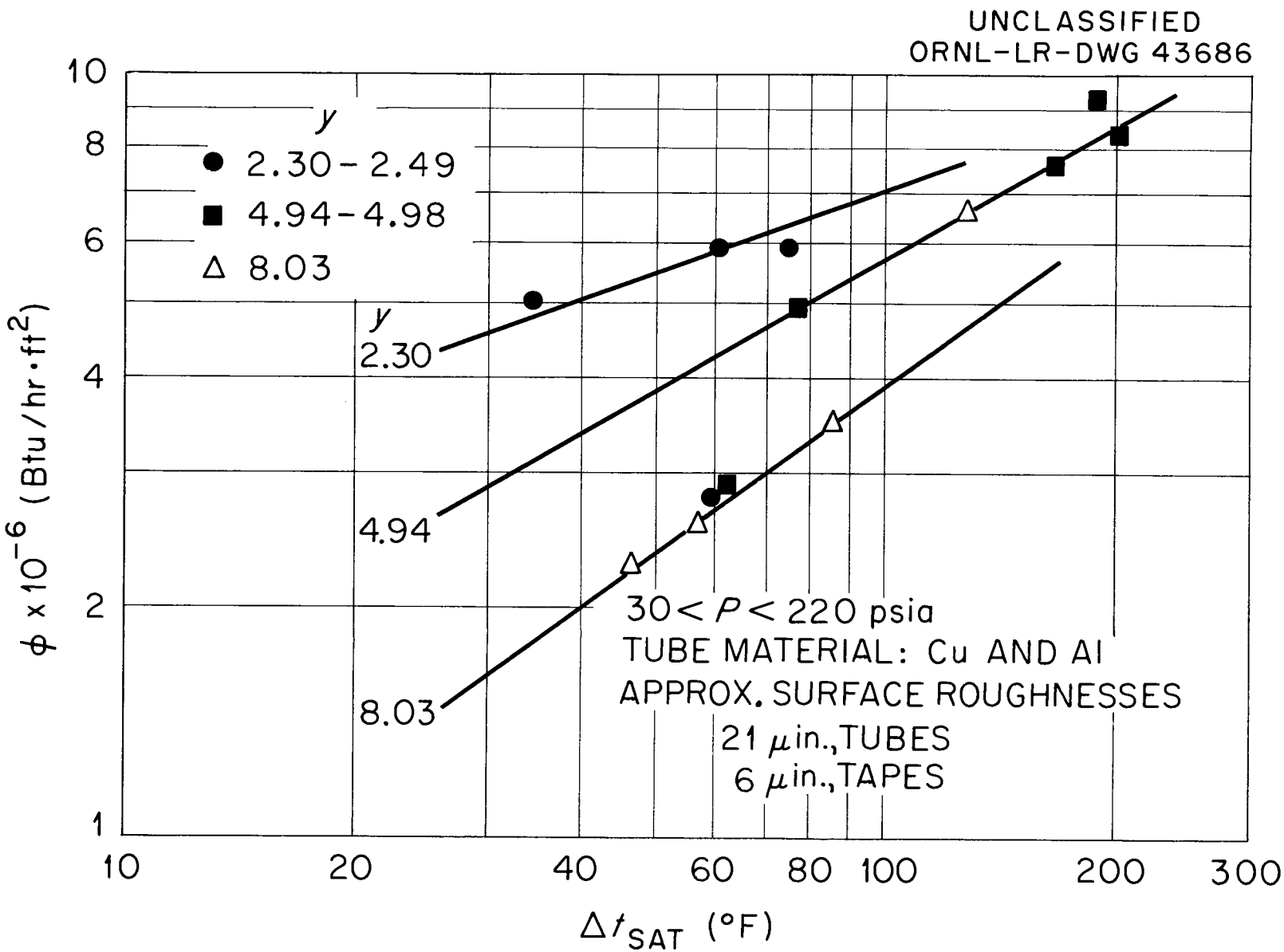

Fig. 7. Local-Boiling Vortex-Flow Heat Transfer Data, Heat Flux vs. Liquid-Film Superheat.

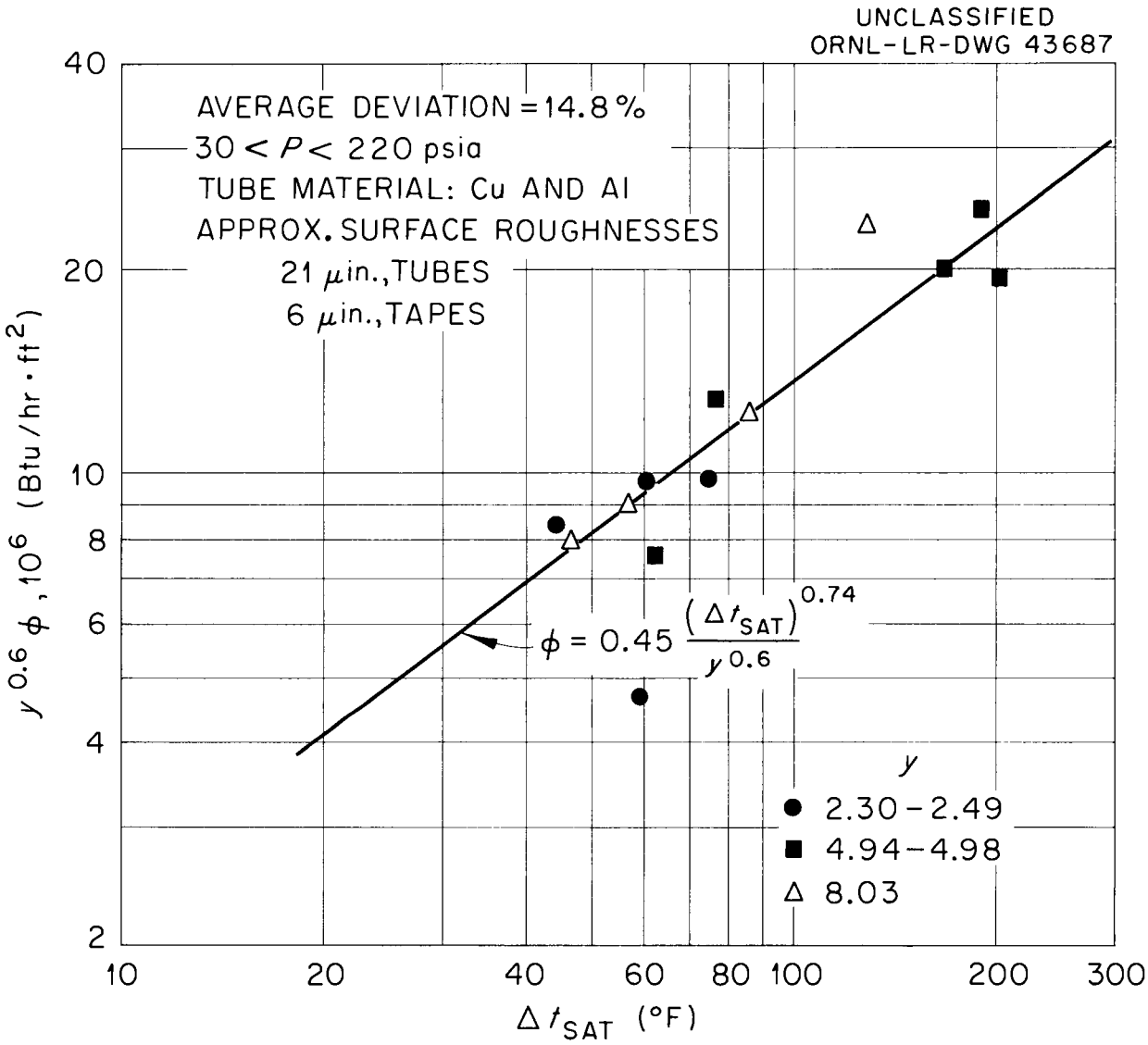

Fig. 8. Local-Boiling Vortex-Flow Heat Transfer Data, Heat Flux Times $y^{0.6}$ vs. Liquid-Film Superheat.

Table 1. Twisted-Tape Vortex-Flow Burnout Data

Test No.	Tube Characteristics[a] D_i, in.	D_o, in.	L_h, in.	L_h/D_i	y	Material	V_{a2}, fps	$(V_{ri})_2$, fps	P_2, psia	Pressure Tap Location[c]	ΔP, psi	t_{b1}, °F	t_{b2}, °F	$(\Delta t_{sub})_2$, °F[d]	ϕ_{bo}, Btu/hr·ft²[e]
1	0.402	0.500	10.48	26.0	2.99	Al	14.7	16.6	19.1	External	4.8	61.9	185.0	42	3.62×10^6
2	0.402	0.500	8.05	20.0	2.99	Al	16.0	18.1	19.7		6.0	64.0	177.9	52	4.75×10^6
3	0.305	0.376	16.20	53.0	2.42	"A" nickel	24.2	28.9	19.5		20.5	47.8	201.2	29	3.56×10^6
4	0.305	0.376	8.15	26.7	2.42		38.4	46.0	29.9		30.1	50.0	141.9	110	6.85×10^6
5	0.305	0.376	4.00	13.1	2.42		60.7	72.5	55.0		54.2	51.8	121.1	169	16.72×10^6
6	0.305	0.376	2.02	6.6	2.42		60.7	72.5	55.0		56.2	51.4	90.7	199	18.80×10^6
7	0.181	0.250	3.80	21.0	2.08[b]		107.8	135.0	20.2		242.0	70.2	150.2	72	20.40×10^6
8	0.181	0.250	2.48	13.7	2.08		110.0	137.8	23.0		235.0	65.8	128.7	99	24.95×10^6
9	0.181	0.250	1.49	8.23	2.08		110.0	137.8	21.6		228.0	64.0	105.6	118	28.00×10^6
10	0.181	0.250	3.80	21.0	2.08		81.0	101.6	17.2		175.0	70.3	159.2	57	16.92×10^6
11	0.181	0.250	2.50	13.8	2.08		84.6	106.0	17.7		166.0	69.1	137.0	80	20.75×10^6
12	0.181	0.250	1.50	8.28	2.08		80.3	100.6	17.5		175.0	68.9	120.2	97	24.77×10^6
13	0.181	0.250	3.80	21.0	2.08		52.8	66.1	15.0		58.7	65.6	147.2	64	10.12×10^6
14	0.181	0.250	2.47	13.66	2.08		55.2	69.2	15.1		55.6	66.2	123.2	88	11.48×10^6
15	0.181	0.250	1.50	8.29	2.08		55.0	68.9	15.0		55.0	66.4	110.4	100	14.57×10^6
16	0.181	0.250	1.45	8.0	2.08		148.0	185.2	29.7		423.0	72.5	111.1	130	37.35×10^6
17	0.181	0.250	3.75	20.7	2.08		149.1	187.0	27.9		432.0	63.2	151.0	85	31.22×10^6
18	0.181	0.250	2.50	13.8	2.08		156.0	195.3	29.7		400.0	62.6	120.7	119	32.75×10^6
19	0.249	0.355	12.03	48.3	2.30	Cu	35.4	42.9	15.7		44.0	64.4	210.8	4	3.35×10^6
20	0.249	0.355	12.00	48.2	2.30		34.0	41.1	545.0		40.0	75.1	221.0	255	5.14×10^6
21	0.189	0.269	12.00	63.5	7.70		67.4	68.9	34.9		108.0	76.6	210.9	48	6.90×10^6
22	0.189	0.269	12.00	63.5	7.70		67.4	68.9	470.0		115.0	80.3	213.1	248	6.82×10^6
23	0.136	0.206	11.97	88.0	2.46		74.4	88.1	495.0		235.0	92.4	350.0	116	9.41×10^6

Table 1. Twisted-Tape Vortex-Flow Burnout Data (Continued)

Test No.	Tube Characteristics[a] D_i, in.	D_o, in.	L_h, in.	L_h/D_i	y	Material	V_{a2}, fps	$(V_{ri})_2$, fps	P_2, psia	Pressure Tap Location[c]	ΔP, psi	t_{b1}, °F	t_{b2}, °F	$(\Delta t_{sub})_2$[d], °F	ϕ_{bo}[e], Btu/hr·ft^2
24	0.136	0.206	12.00	88.2	2.46	Cu	69.4[f]	82.2[f]	14.7	External	292.0	75.2	212.0	17 wt % quality	10.82×10^6
25	0.249	0.355	11.44	46.0	2.30		31.1	37.7	46.7	At tube inlet & exit	20.0	66.0	247.0	30	5.99×10^6
26	0.249	0.355	11.31	45.5	4.94		29.3	30.8	33.7		13.0	67.6	218.9	38	4.83×10^6
27	0.249	0.355	11.44	46.0	8.03		32.8	33.4	36.3		10.9	74.6	201.2	60	4.51×10^6
28	0.189	0.269	11.44	60.55	2.49		75.1	88.9	123.0		84.0	68.2	310.0	33	13.80×10^6
29	0.189	0.269	11.44	60.55	4.98		73.9	77.4	30.3		91.7	71.8	228.2	23	9.15×10^6
30	0.249	0.355	11.38	45.6	2.30		27.6	33.5	95.0		13.0	138.1	318.0	6	5.11×10^6
31	0.189	0.269	11.36	60.0	2.49		73.6	87.0	445.0		90.0	69.8	259.7	195	10.92×10^6
32	0.189	0.269	11.42	60.5	2.49		71.2[f]	84.1[f]	28.7		130.3	64.8	240.0	1.9 wt % quality	11.00×10^6
33	0.136	0.206	10.98	80.7	7.84		135.4	138.1	29.0		346.0	76.6	248.0	0.4	13.11×10^6
34	0.249	0.354	11.00	44.1	4.95	Al	53.3	56.0	84.7		30.3	68.9	194.9	121	7.61×10^6
35	0.249	0.355	17.34	69.7	12.03	Cu	27.8	28.0	46.7		----	82.2	270.2	6.7	3.64×10^6
36	0.249	0.354	17.37	69.7	12.03	Cu	25.8	26.0	245.0		10.0	78.5	324.0	75	4.26×10^6
37	0.249	0.353	11.52	46.4	8.03	Al	25.8	26.2	44.7		8.0	66.6	228.0	46	4.45×10^6
38	0.249	0.353	5.85	23.5	4.95	Al	89.7	94.6	225.0		~ 50.0	70.3	132.0	260	12.03×10^6
39	0.249	0.353	11.52	46.4	2.47	Al	14.77	17.5	24.1		~ 3.0	68.6	246.0	0.84 wt % quality	2.77×10^6
40	0.249	0.353	11.40	45.8	8.03	Cu	46.45	47.2	56.7		~ 27.3	64.8	198.2	91	6.79×10^6

a. Twisted tapes were all 0.015-in.-thick Inconel.

b. For tests 7 to 18, the tape fitted into double internal grooves each 0.008 in. deep and 0.020 in. wide.

c. "External" refers to tap-location indicated by dotted lines in Fig. 1; for tests 25 to 40, the taps entered the test-section wall radially through the electrodes.

d. Values for the inner exit wall location; where pressure taps were externally located, the subcooling at the exit wall was based on a calculated correction of measured exit pressure back to the tube exit.

e. Total water heat-absorption rate divided by internal test-section area, not excluding that covered by the tape edges.

Table 2. Comparative Straight-Flow Burnout Data

Test No.	Tube Characteristics[a] D_i, in.	D_o, in.	L_h, in.	L_h/D_i	V_2, fps	P_2, psia	Pressure Tap Location	ΔP, psi	t_{b_1}, °F	t_{b_2}, °F	$(\Delta t_{sub})_2$, °F	ϕ_{bo}, Btu/hr·ft^2 [b]
1	0.180	0.250	3.80	21.12	144.7	21.7	External	176.3	75.0	110.8	109	12.33×10^6
2			2.50	13.89	148.0	17.6		176.4	70.2	92.1	115	11.65×10^6
3			1.47	8.17	148.0	19.7		170.3	70.0	85.2	130	13.76×10^6
4			3.75	20.81	113.9	18.2		116.8	68.0	106.0	111	10.39×10^6
5			2.48	13.78	120.0	18.9		114.1	67.2	91.0	126	10.40×10^6
6			1.50	8.33	118.0	19.2		114.8	67.3	84.6	134	12.30×10^6
7			3.78	21.00	70.5	15.2		41.8	59.0	90.0	120	5.27×10^6
8			2.50	13.89	75.1	16.3		40.5	59.0	84.9	129	7.08×10^6
9			1.50	8.33	79.4	15.8		38.1	61.7	77.4	138	7.55×10^6
10			3.80	21.12	171.8	26.2		313.8	61.2	99.4	130	17.25×10^6
11			2.48	13.78	174.0	29.2		305.8	60.8	80.2	156	13.65×10^6
12			1.47	8.00	171.0	28.2		311.8	60.6	74.0	160	15.29×10^6
13			3.78	20.80	162.7	29.7		322.0	60.8	97.0	142	15.47×10^6
14			3.78	20.80	123.0	22.7		181.0	60.8	99.9	128	12.61×10^6
15	0.305	0.375	16.38	53.60	33.4	25.2		13.5	49.1	142.7	99	3.22×10^6
16			8.10	26.55	52.0	40.7		23.0	47.8	119.4	151	7.85×10^6
17			4.04	13.21	73.9	73.7		39.0	52.6	91.0	219	11.99×10^6
18			2.02	6.62	67.7	62.2		37.5	53.2	76.4	222	13.20×10^6
19			16.20	53.10	23.6	18.1		8.6	56.1	147.1	78	2.23×10^6
20			7.94	26.00	38.4	26.0		16.7	55.1	133.0	111	6.35×10^6
21			4.06	13.33	56.6	44.0		25.2	54.2	92.9	183	9.17×10^6
22			2.00	6.55	60.0	48.1		27.0	52.7	76.6	205	12.29×10^6
23	0.125	0.250	11.05	88.40	169.9	9.7		545.0	55.0	174.2	1.1 wt % quality	12.52×10^6
24	0.125	0.250	4.00	32.00	93.00	13.3		132.0	52.5	143.6	58	14.59×10^6

a. Test-section material was "A" nickel for tests 1 to 22, and Al for tests 23 and 24.

b. See footnote d of Table 1.

Table 3. Ranges of Test Conditions at Burnout

Variable	Swirl Flow (40 tests)	Straight Flow (24 tests)
D_i, in.	0.136 – 0.402	0.125 – 0.305
y, diameters/180-deg twist	2.08 – 12.03	–
L_h/D_i	6.6 – 88.2	6.55 – 88.4
Tube material	Al, Cu, "A"-nickel	Al, "A"-nickel
V_{a2}, fps	14.7 – 156.0*	23.6 – 174.0
t_{b1}, °F	48 – 138	48 – 75
t_{b2}, °F	91 – 350	74 – 174
ΔP (over-all), psi	3.0 – 432	8.6 – 545
$(\Delta t_{sub})_2$, at wall	17 wt % quality – 260°F subcooling	1.1 wt % quality – 222°F subcooling
ϕ_{bo}, Btu/hr·ft^2	$2.77 \times 10^6 - 37.35 \times 10^6$	$2.23 \times 10^6 - 17.25 \times 10^6$

*Which corresponds to a range of exit resultant velocity of 16.6 – 195.3 fps.

terminated by physical burnout of the test sections, which always occurred in the vortex tests at the downstream end quite near the exit electrode. In most cases, burnout of the tube wall did not destroy the twisted tape. Burnout was usually attained by slowly increasing the voltage drop across the test section at essentially constant coolant flow rate. In a few of the tests, however, the available voltage was not sufficient to cause burnout at high coolant velocity, in which case the flow rate was slowly reduced at constant (maximum) voltage.

Appreciable bowing of some of the tubes of vortex tests 19 to 40 was caused by thermal expansion at the higher temperature levels; the axial curvature thus introduced did not appear, however, to affect the values of ϕ_{bo}.* Figure 9-a is an X ray of the aluminum tube used in vortex test 1 before heating. Figure 9-b is an X ray of a similar aluminum tube after burnout in vortex test 34; the curvature shown was the largest encountered in any of the tests. The irregularly shaped spots on the tube wall were the thermocouple attachment locations and are caused by the presence of brazing compound residue.

Alternating current (60 cps) was used for energy generation in all tests; as discussed in ref 1, a-c heating gives smaller measured values of ϕ_{bo} than d-c (or nuclear) heating because of the ripple of tube metal temperature and heat flux. Italian workers[11] also indicate that the scatter of ϕ_{bo} values is greater when a-c heating is used. An approximate analysis[12] which gives the effect of a-c heating on burnout heat flux may be expressed in the following form:

---

*This is reasonable because of the rotational flow, which keeps the wall wetted so long as any liquid is present.

(*a*) X-ray of Aluminum Vortex Tube Before Heating in Test No. 1.

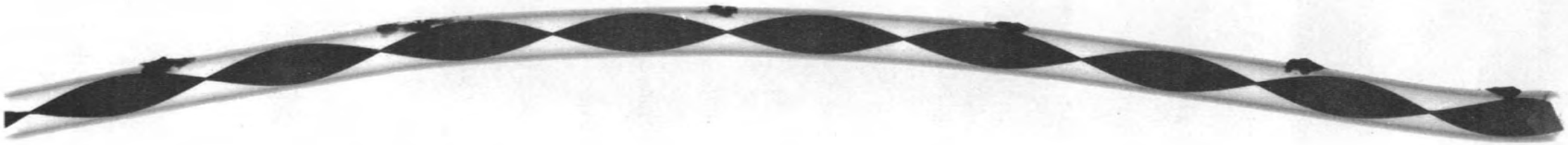

(*b*) X-ray of Aluminum Vortex Tube After Burnout in Test No. 34.

Fig. 9

$$\frac{\left(\phi_{bo}\right)_{a-c}}{\left(\phi_{bo}\right)_{d-c}} = \frac{\left[1 + (2\,\omega\tau)^2\right]^{1/2}}{1 + \left[1 + (2\,\omega\tau)^2\right]^{1/2}} \quad , \tag{21}$$

where

$$\omega = 2\,\pi\,f \tag{22}$$

and

$$\tau = \frac{cv}{hs} \quad . \tag{23}$$

Estimates of the reduction of ϕ_{bo} due to a-c heating were made for a number of the burnouts of this study; the reduction ranged from ~ ~~10%~~ 2% minimum to ~~20%~~ 16% maximum. One might therefore increase the correlated ϕ_{bo} values by ~ ~~15%~~ 10% for applications in which the heat input does not vary with time. *

B. Straight-Flow Burnout Tests

The 24 high velocity, low pressure burnout tests of Table 2 were made for purposes of comparison with the vortex data. Flow development at test-section entry was accomplished with either an upstream cone or an unheated tube ~ 40 diameters long. For all tests where the test-section pressure drop was less than 40 psi, the flow was restricted with a needle valve located upstream of the test section in order to reduce fluctuations of flow rate as burnout was approached. As demonstrated by Lowdermilk and co-workers[13,14] and others,[15] the stability of coolant flow during boiling is influenced by the pump and system flow characteristics. Stability is improved as the test-section pressure drop becomes a smaller part of the total system pressure drop. Under these conditions, the change in pressure drop caused by a phase change of the coolant has less influence on the flow rate since this pressure drop is a smaller part of the total pump head. The test-section pressure drop ranged from 4.5 to 40.0% of the system ΔP for the tests of Table 2 in which the flow was restricted.

* See errata

The burnout location became indeterminate at extreme velocities (V_a greater than ~ 150 fps), generally moving upstream with velocity and increasing in axial extent. In the worst cases, the entire downstream half of the tube was destroyed. The small change with length of degree of subcooling might have been responsible for this effect — i.e., the tube surface might have been covered by vapor to very nearly the same extent over a considerable area just before burnout.

The straight-flow burnout data have been compared with the Gunther equation[16]:

$$\phi_{bo} = 7{,}000\ V_{a_2}^{1/2}\ (\Delta t_{sub})_2 \tag{24}$$

in Fig. 10, and with the extended Bernath correlation[17]:

$$\phi_{bo} = 1.8\ h_{bo}\ (t_i - t_b)_{bo} \tag{25}$$

$$h_{bo} = 10{,}890 \left(\frac{D_e}{D_e + D_h} \right) + mV \tag{26}$$

$$(t_i)_{bo} = 57 \ln P - 54 \left(\frac{P}{P + 15} \right) - \frac{V}{4} \tag{27}$$

where

$$D_h = (\text{heated perimeter})/\pi,\ \text{ft} \tag{28}$$

$$m = 48/D_e^{0.6} \text{ for } D_e < 0.1 \text{ ft}, \tag{29}$$

and

$$m = 90 + \frac{10}{D_e} \text{ for } D_e \geq 0.1 \text{ ft}, \tag{30}$$

in Fig. 11. In Eqs. 25 to 30, temperatures are in °C, diameters in feet, velocity in fps, and pressure in psia; the units of h are Pcu/hr·ft^2·°C, and of ϕ_{bo}, Btu/hr·ft^2.

The more specialized, simpler Gunther expression, which is applicable to low-pressure water, fits the present data somewhat better than the

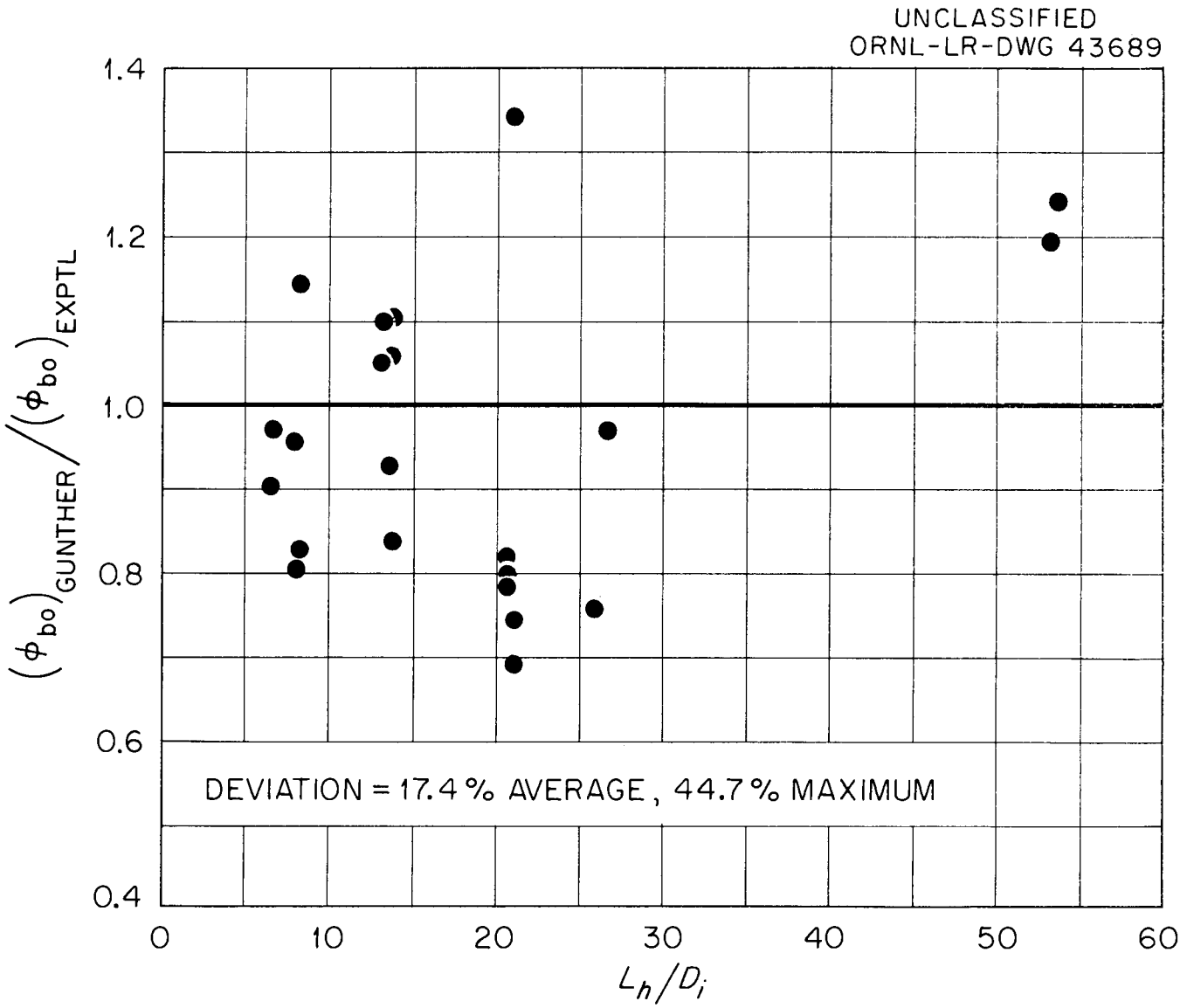

Fig. 10. Burnout Heat Fluxes of Straight-Flow Tests 1-22 Compared with Gunther's Correlation.

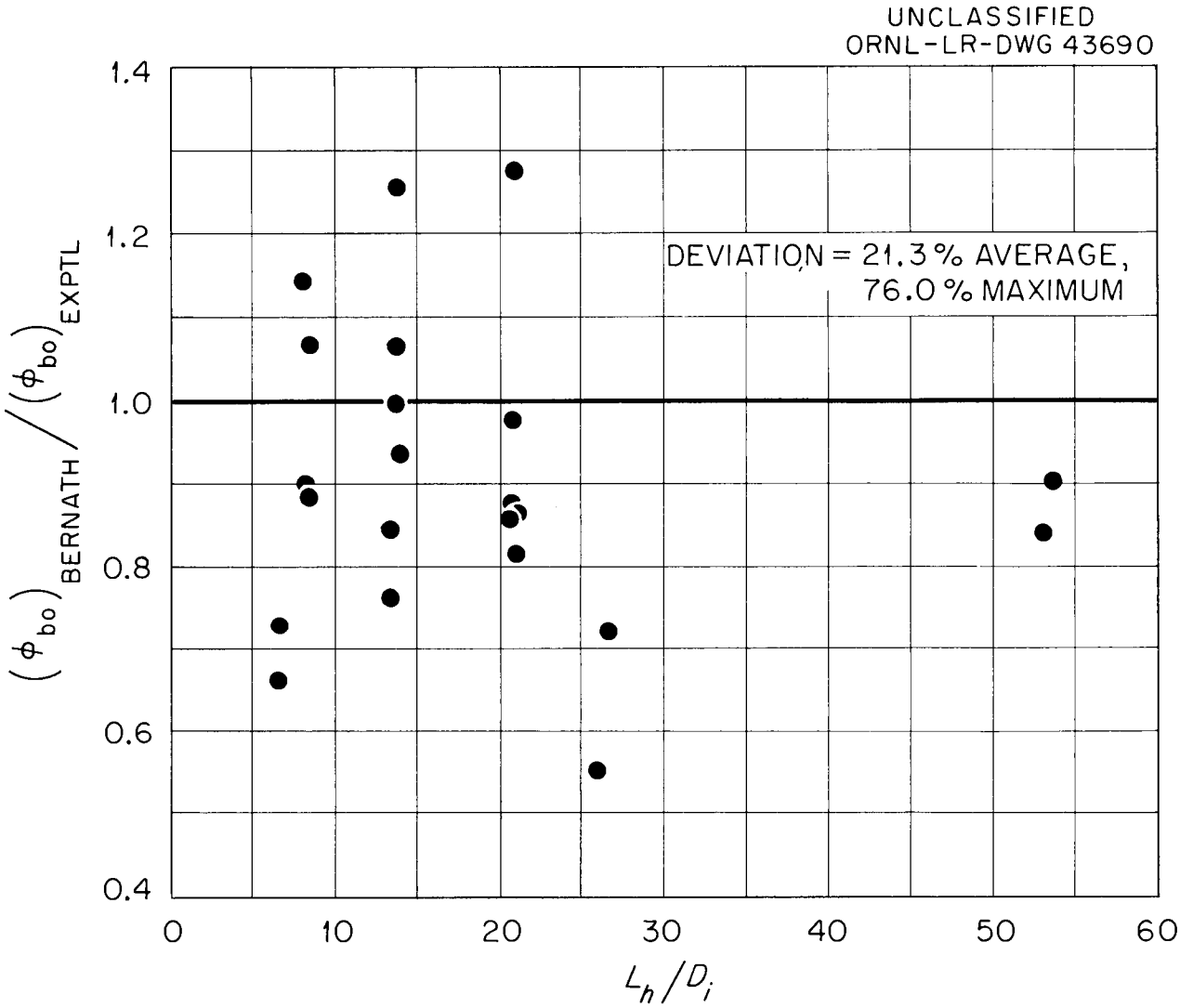

Fig. 11. Burnout Heat Fluxes of Straight-Flow Tests 1-22 Compared with Bernath's Correlation.

generalized Bernath correlation, which is based on almost all the existing burnout data for water. The data generally fall within the ±40% maximum deviation limits which seem to apply to most existing burnout correlations, and the agreement is considered fairly good, especially since the coolant velocities were considerably higher than in the tests on which the correlations were based. There is no distinct trend of ϕ_{bo} with L/D, which tends to confirm Bernath's contention[18] that L/D does not effect ϕ_{bo} directly in straight-flow local boiling burnout.

C. Swirl-Flow Burnout Tests

Pumping Power Dependence. The most important preliminary conclusion of the earlier vortex burnout study conducted at ORNL[1] was that the ratio of vortex-flow to axial-flow burnout heat fluxes is ~ 2 for water flow in identical tubes at equal pumping powers. This conclusion has been confirmed during the present study for twisted-tape vortex flow as shown in Fig. 12. Twelve pairs of tests were conducted, burnout heat fluxes being determined for four pumping powers at each of three L/D ratios for both vortex and axial flow. For the three upper curves of Fig. 12, the test sections were A-nickel tubes, 0.18-in. ID, fitted with twisted tapes for which y was 2.08; the plotted points correspond to tests 7 – 18 of Table 1. The straight-flow tests of Fig. 12, which correspond to tests 2 – 9 and 11 – 14 of Table 2, were made with identical tubes without tapes. The pressure level at tube exit varied from 15 to 30 psia for the 24 tests. For the second test of a given pair, the flow rate was adjusted so that the product of pressure drop and volumetric flow rate – i.e., the test-section pumping power – remained constant. The values of the ratio $(\phi_{bo})_v/(\phi_{bo})_a$ obtained from the curves of Fig. 12 at a constant value of pumping power range from 1.6 to 2.4, 2.0 being a good average.

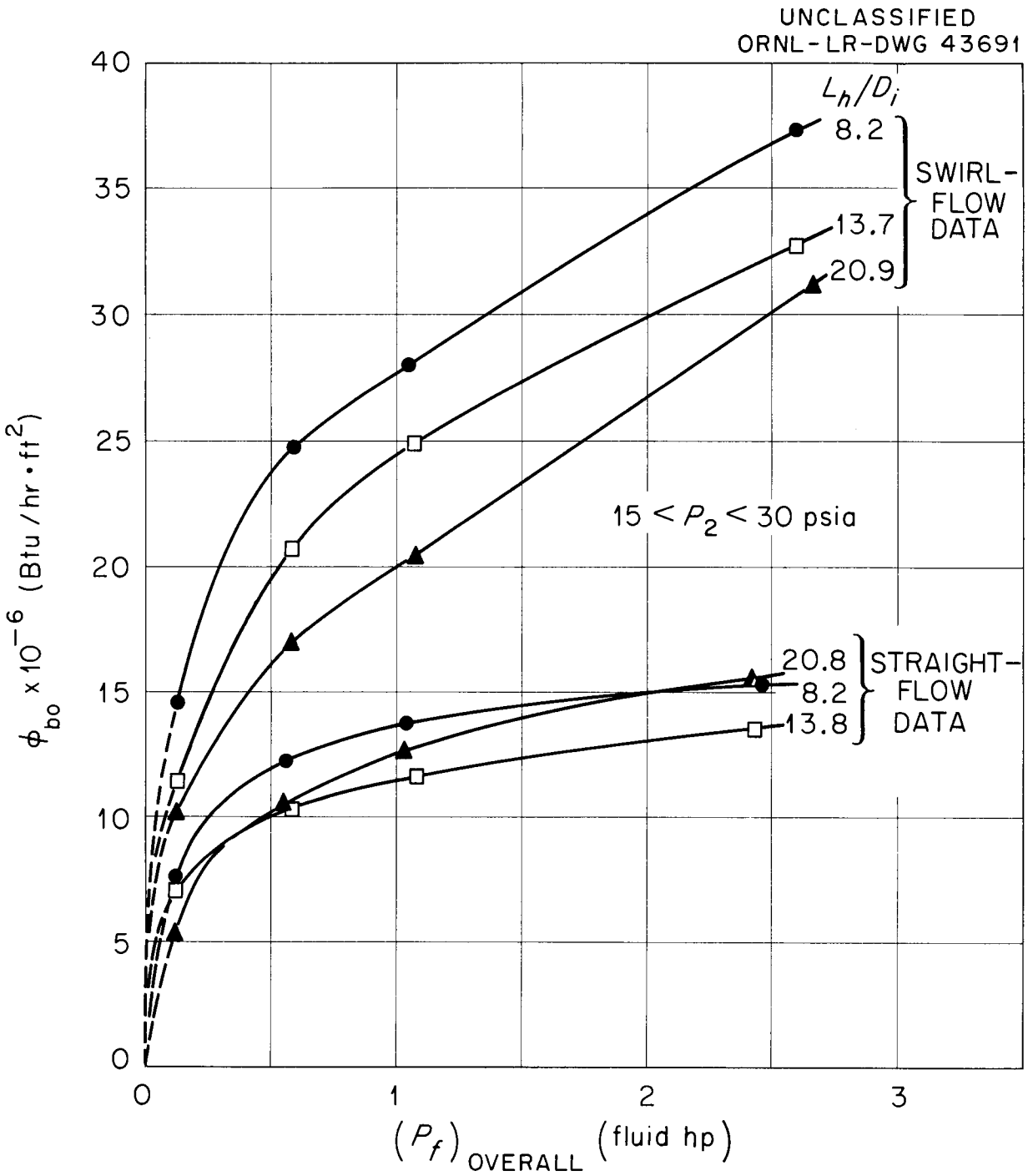

Fig. 12. Comparison of Swirl-Flow and Straight-Flow Burnout Heat Fluxes in Identical Tubes at Constant Pumping Power.

Subcooling Dependence. One of the more interesting aspects of swirl-flow burnout is its insensitivity to the degree of subcooling and pressure level at the burnout site. Such a phenomenon was indicated in our earlier work[1] but is demonstrated more explicity by the twisted-tape data tabulated in Table 4. For these comparative tests, all variables except exit pressure level were held constant. In the first test of a given pair, the exit pressure was minimized; and in the second test, maximized for the given velocity. It is apparent that for pressures up to at least 545 psia, the influence of P and Δt_{sub} on $(\phi_{bo})_v$ is negligible. For tests 35 and 36, where a very loosely twisted tape was used, the subcooling effect begins to appear, as it should since the flow was largely axial.

A possible reason for such behavior (which is contrary to that of straight-flow burnout) is that simultaneous alteration of P and of Δt_{sub} causes a cancellation of effects; i.e., increased pressure reduces the bubble diameters and buoyant force (by increasing ρ_v) so that centrifugal removal of bubbles from the surface is reduced; while at the same time, the increased subcooling tends to increase ϕ_{bo} in the usual straight-flow fashion -- by causing bubble collapse on or very near the surface. It is highly unlikely that this description is adequate, however, since its validity would require almost exact compensation of two independent mechanisms.

Another explanation,[19] which at first seems more plausible, is depicted schematically in Fig. 13. Assuming a McAdams-type variation of axial ϕ_{bo} with Δt_{sub}* in order to obtain a finite value of ϕ_{bo} at $\Delta t_{sub} = 0$, a line has been drawn on the graph (Fig. 13) which corresponds to the predicted equivalent axial ϕ_{bo} for a given vector velocity. The relative position of the vortex

---

*$\phi_{bo} = (a + b\ \Delta t_{sub})\ V^n$, where a, b, and n are constants.

Table 4. Effect of Exit Subcooling and Pressure Level on Swirl-Flow Burnout Heat Flux

Test No.	D_i, in.	L_h/D_i	y	V_{a2}, fps	P_{2i}, psia	$(\Delta t_{sub})_{2i}$, °F	ϕ_{bo}, Btu/hr·ft^2 [b]
19	0.249	48.4	2.30	35.4	16	4	5.35×10^6
20	0.249	48.2	2.30	34.0	545	255	5.14×10^6
21	0.189	63.5	7.70	67.4	35	48	6.90×10^6
22	0.189	63.5	7.70	67.4	470	248	6.82×10^6
24	0.136	88.2	2.46	69.4[a]	15	17 wt % qual.	10.82×10^6
23	0.136	88.0	2.46	74.4	495	116	9.41×10^6
32	0.189	60.5	2.49	71.2[a]	29	1.9 wt % qual.	11.00×10^6
31	0.189	60.1	2.49	73.6	445	195	10.92×10^6
35	0.249	69.7	12.03	27.8	47	7	3.64×10^6
36	0.249	69.7	12.03	25.8	245	75	4.26×10^6

[a] Based on exit flow of liquid only.

[b] Average difference for the five pairs of tests is 7.6%.

UNCLASSIFIED
ORNL-LR-DWG 44836

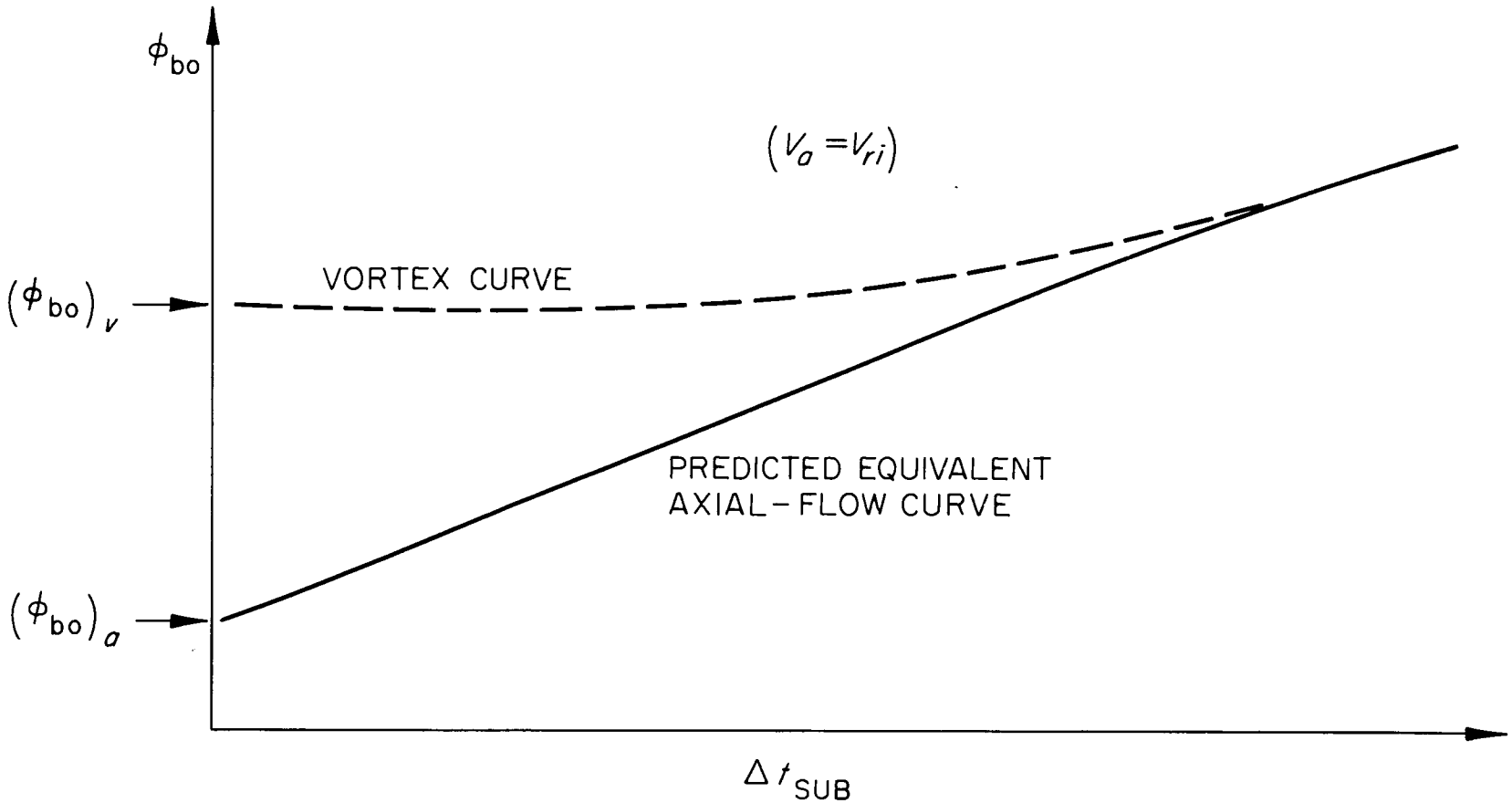

Fig. 13. Schematic Representation of the Small Effect of Subcooling on Vortex-Flow Burnout (See Text).

curve can then be based on considerations of bubble size variation with Δt_{sub}; i.e., at large Δt_{sub}, bubbles are probably so minute that even a large centrifugal acceleration will not cause a significant bubble displacement rate from the heated surface, whereas at lower subcoolings, the gee effect could become appreciable, with the Kutateladze-Zuber equation[20]:

$$\phi_{bo} \propto g^{1/4} \; a_t/g \; {}^{1/4} \tag{31}$$

applying in the limit of $\Delta t_{sub} = 0$ (i.e., bulk boiling with net steam generation). We would thus draw the vortex curve of Fig. 13 as asymptotically approaching the axial-flow curve at large Δt_{sub}, and satisfying the relation:

$$(\phi_{bo})_v = g^{1/4} \; (\phi_{bo})_a \; a_t/g \; {}^{1/4} \tag{32}$$

at $\Delta t_{sub} = 0$. The effect of gee is thus to modify ϕ_{bo} dependence on Δt_{sub} in such a way as to greatly reduce the dependence.

Comparison with Calculated Straight-Flow Burnout Values. Some investigators have apparently felt that ORNL swirl-flow burnout heat fluxes could be correlated by available straight-flow burnout equations if the resultant coolant velocity and actual wall pressure were used. This viewpoint is based on the assumption that centrifugal acceleration plays no important role in reducing the vapor coverage of the heated surface. That the viewpoint is erroneous is clearly shown by Figs. 14 and 15, on which are plotted comparisons of experimental $(\phi_{bo})_v$ with values of $(\phi_{bo})_a$ calculated by the extended Bernath method[17] (see Eqs. 25 to 30).

In Fig. 14, the comparison is made on a local basis — i.e., with local exit vortex values of wall pressure, resultant wall velocity, and bulk water temperature substituted into the Bernath relation to obtain the equivalent

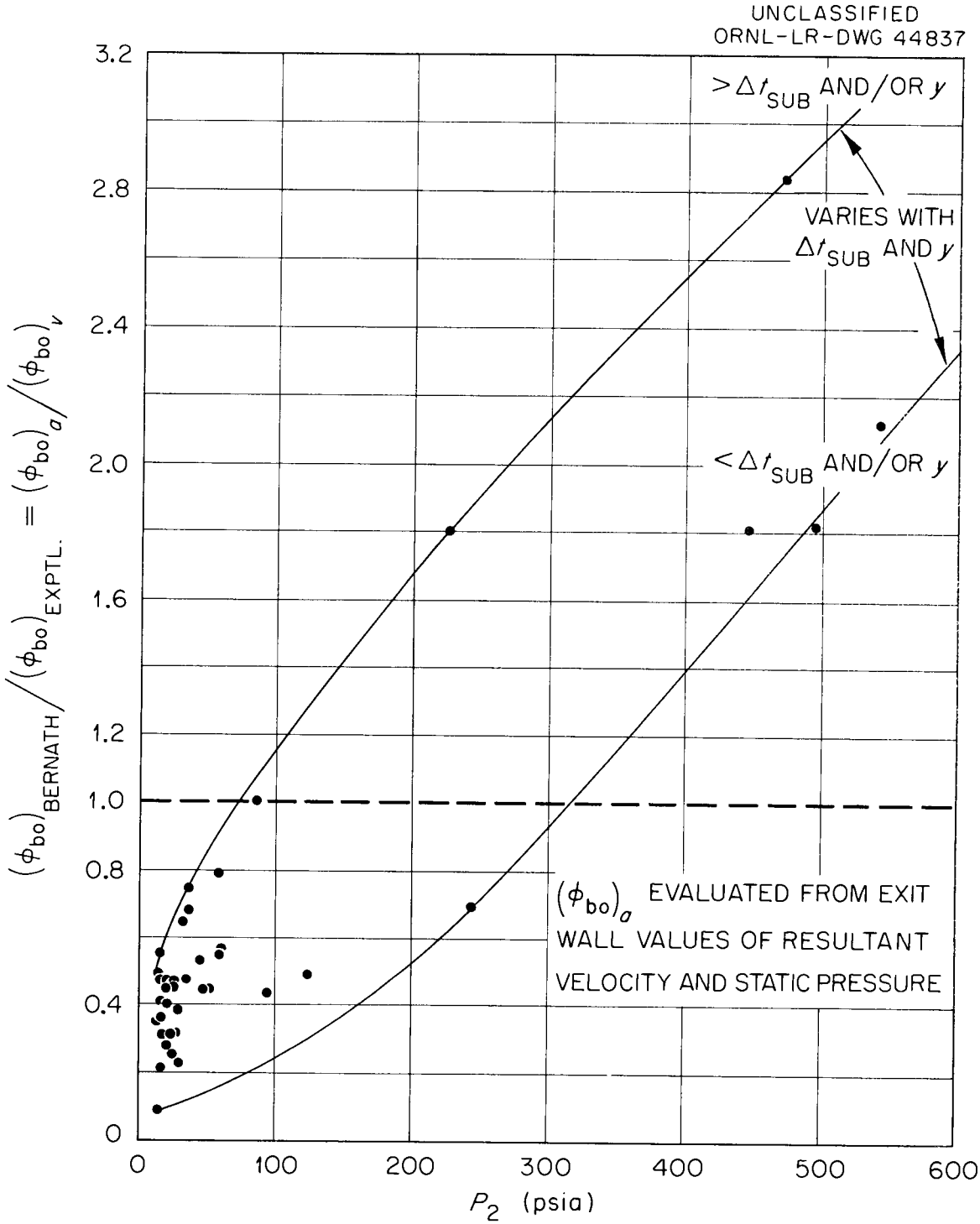

Fig. 14. Comparison of Experimental Vortex Burnout Heat Fluxes with Straight-Flow Burnout Fluxes Calculated by the Extended Bernath Method with the Exit Velocity, Pressure, and Bulk Water Temperature Held Constant.

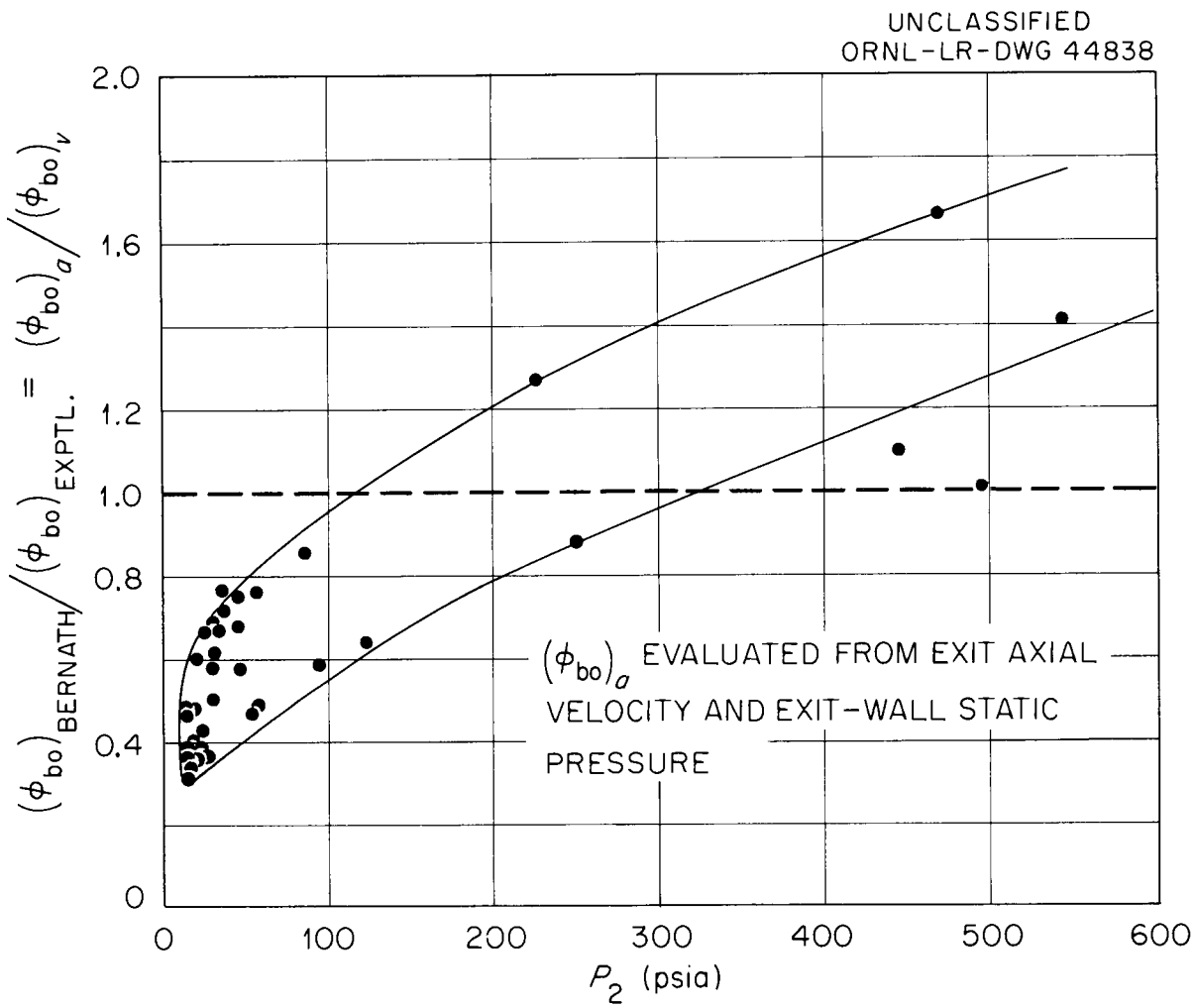

Fig. 15. Comparison of Experimental Vortex Burnout Heat Fluxes with Straight-Flow Burnout Fluxes Calculated by the Extended Bernath Method with the Exit Velocity, Exit Pressure, and Inlet Bulk Water Temperature Held Constant.

axial-flow burnout heat flux. In Fig. 15, the comparison is made on an over-all test-section basis, in which the vortex values of inlet bulk water temperature, exit axial velocity, and exit wall pressure were combined with the Bernath relation and iteratively solved to obtain $(\phi_{bo})_a$. An iterative calculation is required since $(t_b)_{bo}$ in Eq. 25, on which $(\phi_{bo})_a$ depends, is in turn dependent on the heat flux existing upstream of the exit burnout location. The authors feel that this distinction is an important one, and that whenever ϕ_{bo} data for new configurations (rough surfaces, twisted tapes, etc.) are to be compared with calculated axial-flow values, the iterative procedure gives a more significant result, since only in this way can the test-section heat balance be satisfied.

Figures 14 and 15 show clearly the consequences of the P-Δt_{sub} independence of $(\phi_{bo})_v$ as discussed in the previous subsection. At greater pressures, and therefore greater Δt_{sub} for essentially constant t_b, the equivalent axial-flow burnout values can exceed the vortex values, since $(\phi_{bo})_a$ is strongly dependent on Δt_{sub} and P in the present pressure range. At low P or Δt_{sub}, the axial-flow burnout values are, conversely, penalized relative to the vortex values, and the ratio $(\phi_{bo})_v/(\phi_{bo})_a$ becomes as large as 3 – 10, depending on the basis of comparison. It may be concluded that vortex flow is most beneficial from a burnout standpoint with either (a) bulk boiling and net steam generation ($\Delta t_{sub} = 0$), or (b) local boiling under conditions of small or moderate subcooling.

The calculated comparisons of Figs. 14 and 15, which indicate that the ratio $(\phi_{bo})_a/(\phi_{bo})_v$ can exceed unity, are not compatible with the mechanism postulated for subcooling dependence, and illustrated in Fig. 13. The postulated mechanism requires that the vortex-flow ϕ_{bo} curve merge into the

axial-flow curve at large Δt_{sub}, and it is difficult to so interpret the mechanism as to justify a crossover of the two curves. At present, it may only be concluded that either the proposed mechanism is invalid or that it becomes so when the subcooling is large.

Correlation of Vortex-Flow Burnout Heat Fluxes. Elimination of coolant pressure and subcooling as significant variables considerably simplified the task of correlating the experimental values of $(\phi_{bo})_v$. The first such attempt was made when only the data of tests 7 – 18 of Table 1 were available; for these tests, y was constant and equal to 2.08. A plot of $(\phi_{bo})_v$ vs L_h/D_i with V_a as a parameter for these data showed that, on the average, $(\phi_{bo})_v$ varied inversely with $(L_h/D_i)^{0.3}$. Another plot of $(\phi_{bo})_v$ vs V_a with L_h/D_i as a parameter showed that $(\phi_{bo})_v$ varied directly with V_a. The best values for these exponents were 0.29 and 0.95, but they were subsequently rounded to 0.3 and 1.0, respectively, and the initial data were well correlated by a plot, on rectangular co-ordinates, of $(\phi_{bo})_v$ vs $V_a/(L_h/D_i)^{0.3}$. This procedure did not hold up well, however, for later data where y was significantly different from 2.08. For all the vortex burnout data (40 points), the correlating group was changed to $V_{ri}/(L_h/D_i)^{1/3}$, with the results shown in Fig. 16. The resultant wall velocity was calculated from the relation (see Appendix 1 for derivation):

$$V_{ri} = V_a \left[1 + \left(\frac{\pi}{2y} \right)^2 \right]^{1/2} \tag{33}$$

In Fig. 16, both mean and minimum (design) curves are shown; the insert is an expansion of the larger plot for the region $(\phi_{bo})_v < 10 \times 10^6$ Btu/hr·ft^2. Arithmetic average deviations of the data points from the minimum (design) curves are noted on Fig. 16; the average error of the mean curve through

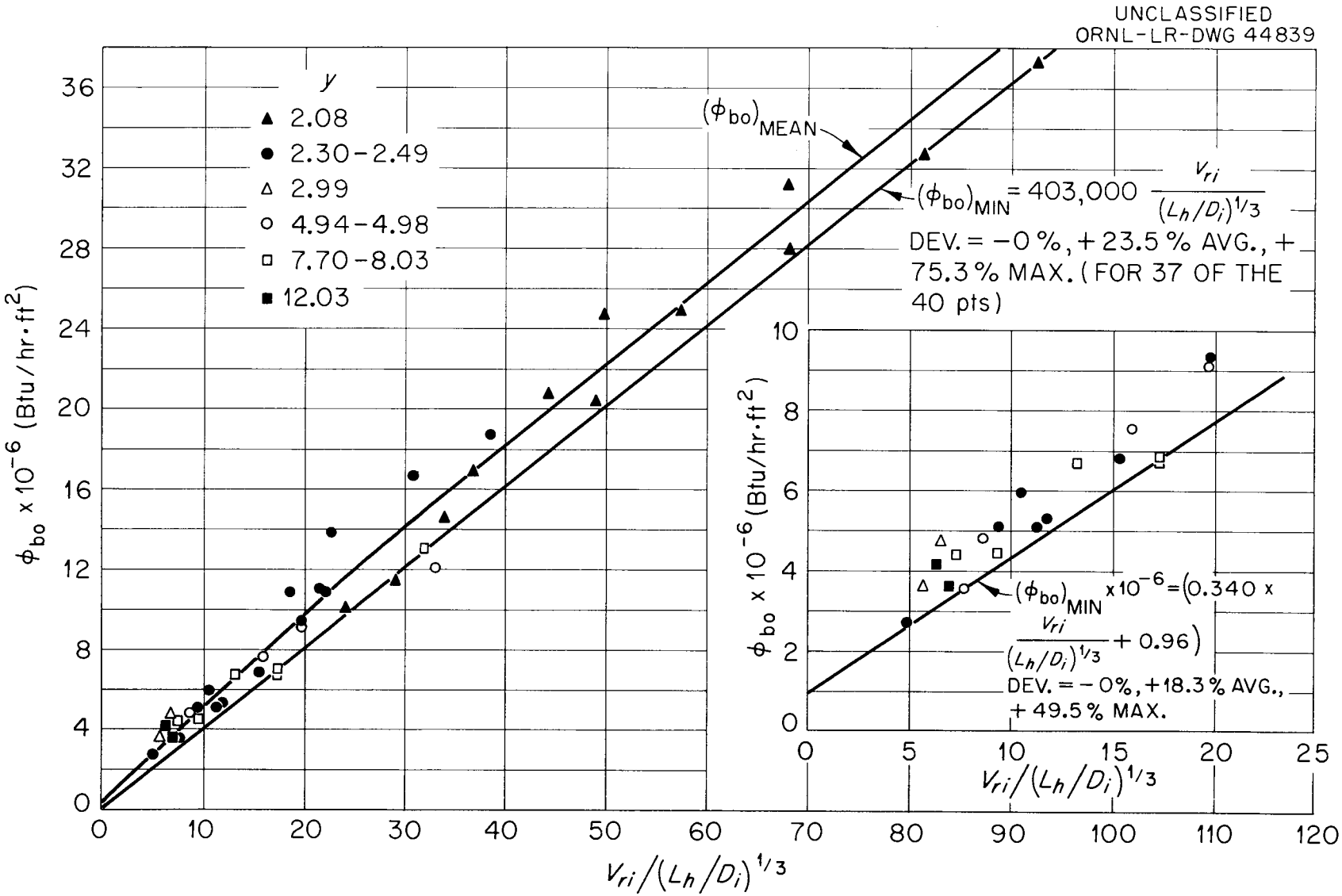

Fig. 16. Twisted-Tape Vortex-Burnout Correlation I.

all the data is ~ ±12%. It appears that use of the resultant wall coolant velocity gives fair representation of the data for various tape twist ratios. It is interesting to note that the variation

$$(\phi_{bo})_v \propto V_{ri} \tag{34}$$

predicts a constant exit bulk water temperature at burnout for all coolant velocities with a fixed geometry and inlet water temperature; this is true since the coolant temperature rise is inversely proportional to V (with ϕ fixed).

A second burnout correlation was based on the premise that the circumferential motion <u>alone</u> would affect burnout according to Zuber's equation[20]:

$$(\phi_{bo})_t \propto \cancel{g^{1/4}}^{*}\ a_t\, g^{1/4} \tag{35}$$

and since

$$* \quad a_t \cancel{g} = \frac{V_t^2}{g_{\cancel{c}}\, R_i} \propto \frac{V_t^2}{D_i} \tag{36}$$

one obtains,

$$(\phi_{bo})_t \propto \frac{V_t^{1/2}}{D_i^{1/4}} \quad . \tag{37}$$

The assumption was then made that the purely axial motion would affect ϕ_{bo} according to:

$$(\phi_{bo})_a \propto V_a^{1/2}\,(L/D)^{-n} \tag{38}$$

which is valid for most straight-flow data. It was further assumed that a product-type solution:

$$(\phi_{bo})_v = f(\phi_{bo})_t \cdot g(\phi_{bo})_a \ , \tag{39}$$

where f and g denote functions, would represent the simultaneous effect of the tangential and axial motions on $(\phi_{bo})_v$. Combination of Eqs. 37 to 39

* See note

with the equations connecting velocity with tape twist ratio (see Appendix 1 for derivations):

$$V_{ti} = \frac{\pi}{2y} V_a \tag{40}$$

$$V_{ri} = V_a \left[1 + \left(\frac{\pi}{2y} \right)^2 \right]^{1/2} \tag{33}$$

results in:

$$(\phi_{bo})_v \propto \frac{V_a}{y^{1/2} D_i^{1/4} (L_h/D_i)^n} . \tag{41}$$

When n in Eq. 41 was taken as 1/3, as in the previous correlation method, and the vortex data were plotted according to Eq. 41, the correlation was inferior to that of Fig. 16 (data deviation 14 – 54% greater).

A refinement to the above scheme was made after an apparent interaction of L_h/D_i and V was noted. The slopes of lines of $(\phi_{bo})_v$ vs L_h/D_i with V_a as a parameter are inversely proportional to V_a, and approximately satisfy the relation:

$$(\phi_{bo})_v \propto (L_{si}/D_i)^{-32/V_a} \tag{42}$$

where the swirl-flow length at the wall is given by (see Appendix 1 for derivation):

$$L_{si} = \frac{L_a}{2y} (4y^2 + \pi^2)^{1/2} . \tag{43}$$

The L/D function of Eq. 42 was used in Eq. 41 to give:

$$(\phi_{bo})_v \propto \frac{V_a}{y^{1/2} D_i^{1/4} (L_{si}/D_i)^{32/V_a}} . \tag{44}$$

The vortex data have been plotted according to Eq. 44 in Fig. 17. The non-linear minimum (design) curve deviates from the data to a somewhat smaller extent than does the corresponding curve of Fig. 16.

A third vortex-burnout correlation was made by plotting the data according to an NACA form,[14] which was developed for bulk boiling of water in axial

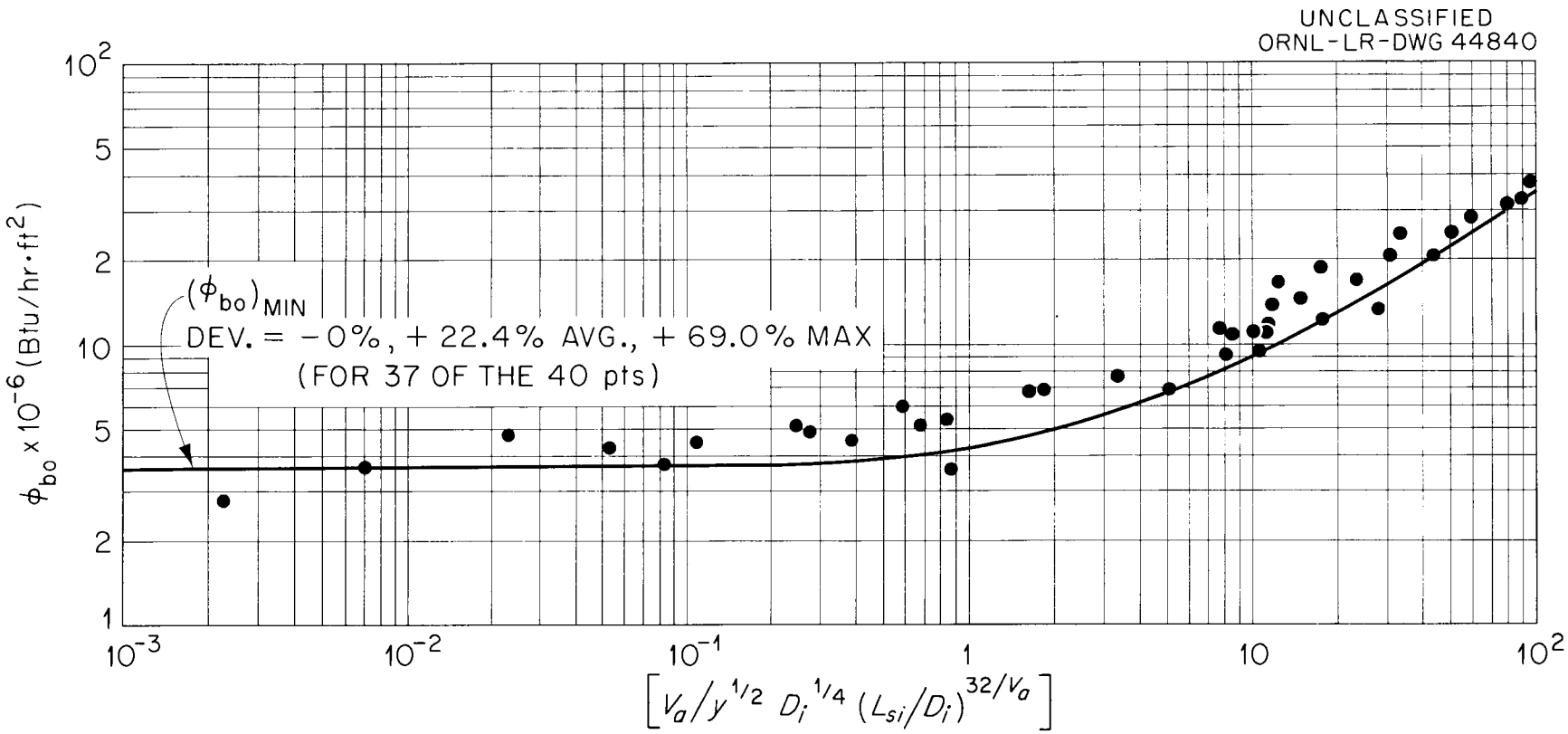

Fig.17. Twisted-Tape Vortex-Burnout Correlation II.

flow. Figure 18 shows the results when axial mass velocity is used. Use of resultant mass velocity, defined as:

$$G_r = 3600\ \rho_b\ V_{ri} \tag{45}$$

gives somewhat better correlation, as shown in Fig. 19.

The tree dissimilar burnout heat flux correlations of Figs. 16 – 19 give similar over-all deviations with respect to the experimental vortex data. The recommended burnout design equation is that of the curve of Fig. 19:

$$(\phi_{bo})_{v_{min}} = \frac{398\ G_r^{0.645}}{D_i^{0.20}\ (L_h/D_i)^{0.44}}\ , \tag{46}$$

where D_i is in ft, which may be transformed to:

$$(\phi_{bo})_{v_{min}} = \frac{130{,}000\ (\rho_b\ V_a)^{0.645}\ (D_i)^{0.24}\left(1 + \frac{\pi^2}{4\ y^2}\right)^{0.323}}{(L_h)^{0.44}} \tag{47}$$

where tube ID (D_i) and heated length (L_h) are in inches.

The appearance of the L/D ratio as a significant variable in each of the vortex burnout correlations may be felt disturbing, since no mechanism has been envisaged which clearly explains such a dependence. In axial-flow bulk boiling burnout, both U.S. and Soviet data show a definite L/D dependence, which is reasonable since the two-phase flow regime, in the presence of net vaporization, can change drastically with heated length. In axial-flow subcooled boiling burnout, the situation is less clear; and two camps exist, one of which supports a fairly strong L/D dependence, the other disclaiming it completely. The recent measurements by Costello[21] of bubble-layer thickness in local boiling of distilled water show that the thickness increases with heated length, and at high heat fluxes and low velocities, the layer can attain a considerable thickness (e.g., 12.2 mils for ϕ =

* See errata

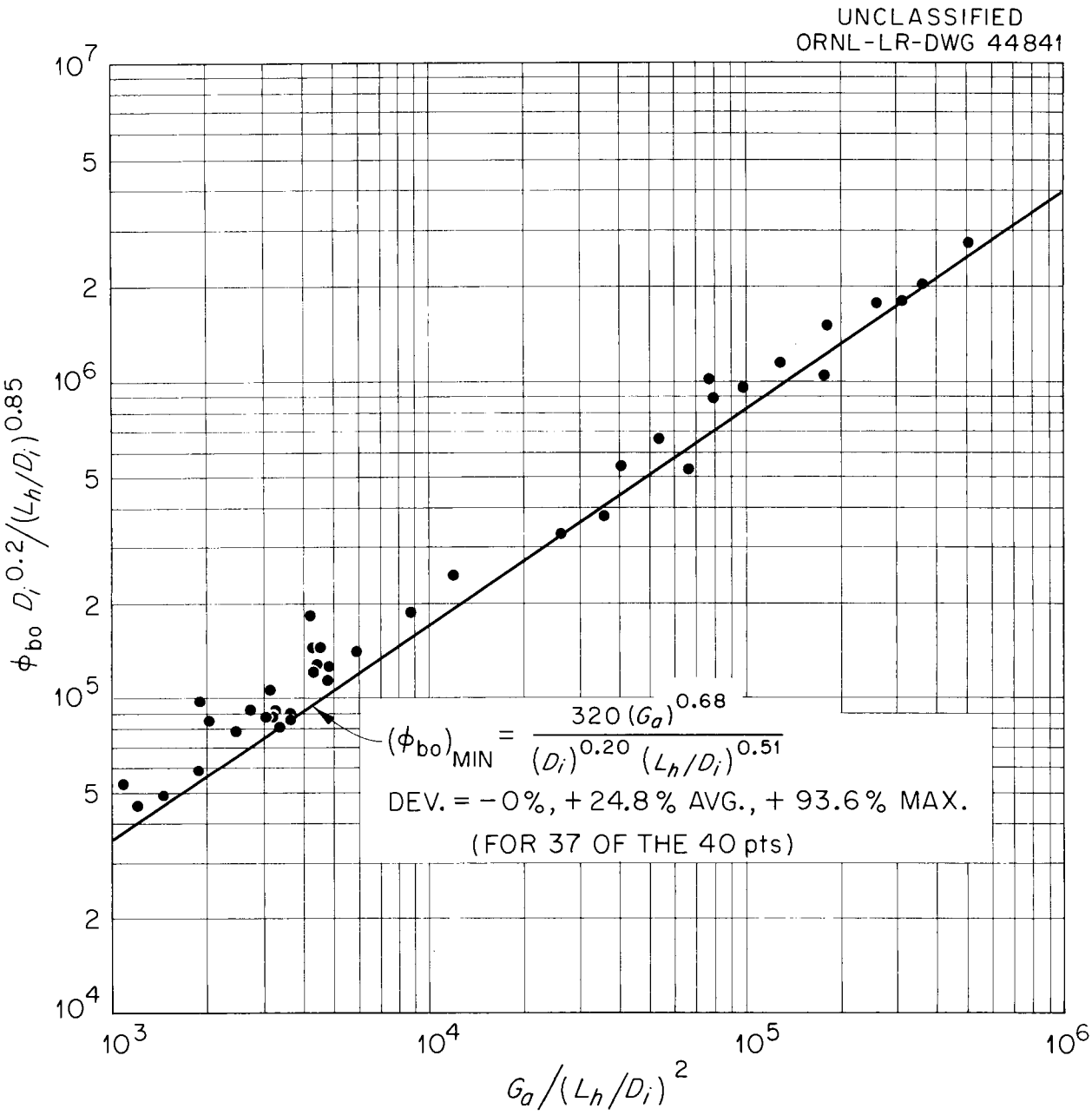

Fig. 18. Twisted-Tape Vortex-Burnout Correlation IIIa.

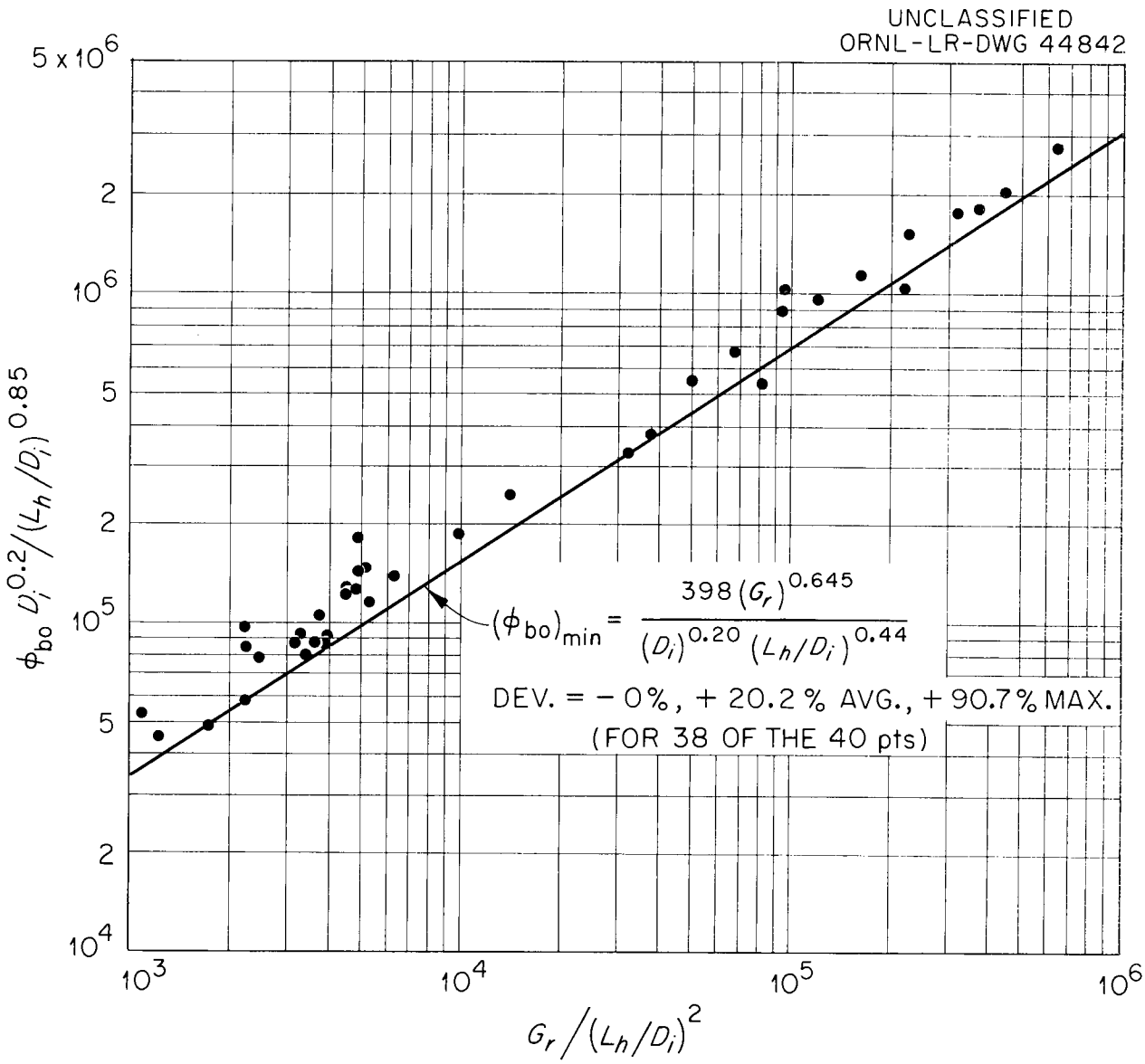

Fig. 19. Twisted-Tape Vortex-Burnout Correlation IIIb.

0.40×10^6 Btu/hr·ft^2, V = 1.5 fps, and P = 17 psia). These data indicate a type of "sliding build-up" of vapor bubbles with length, and may help to explain the ϕ_{bo} dependence on L/D for both axial flow and vortex flow. In any case, the ϕ_{bo} data of the present study definitely vary with L/D at constant V, and the variation is reasonably well characterized by the burnout correlations presented above.

Burnout Test of Oval Twisted Tube. A "slotless, tapeless" vortex tube was produced by flattening a copper tube to an oval cross section, packing its interior with sand, and then twisting the entire tube about its axis. Such an oval twisted tube was mentioned as a possible swirl inducer by Kreith and Margolis;[22] and, apparently, friction factor and pressure distribution tests for such a configuration have been made at KAPL.[23] The final dimensions of the oval tube tested were as follows: flow area = 0.0617 in.^{2}, wetted perimeter = 0.938 in., d_e = 0.264 in., L_h = 11.77 in., and y = 4.03 equivalent diameters/180-deg twist. With exit conditions of P_{wall} = 19.8 psia, V_a = 8.4 fps, and Δt_{sub} = 12°F, burnout occurred at 1.52×10^6 Btu/hr·ft^2. For identical local exit values of P, V, and t_b in an equivalent cylindrical tube, Bernath's extended method[17] predicts an axial-flow burnout of 0.58×10^6 Btu/hr·ft^2 (2.6-fold smaller).

IV. Friction Factors

A total of 149 pressure-drop determinations* were made for the twisted-tape vortex tubes. Data were taken during 88 isothermal, 47 heated nonboiling, and 14 heated local-boiling tests. Both Al tubes (D_i = 0.249 in.) and Cu tubes (D_i = 0.136 in., 0.188 in., and 0.249 in.) were used; tape twist ratio y

*End-loss corrections for all ΔP data discussed here were eliminated by using terminal pressure taps drilled through both electrode and tube wall.

varied from 2.30 to 8.03. Friction factors for the Al tubes seemed to scatter somewhat more than those for the Cu tubes.

A. Isothermal and Nonboiling Data

Friction factors were initially derived from the measured pressure drops by use of the standard axial-flow friction-factor definition:

$$f_a = \frac{D_i}{L_a} \frac{2g_c}{V_a^2} \frac{144}{\rho_b} \Delta P \quad . \tag{48}$$

Friction factors for heated runs were corrected to isothermal conditions by multiplying the right side of Eq. 48 by the turbulent-flow factor 1.02 $(\mu_b/\mu_i)^{0.14}$. The results of such calculations are shown as f_a vs $(Re)_a$ in Fig. 20. The vortex friction factors based on L_a, V_a, and D_i are larger than straight-flow friction factors and vary widely with both y and D_i. The vortex values of f_a do not decrease with Reynolds number as do smooth-tube axial-flow friction factors in the same Re range. The flatness of the curves in Fig. 20 is characteristic of a relative roughness (in axial flow) one hundred times that measured for some of the vortex tubes (21 μin. rms for the tubes and 6 μin. rms for the tapes). Since relative roughness was not determined for all of the vortex tubes, final conclusions concerning its effect cannot be drawn from the present data.

Though D_i was used above, it is obvious that it is not the true characteristic dimension for flow through a tube with an internal twisted tape. A close approximation to the true equivalent diameter (for turbulent flow) may be obtained by dividing four times the free flow area by the wetted perimeter for the case of a similar, but untwisted, tape in a cylindrical tube:

$$D_e = \frac{\left[(\pi/4)\, D_i^2 - D_i\, t_t \right] 4}{\pi\, D_i - 2t_t + 2D_i} \quad . \tag{49}$$

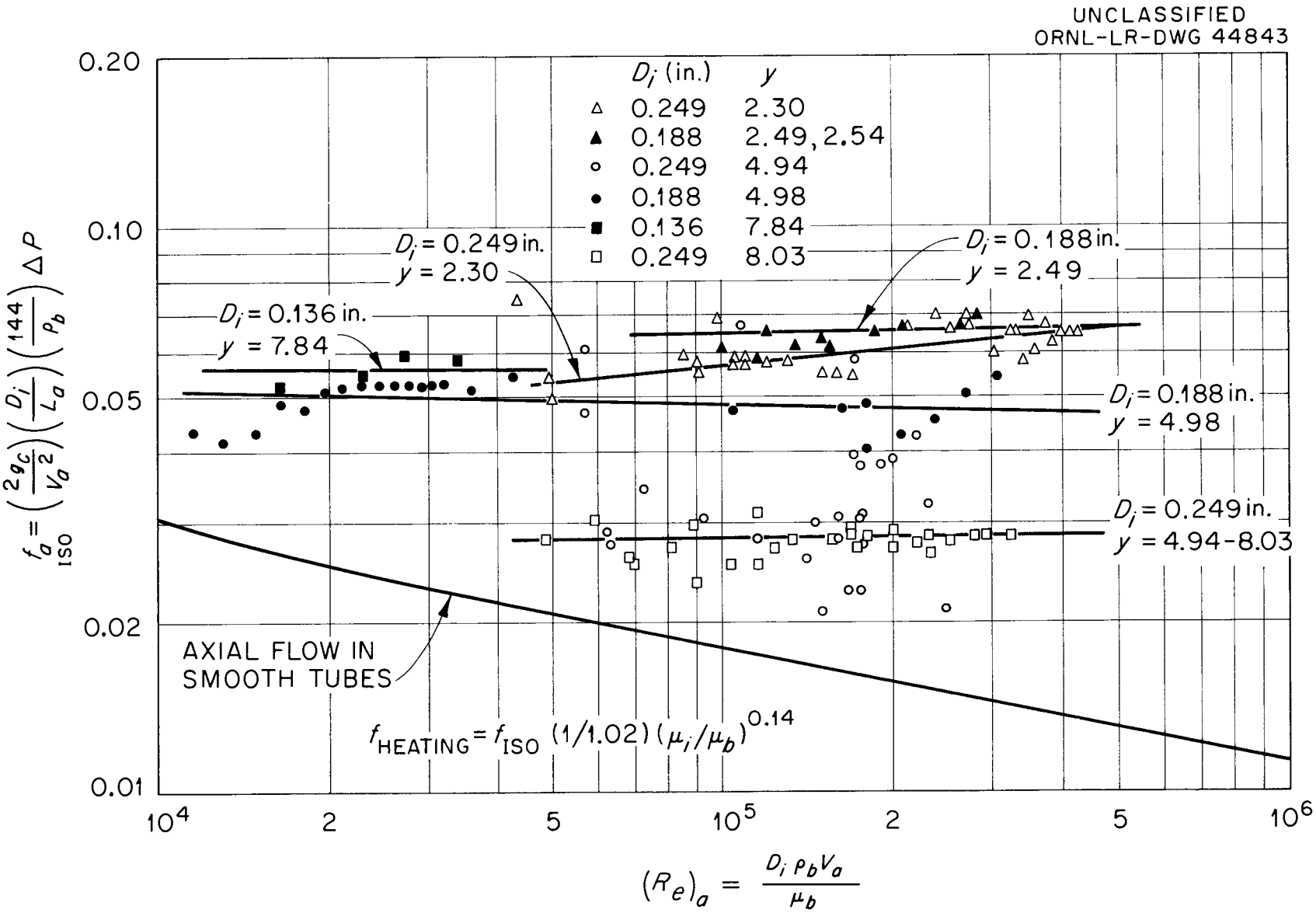

Fig. 20. Vortex-Flow Friction Factors Based on L_a, V_a, and D_i.

The true value of D_e seen by a swirl flow bounded by a tube and internal twisted tape is given by a more complicated function (see Appendix 1 for derivation and discussion), but the true D_e varies from the D_e of Eq. 49 by $< 1\%$ for $1.25 < y < \infty$. Eq. 49 was accordingly used for all calculations of D_e in this report.

The second type of friction factor which was calculated is based on D_e, V_{ri}, and L_{si}, the velocity and length being given by (see Appendix 1 for derivations):

$$V_{ri} = V_a \left[1 + \left(\frac{\pi}{2y} \right)^2 \right]^{1/2} \tag{33}$$

$$L_{si} = \frac{L_a}{2y} \left(4y^2 + \pi^2\right)^{1/2} . \tag{43}$$

This basis of calculation was motivated by the concept that the values of V and L characterizing the frictional pressure loss are those occurring at the flow-inner tube surface interface. The new "rotational" friction factor f_r is thus defined as:

$$f_r = \frac{D_e}{L_{si}} \frac{2g_c}{V_{ri}^2} \frac{144}{\rho_b} \Delta P . \tag{50}$$

Figure 21 is a plot of f_r vs $(Re)_r$ for the data of the present study. $(Re)_r$ is defined by:

$$(Re)_r = \frac{D_e \rho_b V_{ri}}{\mu_b} \tag{51}$$

The friction factors f_r follow approximately the axial-flow smooth-tube curve. The average deviation of experimental f_r values from the curve is $\pm 20.1\%$. However, at any Re, f_r still varies significantly with both D_i and y.

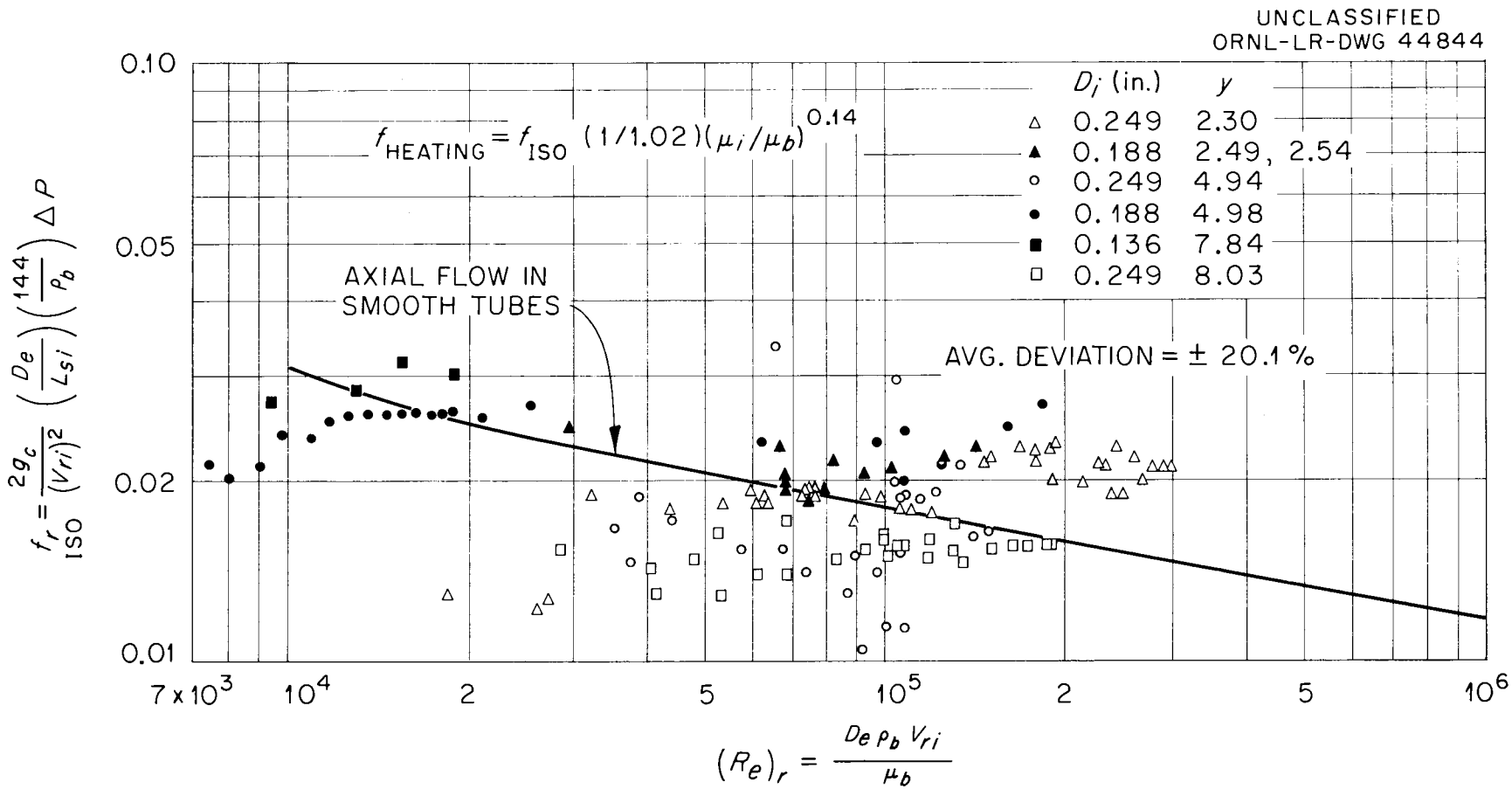

Fig. 21. Vortex-Flow Friction Factors Based on L_{si}, V_{ri}, and D_e.

Correction for the "excess variation" with D_i and y was made empirically, and the best over-all correlation of the twisted-tape vortex data was made in terms of the friction factor f_e, defined as:

$$f_e = \frac{D_i}{L_a} \frac{2g_c}{V_a^2} \frac{144}{\rho_b} \Delta P \, D_i^{1.2} \, y^{0.6} \left(\frac{\mu_b}{\mu_i}\right)^{0.18} \tag{52}$$

for both isothermal and heated nonboiling conditions. This friction factor is plotted in Fig. 22 vs the axial Reynolds number $(Re)_a$, with which it does not vary. The average variation of experimental f_e values from the best mean value of 0.00089 is ±12.3%. The axial friction factor f_a, defined by Eq. 48, may then be expressed by:

$$f_a = 0.00089 \, y^{-0.6} \, D_i^{-1.2} \left(\frac{\mu_i}{\mu_b}\right)^{0.18} \tag{53}$$

and the pressure drop across a twisted-tape vortex tube is given by:

$$\Delta P = 0.00089 \frac{V_a^2}{2g_c} \frac{L_a}{D_i} \frac{\rho_b}{144} D_i^{-1.2} \, y^{-0.6} \left(\frac{\mu_i}{\mu_b}\right)^{0.18} . \tag{54}$$

Equations 53 and 54, the recommended relations, should not be used for extrapolation to diameters and tape twist ratios beyond those of the present tests. Caution should also be exercised if the surface roughness is much different from that given in the text, since there are indications that swirl-flow f is quite sensitive to roughness. If an extrapolation must be made, it is probably best to make it according to Fig. 21, which should possess the greatest generality over very broad variable ranges.

B. Local Boiling Data

In Fig. 23, the ratio of local-boiling to isothermal friction factors is plotted against the dimensional group $\Delta t_{sat} / (\Delta t_{sub} \, P)$. This

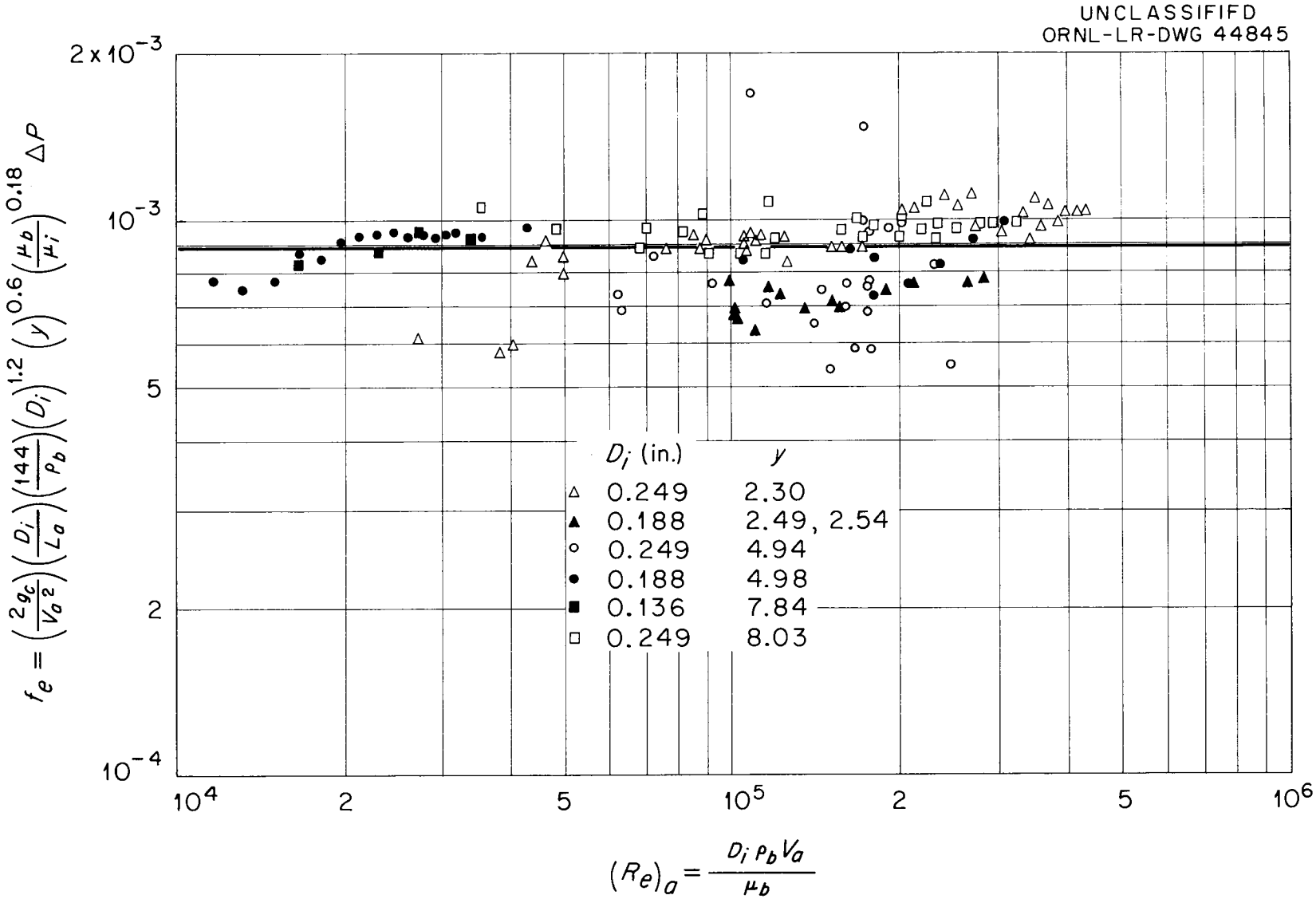

Fig. 22. Vortex-Flow Friction Factors Based on L_a, V_a, D_i, and an Empirical Correction for D_i and y.

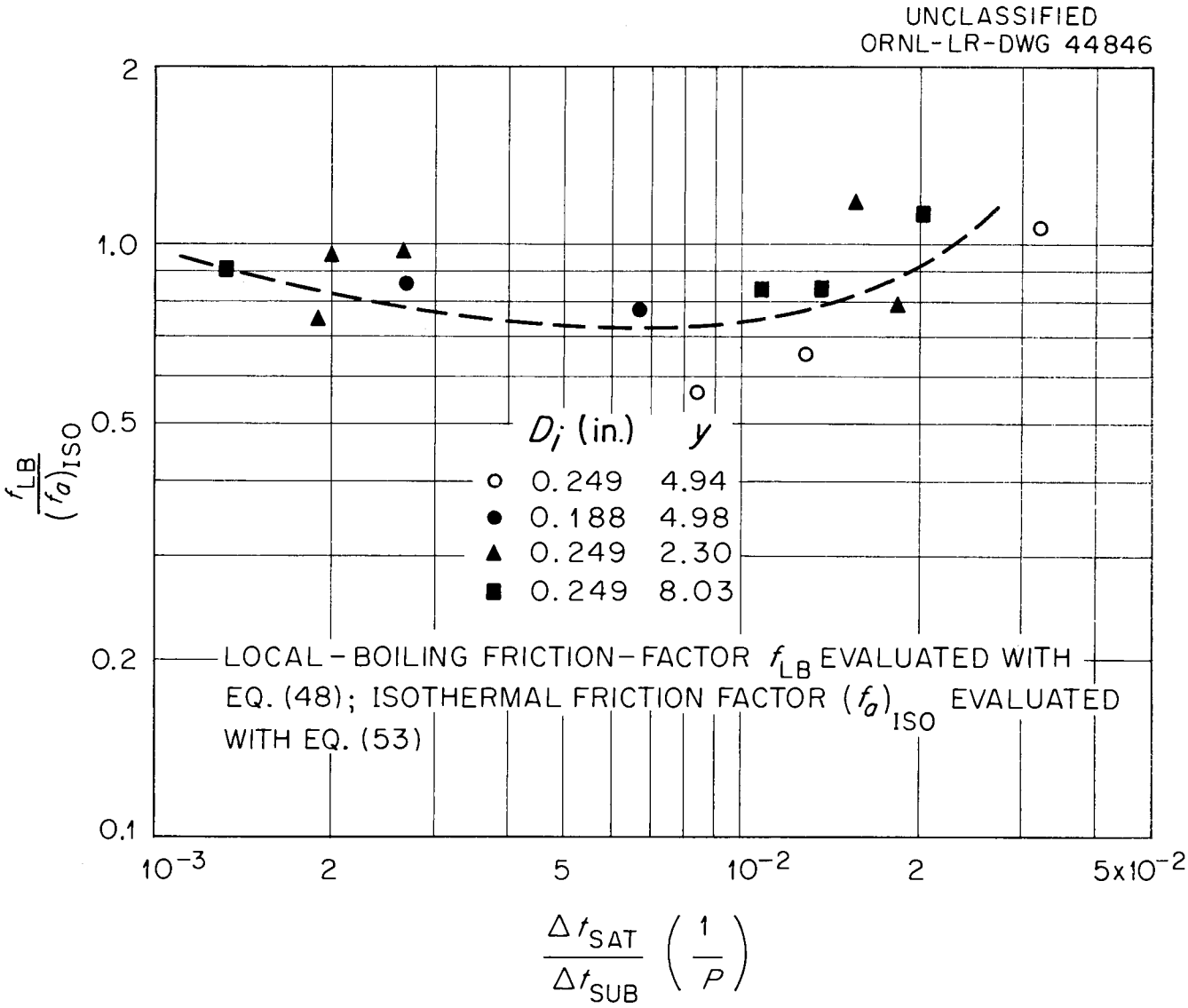

Fig. 23. Ratio of Local-Boiling to Isothermal Friction Factors for Vortex Tubes with Twisted Tapes.

group is a measure of the ratio of bubble-formation potential to bubble-collapse potential (both thermal and mechanical). The f ratio decreases initially, probably because of a decrease of wall viscosity at greater values of liquid-film superheat (Δt_{sat}), but finally increases when the bubble-formation rate is large enough to introduce a significant vapor volume into the coolant stream.

C. Inlet Pressure Loss

Establishment of a tangential flow component, as at the beginning of a tube containing a twisted tape, is accompanied by a decrease of pressure head. If the axial velocity is constant with radius and the twisted tape is very thin, the average pressure drop between planes a and b of Fig. 24-a is given* (neglecting friction losses) by:

$$\overline{\Delta P}_{a-b} = \overline{P}_a - \overline{P}_b = \frac{\pi^2 \rho V_a^2}{16 g_c y^2} . \tag{55}$$

If the tangential flow component is allowed to degenerate by kinetic loss mechanisms beyond the exit of the tube, the pressure drop $\overline{\Delta P}_{a-b}$ represents a permanent loss.

The swirl flow pattern gives rise to a radial pressure gradient, which may be expressed by the equation*:

$$\Delta P_{\mathbb{C}-R} = \frac{\pi^2 \rho V_a^2}{8 g_c y^2} \frac{R^2}{R_i^2} \tag{56}$$

if axial velocity does not vary with radius. The pressure at the tube wall is thus given by:

$$P_i = P_{\mathbb{C}} + \frac{\pi^2 \rho V_a^2}{8 g_c y^2} . \tag{57}$$

*See Appendix 1 for derivation.

UNCLASSIFIED
ORNL-LR-DWG 45123

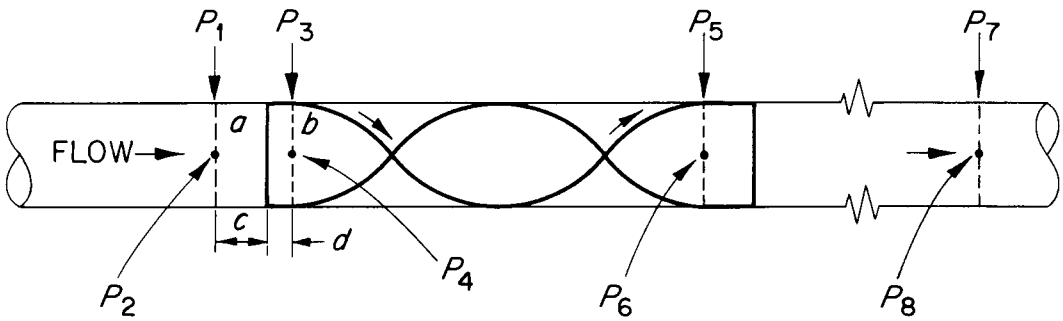

(a)

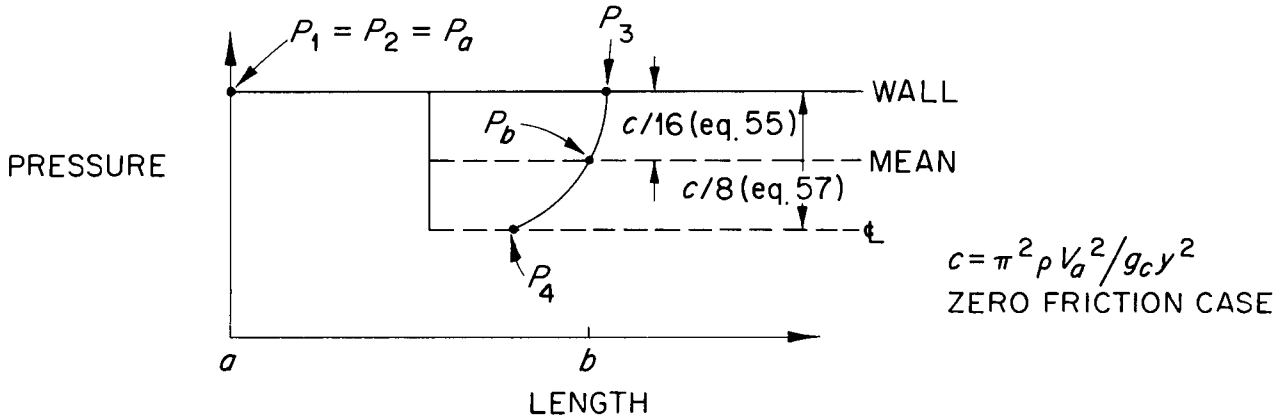

(b)

Fig. 24. Schematic of Entrance Pressure Variation in a Twisted-Tape Vortex Tube.

In Fig. 24-b, Eqs. 55 and 57 have been combined graphically. The curve $P_4 - P_b - P_3$, representing the radial pressure profile at station b, has been rotated 90 deg with respect to the vortex tube's cross section. As indicated by Fig. 24-b:

$$P_3 = P_1 \tag{58}$$

and

$$P_4 = P_2 - \frac{\pi^2 \rho V_a^2}{8 g_c y^2} \tag{59}$$

if frictional losses in the entrance are neglected. An independent derivation based on the Navier-Stokes equations gave identical results. The pressures P_5 and P_6 differ from P_3 and P_4, respectively, by the amount of frictional pressure loss along the tube. P_7 and P_8 are considered to be far enough removed from the tube exit that the flow is purely axial. P_7 equals P_8 and both differ from P_1 and P_2 by the sum of the pressure permanently lost in establishing the tangential velocity and the frictional losses between plane b and station $P_7 - P_8$.

The simplifying assumption that V_a is invariant with radius permitted ready solution of the hydrodynamic equations, but its validity is uncertain. For the case of compressed air entering an empty tube through tangential inlet nozzles, both Hartnett and Eckert[24] and Lay[25] found extremely nonuniform radial profiles of axial velocity, with sharp peaking near the tube wall. However, the conditions of these investigations were not very similar to those of the present study.

Some experiments have been conducted to check the prediction of Eq. 58. In these experiments, additional pressure taps enabled measurements to be taken of the frictional pressure loss gradients (at the wall) for both the axial flow and swirl-flow portions of the test section. These gradients were

used to correct the total measured difference $(P_1 - P_3)$ to a pressure difference exclusive of frictional losses, as follows:

$$(P_1 - P_3)_{nonfriction} = (P_1 - P_3)_{measured} - \left(\frac{dP}{dL}\right)_a c - \left(\frac{dP}{dL}\right)_s d \qquad (60)$$

where c and d are the axial lengths designated in Fig. 24-a. The results of this study are presented in Fig. 25, where the entrance loss is plotted vs axial velocity for $1.8 < y < \infty$. The data show that, actually, $P_3 \neq P_1$ and that $P_3 < P_1$. The pressure drop ΔP_e is nearly as large for straight (untwisted) tapes as for the most tightly twisted tapes, which would seem to point to eddy losses associated with the fluid striking the leading edge of the tape as the mechanism. Though the entrance ΔP is slightly greater for twisted tapes than for straight tapes, it does not appear to vary with y. The small amount by which ΔP_e for twisted tapes exceeds that for straight tapes is still a significant part of the predicted centerline-to-wall pressure rise for the more loosely twisted tapes.

Further experiments have been initiated with a view to obtaining more information regarding the radial and axial variations of pressure in a vortex tube. A composite Lucite twisted tape with internal static pressure channels has been fabricated.

V. Other Recent Swirl-Flow Heat-Transfer Studies

A. Boiling Water

The Reactor Engineering Division of Argonne National Laboratory conducted[26] some 52 burnout tests with water at 2000 psia flowing through a vertical 5/16-in. ID, 21 in. long 304 stainless steel tube. The electrically heated length was 18 in. ($L_h/D_i = 57.5$). The tubes were fitted with 0.005-in.-thick 304 stainless steel twisted tapes which fit the inner tube wall snugly

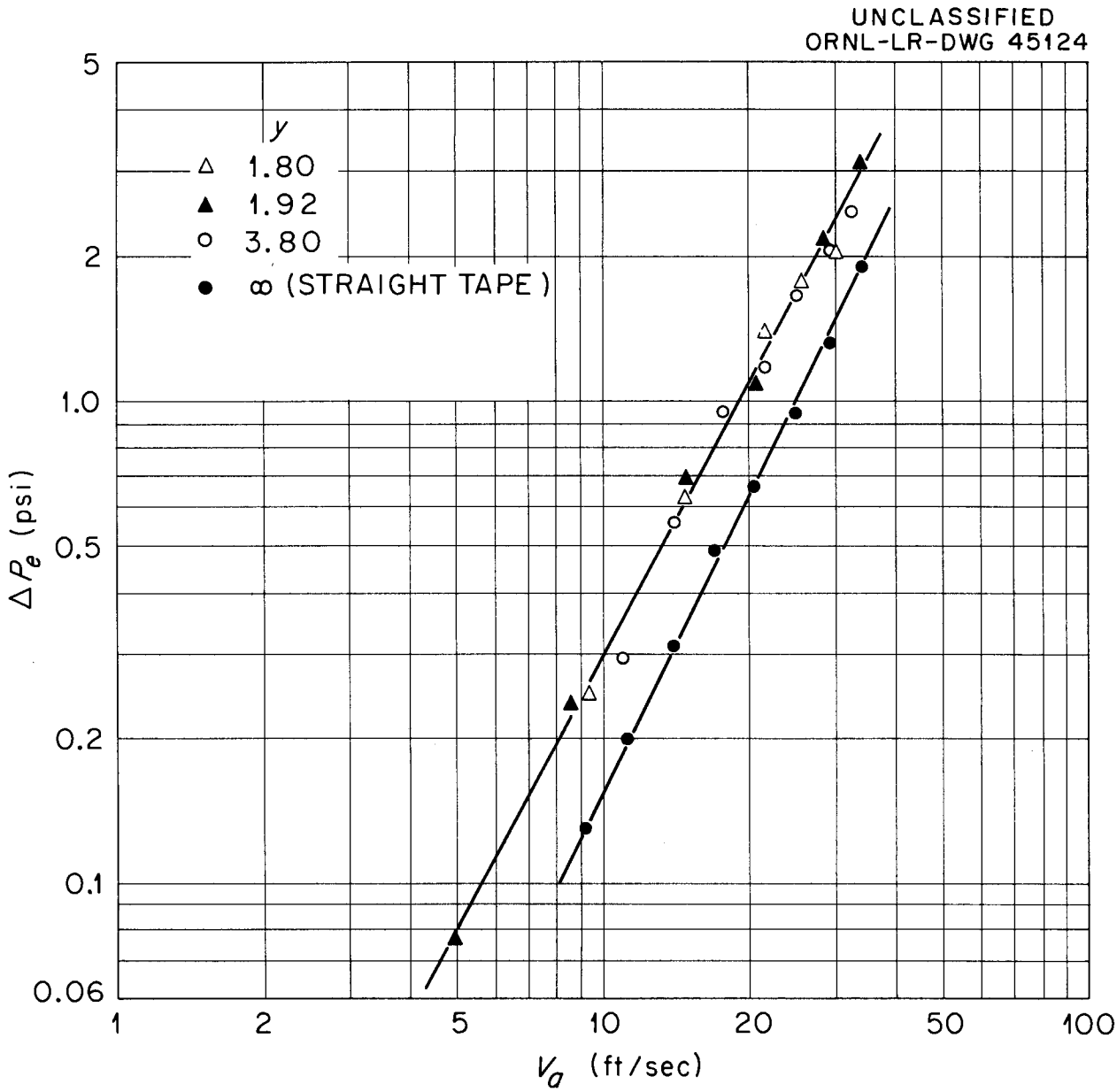

Fig. 25. Entrance Pressure Loss Measured at Wall for ¼-in. ID Tubes with Internal 0.015-in-Thick Twisted Tapes.

$\Delta P_e = P_1 - P_3$ of Fig. 24-a.

See errata

and were welded at the ends. The degree of tape twist corresponded to $y = 2.5$ and 5.0. An electronic burnout detector was used for test termination. Coolant flow rates were moderate ($0.5 \times 10^6 < G_a < 2.0 \times 10^6$), and net steam was generated in 44 of the tests.

Results of the ANL isothermal friction factor tests are shown in Fig. 26. The initial increase in f is considerably larger than is the incremental increase when y is changed from 5.0 to 2.5. Figure 26 is based on equivalent diameter, axial coolant velocity, and axial tube length for the twisted tape data.

Burnout data for $G_a^* \approx 10^6$ lb/hr·ft^2 are plotted in Fig. 27 vs over-all pumping power, calculated from the sum of frictional, momentum, and hydrostatic head losses. The points shown cover the entire experimental range of burnout data with net steam generation. The negative slopes of the curves may be explained as follows: since tube geometry and mass velocity are fixed, the pumping power can increase significantly only through an increase of steam quality, which decreases the mean coolant density. An increase of steam quality can also decrease ϕ_{bo} because of the greater probability of some of the vapor content of the coolant stream being locally smeared over the heated surface. In subcooled boiling burnout, of course, greater P_f is associated with higher velocities, and burnout heat flux increases with P_f.

Figure 27 indicates a maximum 2-1/2-fold improvement in burnout heat flux at constant pumping power. The ANL investigators concluded[26] that centrifugal forces are indeed effective in breaking up vapor films on heated surfaces and that such an action is the mechanism primarily responsible for the observed improvement.

* See note

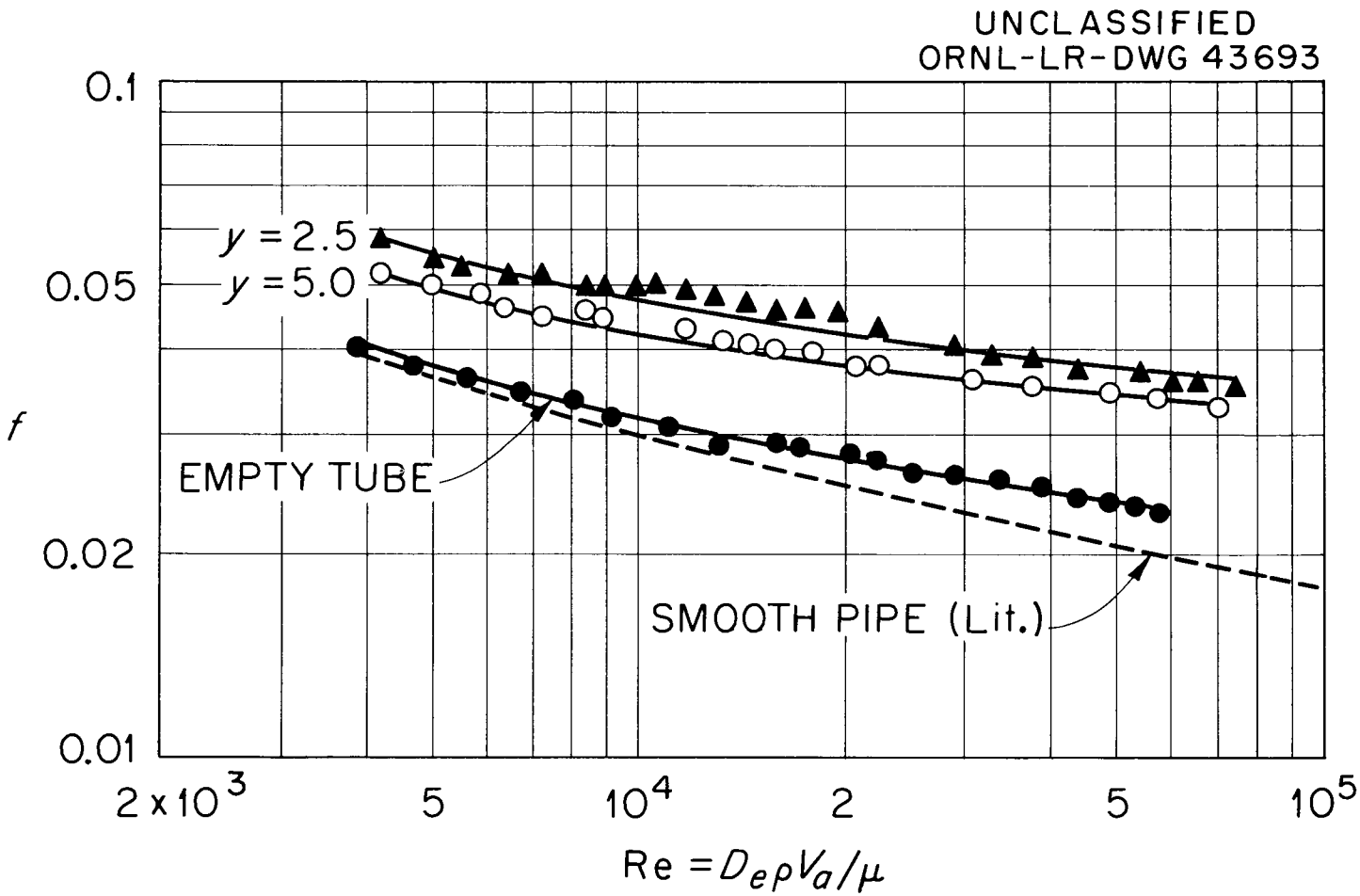

Fig. 26. ANL Twisted-Tape Isothermal Friction Factor Data.

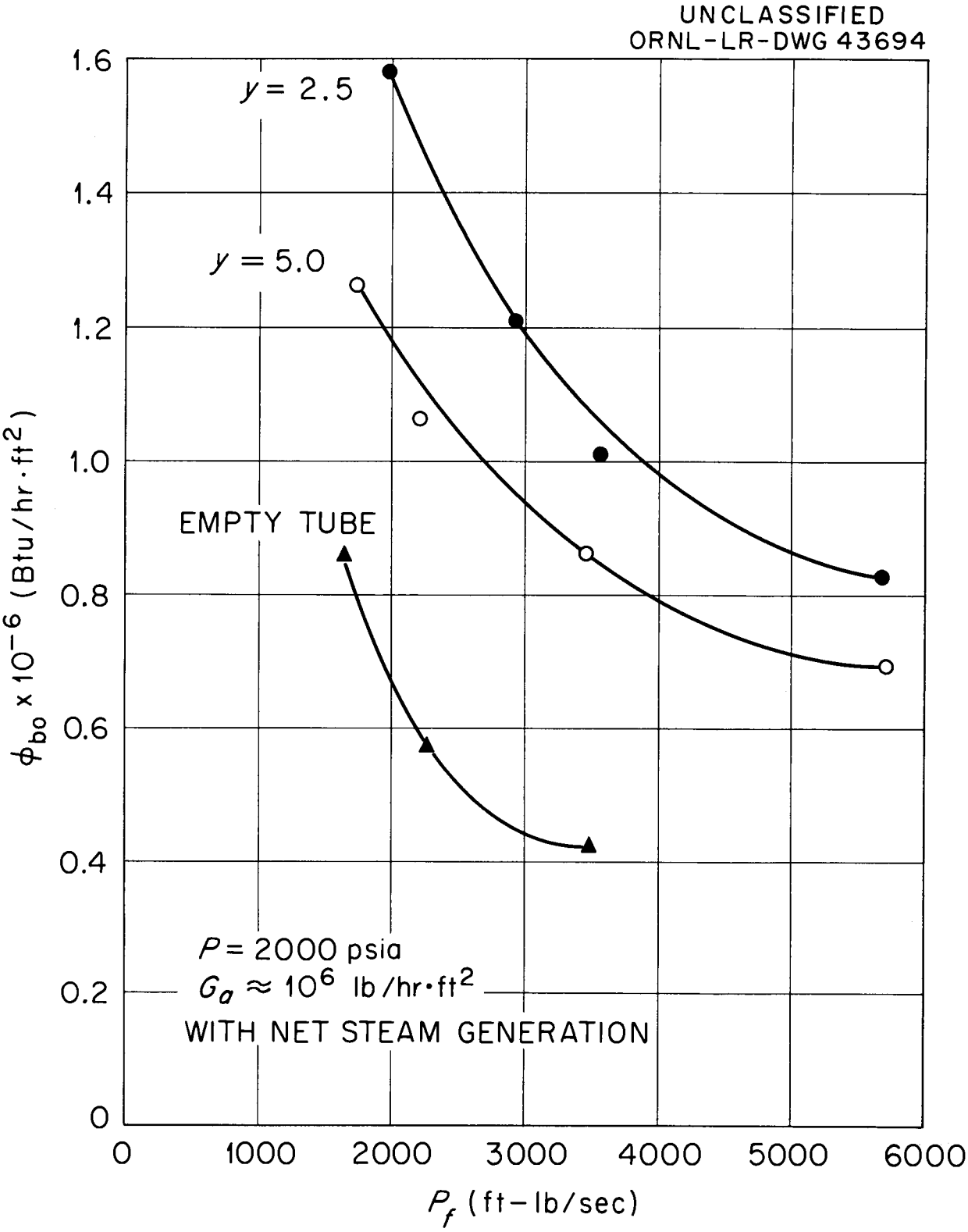

Fig. 27. Burnout Heat Flux vs Pumping Power from ANL Data.

B. Boiling Freon

At the Oak Ridge Gaseous Diffusion Plant, some tests have been recently conducted[27] with Freon-114 in natural circulation through vertical, straight 3/4-in.-ID unpolished copper tubes 3 ft long. Liquid entered the base of the steam-heated tube close to the saturation temperature, and the cold-leg liquid level was maintained 5 ft above the bottom of the test section. Operating pressure was approximately 110 psia.

For straight flow through an empty tube, the maximum values of heat flux and heat-transfer coefficient were approximately 41,000 Btu/hr·ft^2 and 2300 Btu/hr·ft^2·°F, respectively. These values were obtained at the peak of the ϕ (or h) vs Δt_f curve.

Insertion of twisted 2S or 3S aluminum tapes (0.040-in. thick, y = 2.35 and 4.00) caused ϕ_{max} to increase to 67,000 Btu/hr·ft^2 (63% increase), and h_{max} to become 3500 Btu/hr·ft^2·°F (52% increase). Almost identical results were obtained with coiled circular aluminum wires, 1/8-in. and 3/16-in. diameter, hugging the inner tube wall. The wire-coil pitch was 1.9 in. or 2.0 in., corresponding to a y range of 1.27 to 1.33 diameters/180-deg rotation. All inserts were friction fitted.

At Δt_f = 20°F, the ratio (by weight) of liquid to vapor at the tube exit, L/V, decreased from ~ 2.5 to ~ 0.25, illustrating the greatly increased fractional vaporization per pass in the swirl-flow case.

Swirl-flow h began diverging upward from the straight-flow line of h vs Δt_f at ~ 80% of $(\Delta t_f)_{crit.}$; similarly, ϕ divergence began at ~ 50% of $(\Delta t_f)_{crit.}$.

It is the writers' opinion that the coiled wires would be less advantageous than the twisted tapes if: (1) the wires were of smaller diameter,

(2) they were spaced on a very small pitch, or (3), if the heat transfer were in the nonboiling regime.

C. Heating Air

An extensive investigation of pressure drop and heat transfer for air flowing in baffled and packed tubes was carried out by R. Koch,[28] who used disks, rings, baffle plates, propellers, and ball and Raschig ring packings as well as twisted tapes. Koch's apparatus consisted of a 1.97-in.-ID straight intake section 98.4 in. long, followed by a 38.6 in. long brass test section of the same ID (L_h/D_i = 19.6). Clean, undehumidified air was blown through the test section, which was externally heated by atmospheric-pressure steam. The inner surface of the test section was "very smooth" and was the heat-transfer plane on which all heat-transfer coefficients were based. The twisted tapes were of soft aluminum, 0.039-in. thick, and fitted the inner tube wall tightly. The tape twist ratios used were 2.5, 4.25, and 11.0 diameters/180-deg twist.

Figure 28 shows smoothed curves representing the Reynolds number variation of Koch's isothermal friction factors. The original data points deviated negligibly from the curves. The quantities f and Re in Fig. 28 are based on internal tube diameter, axial velocity, and axial tube length. The line for the empty tube corresponds to Blasius' equation for fully developed turbulent flow in a smooth tube:

$$f_a = (100\ \mathrm{Re})^{-1/4} \tag{61}$$

with which Koch's straight-flow data agree very closely for $3500 < \mathrm{Re}_a < 80{,}000$. For y = 11.0, the friction factors are considerably greater than for the empty tube; but for more tightly twisted tapes, further increases in f are relatively small. The same behavior was noted in the ANL f,Re data (Fig. 26).

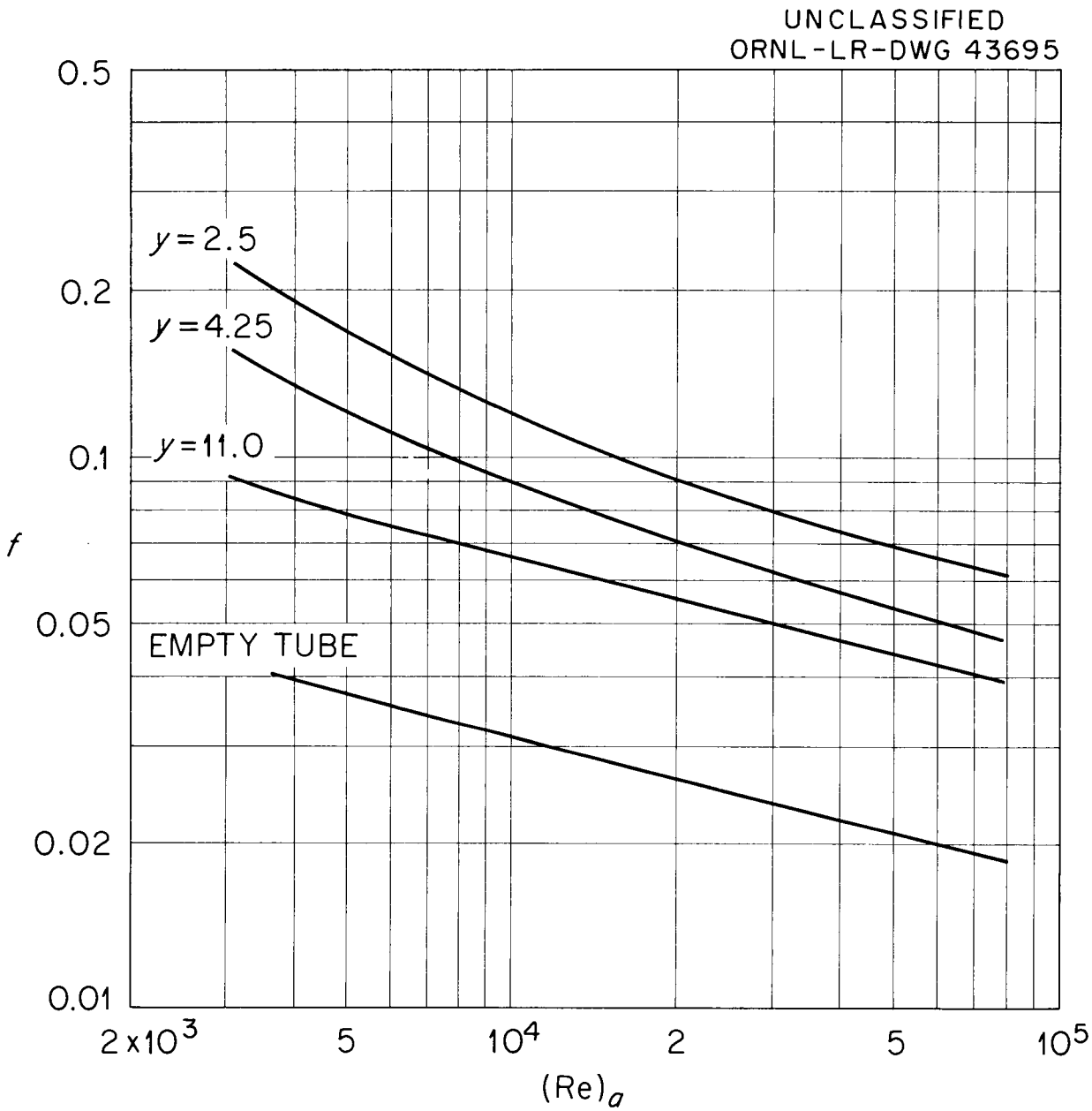

Fig. 28. Twisted-Tape Isothermal Friction Factors vs Reynolds Number. (Data of Koch).

Koch reasonably interpreted such a variation to mean that a large part of the observed pressure loss with twisted tapes is caused by friction on the tape surfaces. For the case of an untwisted strip ($y = \infty$) centrally located in a tube, pressure-loss data will closely agree with the empty-tube curve if D_e is used in f and Re. This agreement has been substantiated by measurements made during the present study. For Koch's loosely twisted tape for which $y = 11.0$, the f,Re curve based on D_e lies only ~ 15% above the empty-tube curve, which shows that use of D_e, which characterizes changes in geometry and surface drag for turbulent flow, accounts for nearly all the difference in the bottom two curves of Fig. 28. Since Fig. 28 is based on D_i, however, the separation between the two lower curves is large.

In Fig. 29, Koch's heat-transfer data are represented as mean Nusselt number (average for the tube, and including the thermal entrance effect) vs Reynolds number. As before, the smoothed curves are based on axial velocity and tube ID. The empty-tube line corresponds to Nusselt's equation for turbulent gas flow:

$$(Nu)_f = 0.0326\ (Re)_f^{0.786}\ (Pr)_f^{0.45}\ (D_i/L)^{0.054} \qquad (62)$$

with which Koch's straight-flow data agree very well for $4000 < Re_a < 68{,}000$.

The data of Fig. 29 are replotted in Fig. 30 as a referred Nusselt number; i.e., the ratio of the mean vortex-flow to axial-flow Nusselt number vs twist ratio with Reynolds number as a parameter. The influence of the thermal entrance effect has been eliminated from the Nusselt numbers in Fig. 30 by recalculation to values for fully developed flow with Eq. 25 of the original reference.[28] It is apparent that Nu enhancement increases with decreasing Re. It may also be inferred that for $y \geqq 20$, almost no heat-transfer improvement can be expected; and that at $y \approx 2$, little is to be gained from further (numerical)

* See errata

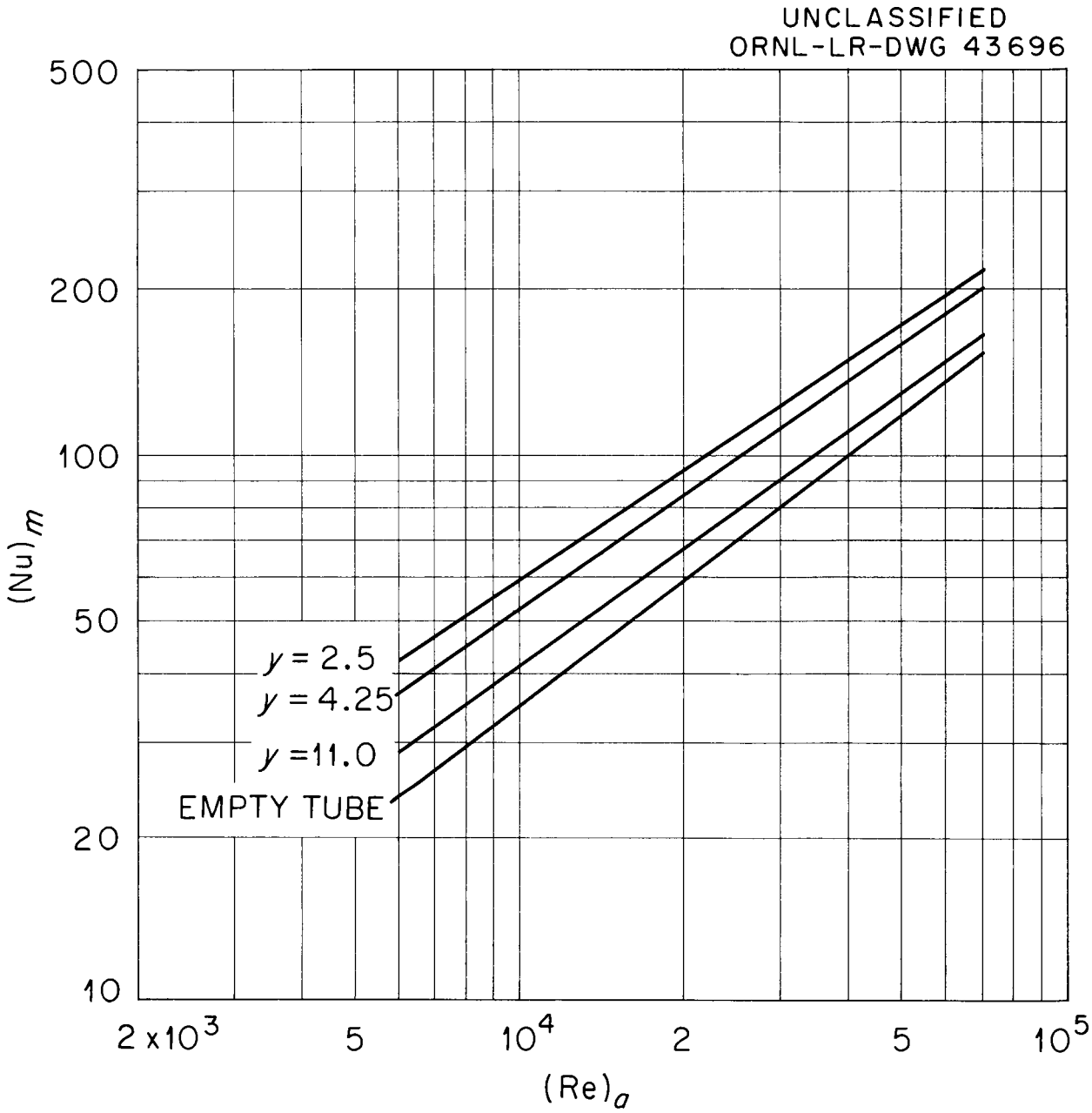

Fig. 29. Mean Nusselt Number vs Reynolds Number for Twisted Tapes. (Data of Koch).

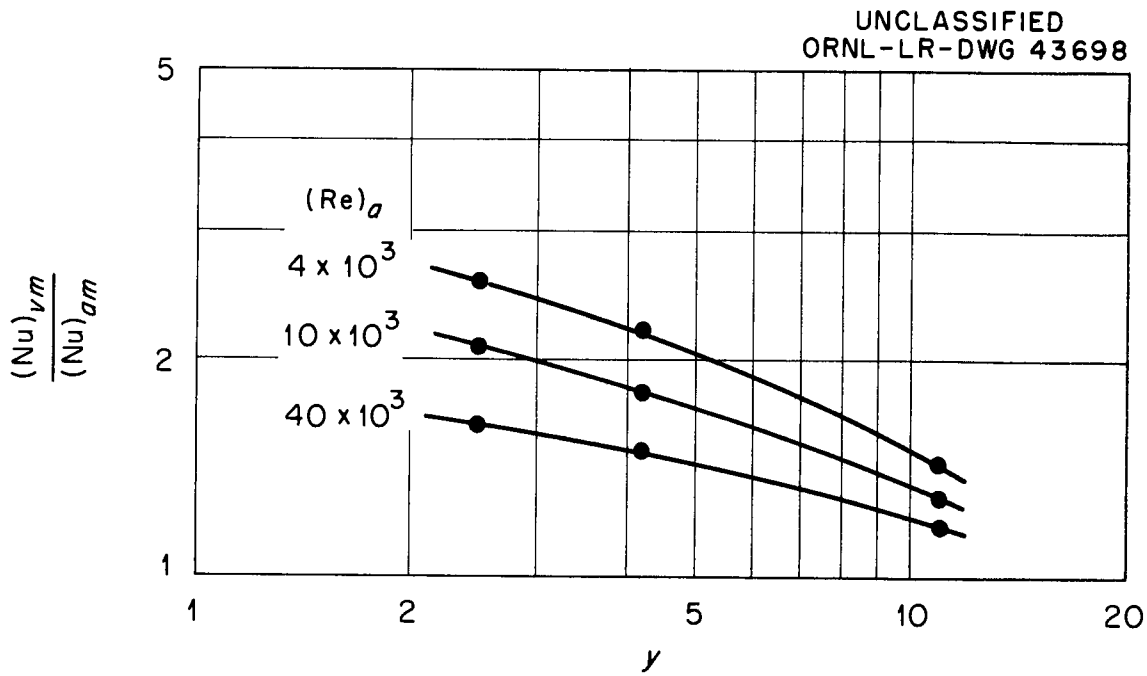

Fig. 30. Ratios of Mean Vortex-Flow Nusselt Number to Mean Axial-Flow Nusselt Number vs Tape Twist Ratio and Reynolds Number. (Data of Koch).

decreases in y.

The agreement of Koch's data for air as shown in Fig. 30 with the data of the present study for water (Fig. 3) is reasonably good. The chief divergence between the sets of data is that Koch's Nu ratio curves vary significantly with Re, whereas ours do not. In water, thermally caused radial density differences are not counteracted by opposing density differences arising from the radial pressure gradient. In air, however, as pointed out by Kreith and Margolis,[22] the fluid density at larger radial distances is increased by the radial pressure gradient, which reduces the free-convection driving force. When Fig. 30 is considered along these lines, the separation of curves according to Re becomes clear, since at higher axial Re, the gas compaction at the wall is increased because of the greater centrifugal forces generated. Accordingly, the Nu ratio decreases with increasing Re.

Koch further plotted $(Nu)_m$ vs f/f_o for an empty tube and for a tube with twisted tape inserts, where f and f_o are the friction factors with and without inserts, respectively, at equal Reynolds numbers. He was thus able to show that at a given pumping power, the turbulated tube gives Nu numbers up to 1-1/2-fold larger than an empty tube in which the velocity has been increased to give the same pumping power.

D. Heating Santowax Liquid

A series of 18 tests was conducted by R. L. Judd[29] with isopropylated Santowax* liquid in swirl flow through an electrically heated 0.48-in.-ID stainless steel tube 21.6 in. long (L_h/D_i = 45.0). Enameled twisted tapes for which y was 2.6, 5.0, and 7.3 were used as swirl generators; the tapes were slightly undersized, and a gap of 0.002 in. to 0.015 in. existed between tape edges and

*A product of the Monsanto Chemical Company.

the inner wall surface. The velocity range was 10 to 30 fps, and bulk coolant temperature was varied from 300 to 500°F.

The swirl-flow data were compared at constant Re and Pr with a correlation equation for straight-flow data taken with the same equipment; the Nu and Re were based on D_e. The comparison failed to show an improvement in Nu greater than ≈ 25%.

That Judd's data showed less improvement than those of Kreith and Margolis,[22] of Koch,[28] and of the present study may be traced in part to his use of undersized tapes. Similarly underdimensioned tapes were used by Evans and Sarjant;[30] and Koch, in comparing their data with his own, showed that the improvement in their Nusselt numbers was considerably smaller than that shown by his data. The ratio of wall gap to tube ID was ≈ 0.08 for the test sections of Evans and Sarjant, and for those of Judd, ≈ 0.03, or of the same magnitude.

E. Boiling Mercury

Soviet workers have heated mercury containing no wetting additives in an empty vertical carbon-steel tube and in the same tube after insertion of a "flat iron helix".[31] No details concerning the twisted strip are given. At ϕ = 9,240 Btu/hr·ft^2, it was estimated that helix insertion increased the fractional contact of the heating surface by the mercury from 12 – 20% to ≈ 70% because of the increased contact rate, or turbulence level. These Russian data are presented in Fig. 31 as h vs ϕ for the top of the tube, where boiling was fully developed; and for the bottom of the tube, where no boiling took place. In the boiling regime, h was increased ≈ 15-fold at a given heat flux, which indicates that swirl flow of nonwetting liquids may be particularly beneficial.

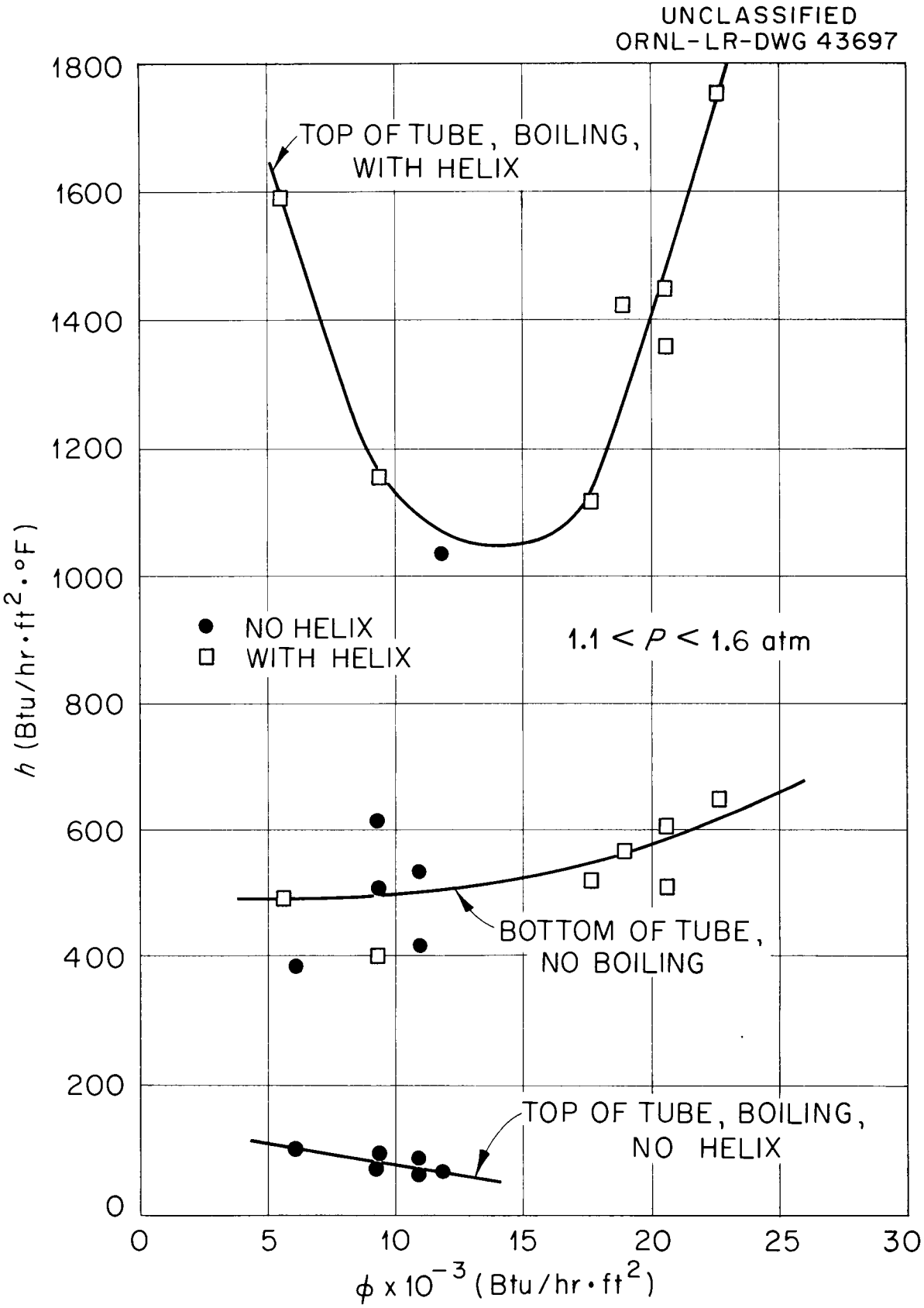

Fig. 31. Soviet Data for Heating Mercury.

F. Heating Air and Water

Kreith and Margolis[22] heated air and nonboiling water in a 0.53-in.-ID tube (very smooth) fitted with 0.032-in.-thick twisted tapes for which y was 2.58, 5.0, and 7.3 diameters/180-deg twist. The range of Reynolds number, based on D_e and V_a, was 10,000 to 100,000. The resulting ratios of vortex-flow to straight-flow Nusselt numbers at a given Reynolds number, each based on D_e and V_a, are summarized in Table 5.

Table 5. Twisted-Tape Heat-Transfer Data of Kreith and Margolis[22]

y	Fluid	$(Nu)_{vm}/(Nu)_{am}$
2.58	Water	3.05 – 3.75[a]
5.0, 7.3	"	1.77 – 2.35
2.58	Air	1.30 – 1.35
5.0, 7.3	"	1.15 – 1.20

[a]When the water was cooled rather than heated, the Nu ratio decreased by ~ 40% to the range 1.82 – 2.15.

The Nusselt number ratios of Table 5 would be ~ 10% larger if the Re and Nu were based on D_i rather than D_e.

VI. General Discussion

A. Relation of Heat Transfer to Friction in Swirl Flow

Many analogies between turbulent momentum and heat transfer have been proposed, and from most of those commonly used, the factor j/f may be extracted, where j is defined as:

$$j = (St)\ (Pr)^{2/3} = \left(\frac{h}{C_p\ G}\right)\left(\frac{C_p\ \mu}{k}\right)^{2/3} . \qquad (63)$$

The empirical Colburn modification of the original Prandtl-Taylor analogy for nonboiling heat transfer with axial flow states that $j/f = 1/2$, when f is defined by:

$$\Delta P = 4 f \frac{\rho V^2}{2 g_c} \left(\frac{L}{D} \right) . \tag{64}$$

Two of the final swirl-flow correlations — Eq. 14 for heat-transfer coefficient and Eq. 53 for friction factor — have been used to calculate swirl-flow nonboiling j/f ratios for 1/4-in.-ID tubes; the results are shown in Fig. 32 for $2 \times 10^4 < (Re)_a < 3 \times 10^5$. Physical properties were evaluated at t_b, and since the friction factors used in this report are four-fold larger than those calculated from Eq. 64, the j/f factors for both axial and swirl flow have been multiplied by four in order to place the straight-flow line at its usual level of 1/2. For $y = 5$ or 8, the vortex tube is clearly superior, on a j/f basis, to axial flow in the empty tube.

The j/f variation of Fig. 32 differs in two essential respects from the corresponding j/f plot of Kreith and Margolis[22] for fluid flow through a 0.53-in.-ID twisted-tape vortex tube. Their plot shows lines of positive slope, j/f increasing with both Reynolds number and with increased tightness of tape twist.

The difference in slope between the lines of our Fig. 32 and those of Kreith and Margolis' j/f plot can be explained on the basis of surface roughness, as depicted schematically in Fig. 33. The tubes used by Kreith and Margolis were described as "polished and very smooth", whereas those of the present study were not. As shown by curves 1 and 3 of Fig. 33, f decreases at a greater rate than j when Re increases for swirl flow through a smooth tube; the j/f ratio consequently increases. The inverse is true for the rougher surface case (curves 1 and 4), for which f remains essentially

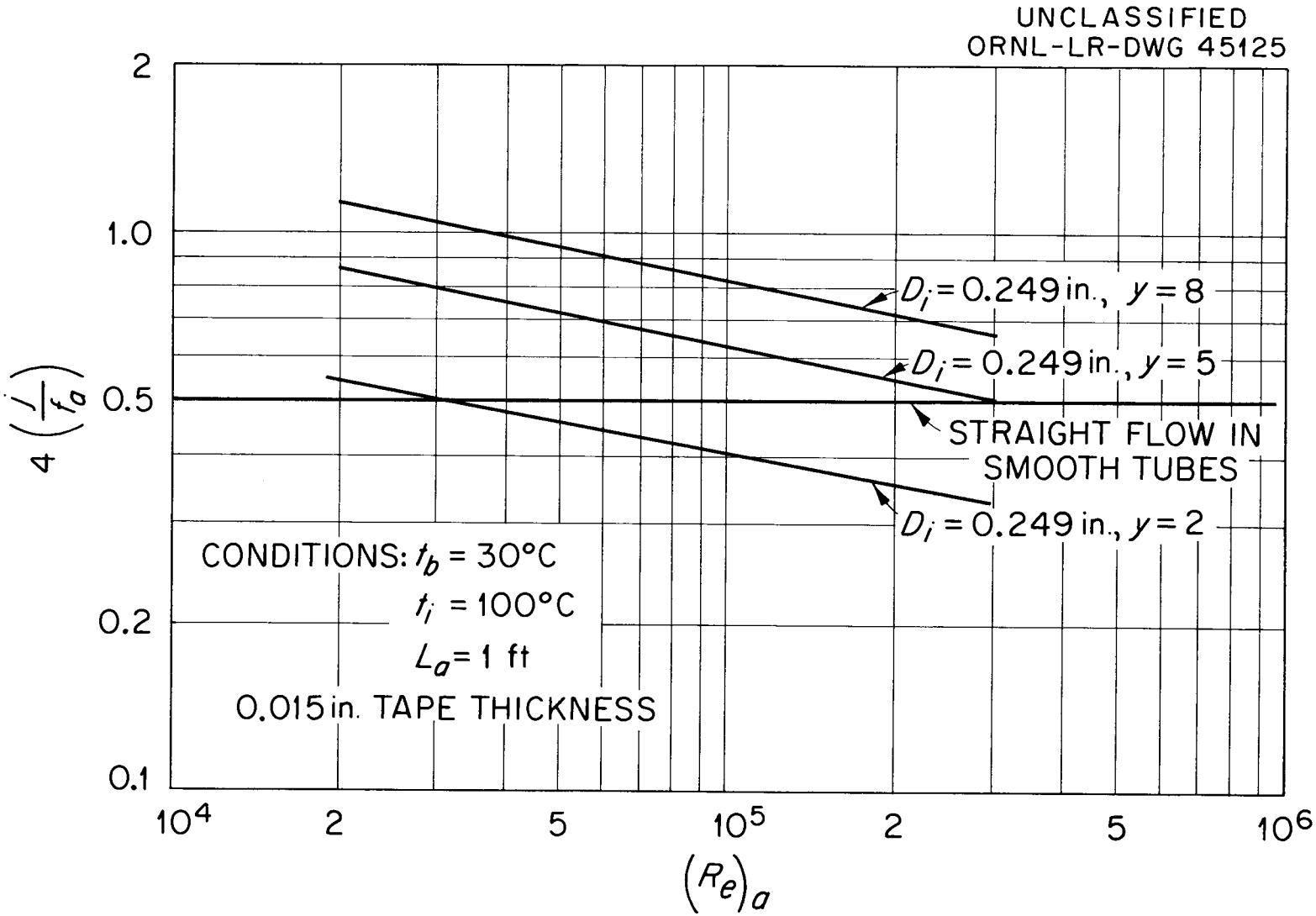

Fig. 32. $4\left(\frac{j}{f_a}\right)$ vs $(R_e)_a$ as Calculated from Final Correlations for Twisted-Tape Vortex Tubes.

UNCLASSIFIED
ORNL-LR-DWG 45126

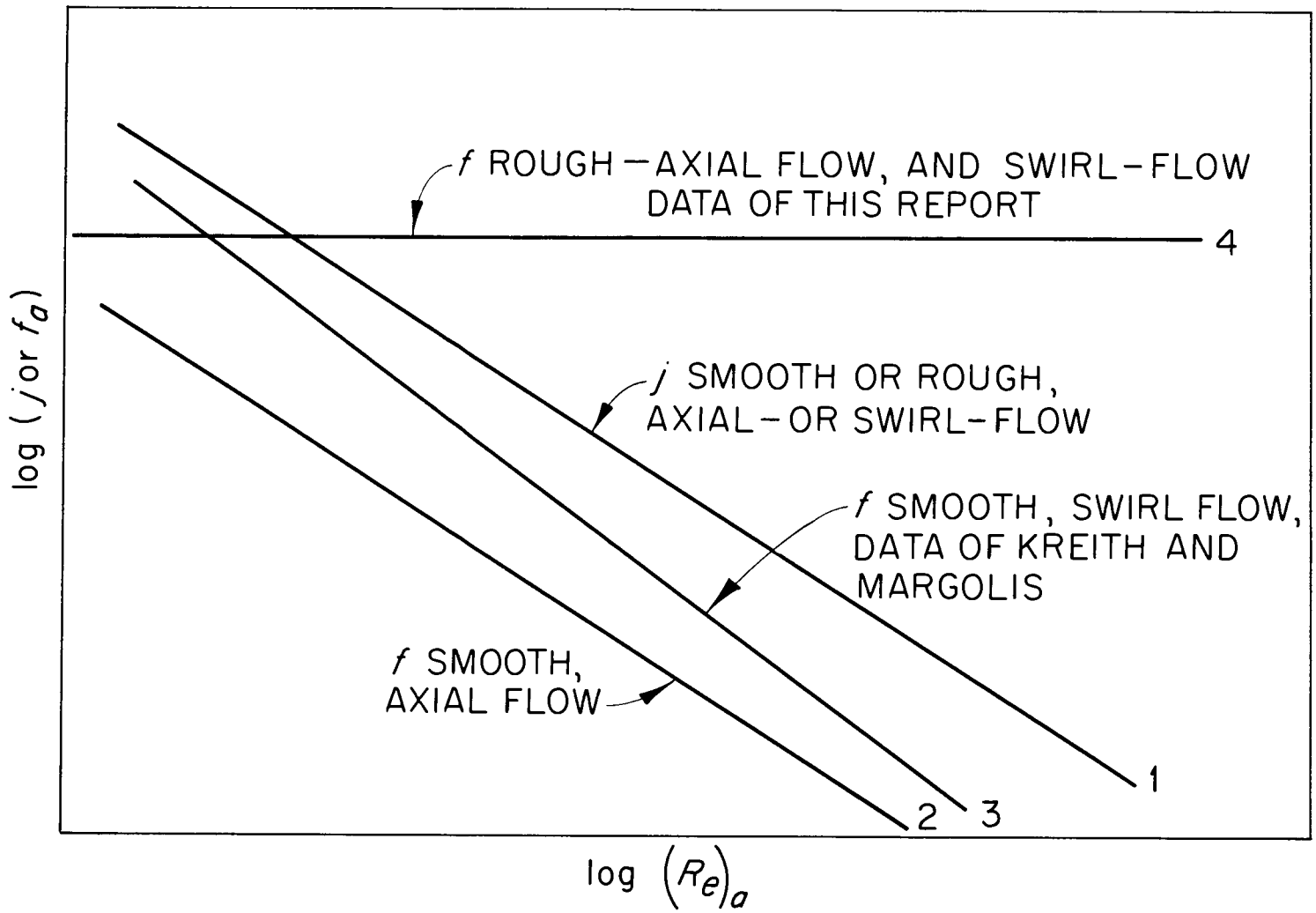

Fig. 33. Schematic Variation of j and of f with Reynolds Number for Turbulent Flow Over Smooth and Rough Surfaces.

constant while j still decreases with Re; j/f thus decreases with Re, as observed in Fig. 32.

The difference in the dependence of j/f on y (in our Fig. 32 as compared with the similar plot of Kreith and Margolis) may be explained in the same fashion: with a fixed flow rate, the "local wall Re", based on the resultant coolant velocity near the tube wall, increases with an increase in tape twist tightness. The j/f ratios for the rougher surfaces of the present study consequently decrease because of the relative variation of curves 1 and 4 of Fig. 33, as discussed above.

It thus appears that the dependence of j/f on other variables is sensitive to surface roughness; and that while j/f can be greater than the straight-flow value of 1/2 for either very smooth or relatively rough surfaces, its variation with Reynolds number and tape twist ratio can be changed by an alteration of the surface microstructure.

In Figs. 34 and 35, the j/f ratios corresponding to individual nonboiling tests have been ploted vs axial Reynolds number and heat flux, respectively. The trend of the points in Fig. 35 indicates a slight increase of j/f when heat flux is increased. This is not unexpected, since the equation used to calculate h (Eq. 14) does not explicitly include the effect of boundary-layer expansion, as Eq. 15 does in the term $\beta\Delta t_f$.

The relation between h and energy expenditure may be seen more clearly, perhaps, if comparisons are made of the dimensionless group $(j/f_a)/(Re)_a$:

$$\frac{j/f_a}{(Re)_a} = \left(\frac{h}{C_p\ \rho\ V_a}\right)\left(\frac{2\ L_a\ \rho\ V_a^2}{g_c\ D_i\ \Delta P}\right)\left(\frac{\mu}{D_i\ \rho\ V_a}\right) \tag{65}$$

which reduces to:

$$\frac{j/f_a}{(Re)_a} = \frac{h}{\Delta P}\ \frac{2\ L_a}{g_c\ D_i^2}\ \frac{\mu}{\rho\ C_p} \tag{66}$$

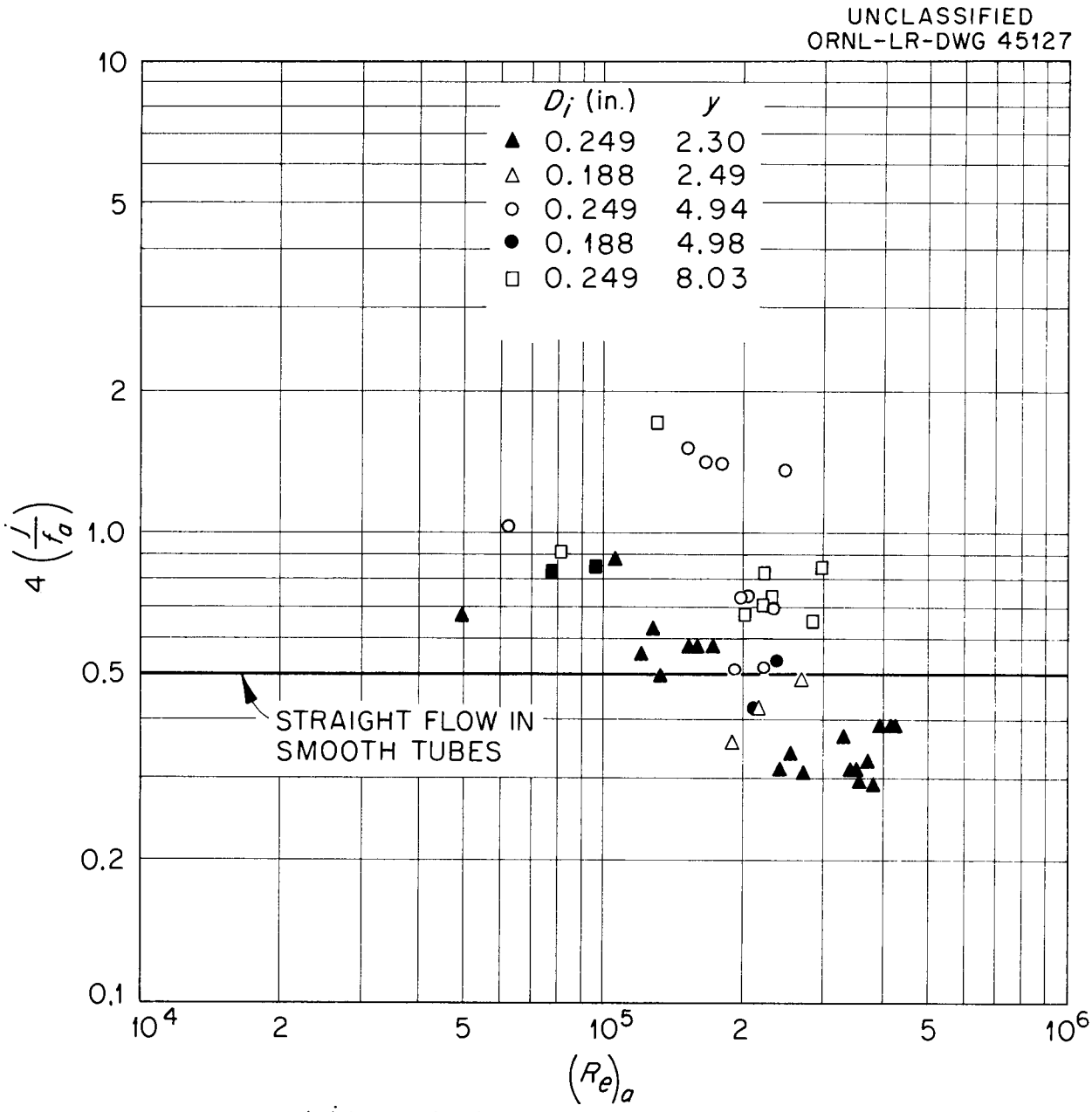

Fig. 34. $4\left(\frac{j}{f_a}\right)$ vs $(R_e)_a$ Based on Individual Vortex-Tube Data Points.

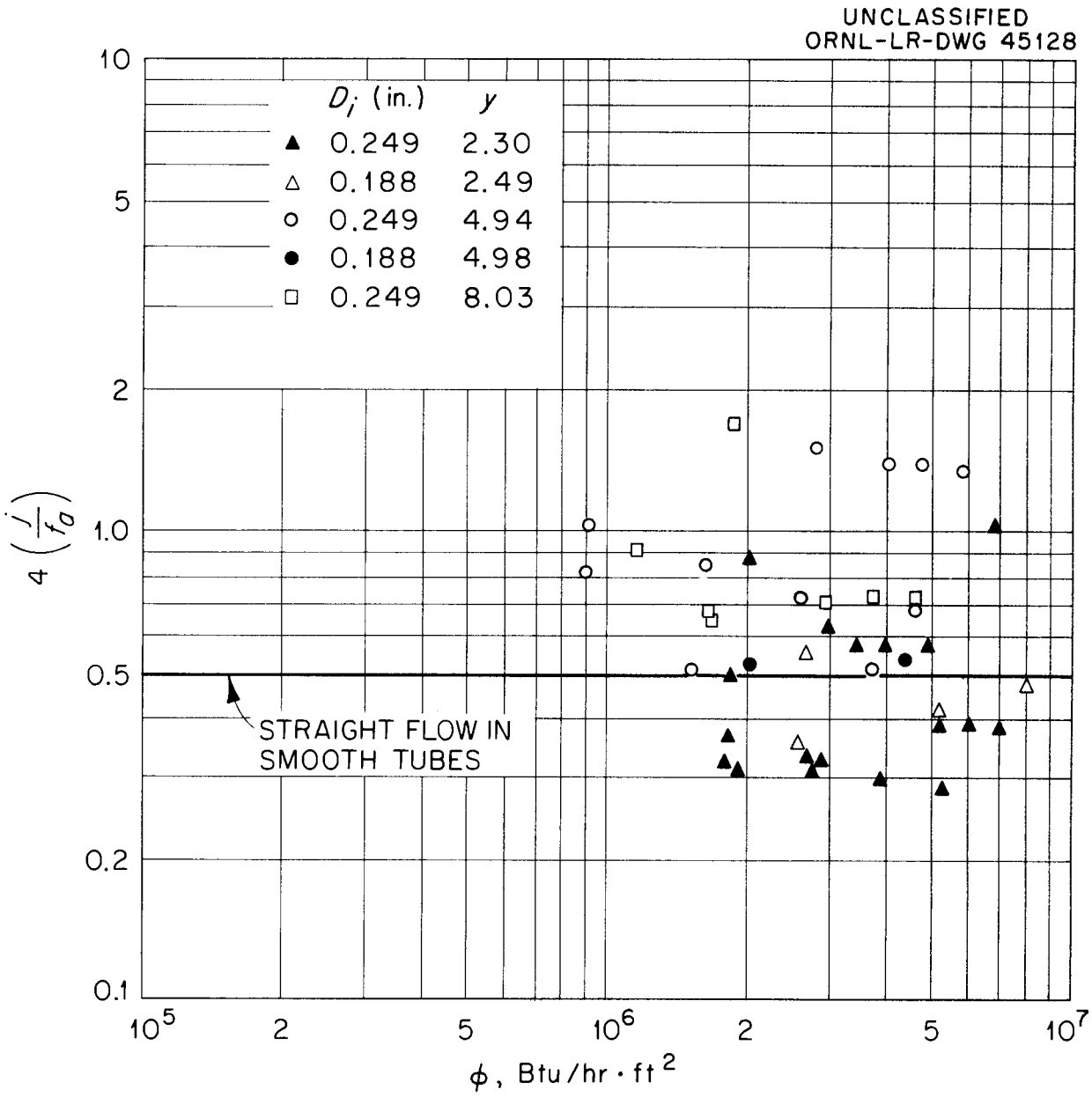

Fig. 35. $4\left(\frac{j}{f_a}\right)$ vs ϕ Based on Individual Vortex-Tube Data Points.

and gives the relative heat-transfer coefficient per unit frictional pressure drop for the same fluid flowing at the same bulk temperature through tubes of equal dimensions.

The group $(j/f_a)/(Re)_a^2$ similarly represents the relative heat-transfer coefficient per unit frictional pumping power, as may be seen when the group is arranged as follows:

$$\frac{j/f_a}{(Re)_a^2} = \frac{h}{\Delta P\ V_a\ (\pi\ D_i^2/4)}\ \frac{\pi\ L_a}{2\ g_c\ D_i}\ \frac{\mu^2}{C_p\ \rho^2}\ . \tag{67}$$

Figure 36 shows a replot of Fig. 32 both as $(j/f_a)/(Re)_a$ vs $(Re)_a$ and as $(j/f_a)/(Re)_a^2$ vs $(Re)_a$. On either a unit pressure drop or a unit pumping power basis, the nonboiling convective heat-transfer coefficient for the vortex tubes is as much as two-fold larger than for axial flow.

The criteria defined by Eqs. 66 and 67 were also used by Smith and Epstein[32] for comparing the relative heat-transfer efficiencies of pipes of different surface roughness. Their study substantiated the prior belief that the smoothest surface is the most efficient (as defined by Eqs. 66 and 67).

B. Swirl-Flow Advantages and Potential Applications

Since swirl flow is inherently associated with a concave cylindrical coolant boundary, it may be well to first consider the general advantages of tubular nuclear fuel elements relative to flat, or slightly curved, plate elements; these have been discussed in part by Cushman & Cunningham[33] and Maxwell[34] and may be stated as follows:

(a) Tubes give greater structural strength and rigidity, especially when they are fabricated into bundles. Conversely, for a given rigidity thinner gage material can be used.

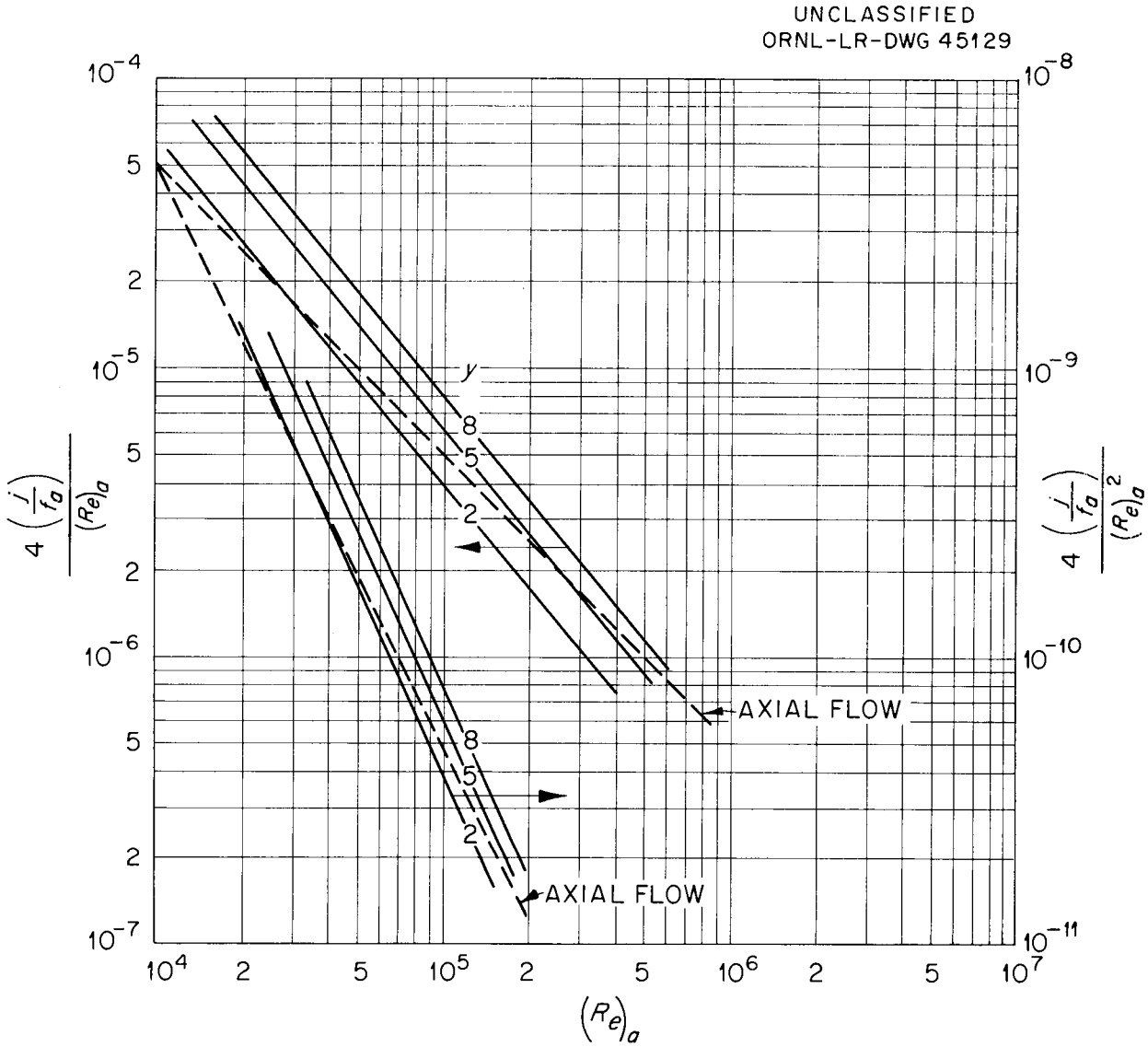

Fig. 36. Heat Transfer Coefficient per Unit Pressure Drop and per Unit Frictional Pumping Power for 1/4-in. ID Tubes.

(b) Tubes cooled externally as well as internally can give a greater heat-transfer surface area per unit volume than all but the tightest plate matrices. In addition, all of the fuel element surface in the active region which is exposed to coolant flow is heat-transfer surface, since the side plates commonly used with plate fuel elements are not needed.

(c) Pressure differentials between the coolant streams inside two adjacent tubes cannot cause the tubes to touch since any internal force tending to cause displacement of a tube acts radially in all directions. Differential pressure between adjacent external flow regions is equalized by transverse coolant flow between the tubes. These considerations point to the further advantage of smaller engineering hot channel factors, since the nominal design geometry can be better assured.

A comparison[33] between existing MTR curved-plate fuel elements and a tubular element design* showed that, on a basis of constant coolant mass flow rate,

$$\frac{(q/\Delta t_f)_{tubes}}{(q/\Delta t_f)_{plates}} = 1.44$$

i.e., the tubular elements would allow a 44% increase in power level for a constant film temperature difference.

Several methods of fabricating tubular elements into core bundles cooled both internally and externally have been investigated.[33] These include tubes with spot-welded flared and fluted ends, terminal element spacing by means of smaller diameter tubing, and wire-mounted tubes (cross wires or bands passing

*Tubes of 1/4-in. OD with 0.030-in. walls on 0.290-in. pitch, cooled on both sides by axial water flow.

laterally through slots cut in the ends of each tube).

Additional specific advantages accruing from inclusion of a twisted-tape swirl generator in a tubular fuel element for a water-cooled reactor include the following:

(d) Still greater structural rigidity.

(e) Significantly enhanced heat-transfer rates at constant pressure drop or pumping power – both below and at burnout.

(f) No large decrease in ϕ_{bo} experienced because of net steam generation. Burnout due to a local liquid deficiency is not possible short of total evaporation.

(g) A smaller incremental pressure drop when net steam is generated because of the existence of a favorable annular two-phase flow regime.

(h) Flow separation from the surface of an axially warped fuel element suppressed by the radial coolant forces.

(i) Operation at a lower pressure level allowable because of the lack of dependence of swirl-flow burnout on pressure and degree of subcooling. For the same reason, a loss of coolant pressure would be less serious.

(j) The L/D ratio required for establishment of a fully developed swirl-flow boundary layer is much smaller than with axial flow; Fraser's visual observations of flow behavior[23] support this contention.

All reactors would not benefit equally from the advantages listed, since some of the heat-transfer aspects would be more important in a specific design than others.

Tube dimensions the same as those used in the MTR comparison (footnote, p 80) correspond to a specific surface area (if both sides are cooled) of 216 ft^2/ft^3. A moderate operating heat flux of 5×10^6 $Btu/hr \cdot ft^2$ for each surface would yield a power density of 3/6 Mw/ft^3. The performance of twisted-tape vortex-tube fuel elements might be increased still more, on a burnout basis, by roughening (e.g., threading) the exterior surfaces, as indicated by recent studies of the influence of surface macro-roughness on burnout heat flux by Durant and Mirshak.[35]

Promising potential applications of swirl-flow heat transfer other than for heat removal in nuclear reactors include the cooling of particle accelerator targets, high-performance electromagnets, and rocket nozzle throats. Swirl-flow of coolant gas through the steam generator of a gas-cooled reactor might also be beneficial, since the size of the steam generator is highly dependent on the magnitude of the relatively small gas-film heat-transfer coefficient.

C. Recommendations for Further Investigation

Since swirl-flow friction factors appear to be strongly dependent on many variables, it would be desirable to have more pressure-drop data, preferably from tests for which surface roughness is either controlled or accurately known.

A better delineation of the burnout subcooling-independence mechanism, and more data on burnout with net steam generation and with inlet-generator vortex tubes of large L/D ratio would be most helpful in filling out the areas for which little information presently exists.

* See errata

ACKNOWLEDGEMENTS

The authors wish to express their appreciation to J. Lones, D. H. Wallace, and T. N. Jones for their able and enthusiastic assistance as project technicians; to J. H. Erwin, ORNL Metallurgy Division, for his rapid delivery of the test sections; to W. D. Powers for the derivation of Eqs. 102 and 106; to W. C. Colwell's Graphic Arts section for their skillful preparation of the figures, and to Dolores Eden for her conscientious typing of the manuscript.

LITERATURE CITED

1. W. R. Gambill and N. D. Greene, "Boiling Burnout with Water in Vortex Flow," Chem. Engrg. Prog. 54, 68-76 (October 1958).

2. F. Kreith and M. Summerfield, Investigation of Heat Transfer at High Heat-Flux Densities: Experimental Study with Water of Friction Drop and Forced Convection with and without Surface Boiling in Tubes, Prog. Rep. No. 4-68, Jet Propulsion Lab., Calif. Inst. of Tech., Pasadena, Calif. (April 2, 1948).

3. W. R. Gambill, Electrical Resistivity Data for Heat-Transfer Test-Section Metals, ORNL CF 59-4-89 (April 15, 1959).

4. E. R. G. Eckert and R. M. Drake, Jr., Heat and Mass Transfer, p 496-498, McGraw-Hill Book Co., New York, 1959.

5. Ibid., p 235-236.

6. R. B. Bird et al., Notes on Transport Phenomena, p 192-194, John Wiley and Sons, Inc., New York, 1958.

7. A. Acrivos, "Combined Laminar Free- and Forced-Convection Heat Transfer in External Flows," AIChE Journal 4, 285-289 (September 1958).

8. S. Ostrach and W. H. Braun, Natural Convection Inside a Flat Rotating Container, NACA-TN-4323 (September 1958).

9. N. E. Dorsey, Properties of Ordinary Water-Substance, pp 231, 592, Reinhold Publishing Co., New York, 1940.

10. W. H. Jens and P. A. Lottes, Analysis of Heat Transfer, Burnout, Pressure Drop and Density Data for High-Pressure Water, ANL-4627 (May 1, 1951).

11. A. Cicchitti, M. Silvestri, G. Soldaini, and R. Zavattarelli, "A Critical Survey of the Literature on Burnout Studies with Wet Steam," Energia Nucleare 6, No. 10, 637-660 (1959).

12. G. Bertolotti, A. Cicchitti, S. Finzi, M. Silvestri, G. Soldaini, and R. Zavattarelli, A Facility Used for Wet Steam Cooling Experiments: Pressure Drop, Heat Transfer, and Burnout, CISE Report No. 64 (April 15, 1959); Energia Nucleare 6, No. 7, 458-471 (1959).

13. W. H. Lowdermilk and W. F. Weiland, Some Measurements of Boiling Burnout, NACA-RM-E54K10 (Feb. 23, 1955).

14. W. H. Lowdermilk, C. D. Lanzo, and B. L. Siegel, Investigation of Boiling Burnout and Flow Stability for Water Flowing in Tubes, NACA-TN-4382 (September 1958).

15. J. A. Clark and W. M. Rohsenow, "Local Boiling Heat Transfer to Water at Low Reynolds Numbers and High Pressures," Trans. ASME 76, 553-562 (May 1954).

16. F. C. Gunther, "Photographic Study of Surface-Boiling Heat Transfer to Water with Forced Convection," Trans. ASME 73, 115-123 (February 1951).

17. L. Bernath, A Theory of Local Boiling Burnout and its Application to Existing Data, Preprint No. 110, Third National Heat Transfer Conference, ASME-AIChE, Storrs, Conn. (August 1959).

18. L. Bernath, in Discussion of the paper "Investigation of Burnout Heat Flux in Rectangular Channels at 2000 psia," by H. S. Jacket, J. D. Roarty, and J. E. Zerbe, Trans. ASME, p 401 (February 1958).

19. R. W. Bowring, Atomic Energy Research Establishment, Reactor Division, Harwell, England, private communication, June 29, 1959.

20. N. Zuber and M. Tribus, Further Remarks on the Stability of Boiling Heat Transfer, Dept. of Engrg., Univ. of Calif., Rep. 58-5 (January 1958).

21. C. P. Costello, Aspects of Local Boiling Effects on Density and Pressure Drop, Paper No. 59-HT-18, Third National Heat Transfer Conference, ASME-AIChE, Storrs, Conn. (August 1959).

22. F. Kreith and D. Margolis, "Heat Transfer and Friction in Turbulent Vortex Flow," Appl. Sci. Res., Section A, 8, 457-473 (1959).

23. J. P. Fraser, Reactor Fuel Element Matrices with Strong Secondary Flows, KAPL-M-S3G-RES-62 (April 15, 1959).

24. J. P. Hartnett and E. R. G. Eckert, "Experimental Study of the Velocity and Temperature Distribution in a High-Velocity Vortex-Type Flow," Trans. ASME, 751-758 (May 1957).

25. J. E. Lay, "An Experimental and Analytical Study of Vortex-Flow Temperature Separation by Superposition of Spiral and Axial Flows, Part 1," J. of Heat Transfer, 202-212 (August 1959).

26. R. Viskanta, internal ANL memorandum, Sept. 30, 1958; received from J. F. Marchaterre (ANL), private communication, May 26, 1959.

27. C. F. Allen, R. L. Higgins, and J. W. Michel, ORGDP, private communication, Aug. 27, 1959.

28. R. Koch, "Pressure Loss and Heat Transfer for Turbulent Flow," VDI-Forschungsheft, Series B, 24, No. 469, 1-44 (1958).

29. R. L. Judd, Canadian General Electric Co., Ltd., private communication, Oct. 27, 1959.

30. J. Evans and R. J. Sarjant, "Heat Transfer and Turbulence in Gases Flowing Inside Tubes," J. Inst. Fuel 24, 216-227 (1951).

31. S. S. Kutateladze et al., p 104-105 of Ch. 10 ("Heat Exchange During Boiling") of Liquid Metal Heat Transfer Media, Supplement No. 2 of the Soviet J. of Atomic Energy. Also, A. N. Loshkin and P. I. Krol, "Characteristics of Mercury Boiling in the Tubes of a Mercury-Vapor Generator," Russ. J. of Tech. Physics 8, No. 21 (1938) (tr-NDA-28, Reactor Heat Transfer Progress No. 10, July 10, 1956).

32. J. W. Smith and N. Epstein, "Effect of Wall Roughness of Convective Heat Transfer in Commercial Pipes," AIChE Journal 3, No. 2, 242-248 (1957).

33. R. A. Cushman and W. W. Cunningham, "Tubular vs Plate Fuel Elements: Heat Transfer and Flow Analysis," 1956 Reactor Heat Transfer Conference Reprints, Book 1 [TID-7529 (Pt. 1)], 248-261 (November 1957).

34. W. A. Maxwell, "Tubular-Type Dispersion Elements," p 170-183 of Nuclear Fuel Elements, ed. by H. H. Hausner and J. F. Schumar, Reinhold Publishing Co., New York, 1959.

35. W. S. Durant and S. Mirshak, Roughening of Heat Transfer Surfaces as a Method of Increasing the Heat Flux at Burnout, DP-380, Prog. Rep. No. 1 (July 1959).

APPENDIX 1

Derivation of Twisted-Tape Vortex-Flow Equations

A. Equivalent Diameter

By definition, the "nominal" equivalent diameter (taken in a plane normal to the tube axis) is four times the free flow area divided by the wetted perimeter:

$$(D_e)_{nom.} = \frac{4\left(\frac{\pi D_i^2}{4} - t_t D_i\right)}{\pi D_i - 2 t_t + 2 D_i} = \frac{\pi D_i^2 - 4 t_t D_i}{\pi D_i + 2 (D_i - t_t)} \tag{68}$$

where t_t is the thickness of the tape. Derivation of the "true" equivalent diameter (taken in a plane normal to the flow streamlines) is given in a later section of this appendix.

B. Swirl-Flow Path Length at Inner Tube Wall

This quantity is identical to the spiral length of an edge of the twisted tape. Since y is defined as the tape twist ratio in internal diameters per 180-deg rotation, the axial tube length required for 360-deg rotation is given by:

$$L_a = 2 y D_i \tag{69}$$

and:

$$L_{si}^2 = (2 y D_i)^2 + (\pi D_i)^2 \tag{70}$$

or:

$$L_{si} = D_i (4 y^2 + \pi^2)^{1/2} . \tag{71}$$

Combination of Eqs. 69 and 71 yields the final relation:

$$L_{si} = \frac{L_a}{2 y} (4 y^2 + \pi^2)^{1/2} \tag{72}$$

C. Resultant Fluid Velocity at Inner Tube Wall

As mentioned in the text, a rotating (forced vortex) slug flow model has been used for evaluation of several quantities appearing in the friction factor, heat-transfer coefficient, and burnout heat flux correlations. On this basis, since V_a does not vary with radius, we may write:

$$V_t = V_a \frac{\pi}{2\,y} \frac{R}{R_i} \tag{73}$$

which, at the wall, reduces to:

$$V_{ti} = \frac{\pi}{2\,y} V_a \quad . \tag{74}$$

The tape must therefore be twisted quite tightly ($y = \pi/2 = 1.571$) for the tangential velocity at the wall to equal the (constant) axial velocity. The resultant wall velocity is consequently given by:

$$V_{ri}^2 = V_a^2 + \left(\frac{\pi}{2\,y} V_a\right)^2 \tag{75}$$

which reduces to:

$$V_{ri} = V_a \left[1 + \left(\frac{\pi}{2\,y}\right)^2\right]^{1/2} \tag{76}$$

or:

$$V_{ri} = \frac{V_a}{2\,y}(4\,y^2 + \pi^2)^{1/2} \quad . \tag{76-b}$$

D. Rotation Rate of Fluid

$$\begin{aligned} \text{rpm} = {} & V_a \text{ ft/sec} \times 1/(y \text{ diameters/twist}) \times (12/D_i)\text{diameters/ft} \\ & \times 1 \text{ revol./2 twists} \times 60 \text{ sec/min} \end{aligned} \tag{77}$$

$$\therefore \text{ rpm} = 360\, V_a/y\, D_i \quad . \tag{78}$$

E. Centrifugal Intensity (gees) at Inner Tube Wall

The number of gees corresponding to a given tangential velocity is, by definition and in consistent units:

$$\text{gees} = \frac{a_t}{g} = \frac{V_t^2}{g\,R} \tag{79}$$

or, at the tube wall:

$$(\text{gees})_i = \frac{V_{ti}^2}{g\,R_i} \; . \tag{80}$$

The tangential velocity may be defined as path length per revolution times rpm, as follows:

$$V_{ti} = \frac{\pi\,D_i\,(\text{rpm})}{(12)(60)} \tag{81}$$

where the units are fps and in. Combination of Eqs. 78, 80, and 81 yields:

$$(\text{gees})_i = \frac{1.845}{D_i}\left(\frac{V_a}{y}\right)^2 . \tag{82}$$

If $D_i = 1/4$ in., $y = 2$, and $V_a = 60$ fps, then $(\text{gees})_i = 6640$.

F. Radial Pressure Gradient

Assuming V_a independent of R, and in consistent units:

$$a_t = \frac{V_t^2}{R} \; , \tag{83}$$

$$dF = dm\,\frac{a_t}{g_c} \; , \tag{84}$$

$$dm = \rho\,dv \; . \tag{85}$$

Combining Eqs. 83 to 85:

$$dF = \frac{\rho\,V_t^2}{R\,g_c}\,dv \tag{86}$$

$$V_t = V_a \frac{\pi}{2\,y} \frac{R}{R_i} \quad . \tag{73}$$

Combining Eqs. 73 and 86:

$$\frac{dF}{A} = \rho \frac{\pi^2}{4\,y^2} \frac{V_a^{\,2}}{R\,g_c} \left(\frac{R}{R_i}\right)^2 dR \tag{87}$$

$$\Delta P_{\mathbb{C}-R} = (P_R - P_{\mathbb{C}}) = \int_0^R dF/A = \rho \frac{\pi^2}{4\,y^2} \frac{V_a^{\,2}}{g_c} \frac{1}{R_i^{\,2}} \int_0^R R dR \tag{88}$$

$$\therefore \Delta P_{\mathbb{C}-R} = \rho \frac{\pi^2}{4\,y^2} \frac{V_a^{\,2}}{g_c} \frac{R^2}{2\,R_i^{\,2}} = \frac{\pi^2}{8\,g_c} \frac{\rho\,V_a^{\,2}}{y^2} \left(\frac{R}{R_i}\right)^2 \tag{89}$$

and,

$$\Delta P_{\mathbb{C}-R_i} = \frac{\pi^2}{8\,g_c} \frac{\rho\,V_a^{\,2}}{y^2} \quad . \tag{90}$$

In units of psi, pcf, and fps,

$$\Delta P_{\mathbb{C}-R_i} = (\rho/3745)(V_a/y)^2 \quad . \tag{91}$$

G. Inlet Pressure Loss due to Swirl Formation

Assume that V_a is invariant with R and that the tape volume is negligible. In the absence of friction and along a constant diameter tube, a mechanical energy balance with respect to the cross-sectional planes **a** and b of Fig. 24-a gives (in consistent units):

$$\overline{P_a}\ v + m \frac{V_a^{\,2}}{2\,g_c} = \overline{P_b}\ v + m \frac{V_a^{\,2}}{2\,g_c} + m \frac{\overline{V_{tb}^{\,2}}}{2\,g_c} \tag{92}$$

V_a is not subscripted since $(V_a)_a = (V_a)_b$

$$\overline{P_b} = \overline{P_a} - \frac{m}{v} \frac{\overline{V_{tb}^{\,2}}}{2\,g_c} \tag{93}$$

and,

$$\overline{\Delta P}_{a-b} = \left(\overline{P_a} - \overline{P_b}\right) = \rho \frac{\overline{V_{tb}^2}}{2\, g_c} \tag{94}$$

$$\overline{V_{tb}^2} = \frac{2\,\pi \int_0^R V_{tb}^2\, R dR}{\pi R^2} \,. \tag{95}$$

Squaring Eq. 73:

$$V_{tb}^2 = \frac{\pi^2}{4\, y^2}\, V_a^2 \left(\frac{R}{R_i}\right)^2 . \tag{96}$$

Combining Eqs. 95 and 96:

$$\overline{V_{tb}^2} = \frac{2\,\pi \left(\frac{\pi^2}{4\, y^2}\right)\left(\frac{V_a^2}{R^2}\right) \int_0^R R^3\, dR}{\pi R^2} = \frac{\pi^2\, V_a^2}{8\, y^2} \,. \tag{97}$$

Combining Eqs. 94 and 97:

$$\overline{\Delta P}_{a-b} = \frac{\pi^2}{16\, g_c} \frac{\rho\, V_a^2}{y^2} \,. \tag{98}$$

In units of psi, pcf, and fps:

$$\overline{\Delta P}_{a-b} = \left(\frac{\rho}{7490}\right)\left(\frac{V_a}{y}\right)^2 . \tag{99}$$

H. "True" Equivalent Diameter

An equivalent diameter calculated from the integrated mean flow area normal to the streamlines and from the corresponding mean perimeter would more nearly satisfy the definition of D_e than does the "nominal" equivalent diameter of Eq. 68. If the length required for one complete (360 deg) fluid rotation is L radii, then:

* See errata

$$\text{"True" Flow Area} = \frac{\text{Volume}}{\text{Path length}} \tag{100}$$

and

$$A_f' = \int_0^{R_i} \frac{2\pi\, R\, R_i\, L\, dR}{(4\,\pi^2\, R^2 + R_i^{\,2}\, L^2)^{1/2}} \tag{101}$$

$$A_f' = \frac{R_i^{\,2}\, L^2}{2\pi} \left[\left(1 + \frac{4\,\pi^2}{L^2}\right)^{1/2} - 1\right] \tag{102}$$

Since $L = 4\,y$, Eq. 102 may be rewritten as:

$$A_f' = \frac{8\, R_i^{\,2}\, y^2}{\pi} \left(\left[1 + \left(\frac{\pi}{2\,y}\right)^2\right]^{1/2} - 1\right). \tag{103}$$

Eq. 102 meets limit requirements, since $A_f' \to 0$ as $L \to 0$, and $A_f' \to \pi\, R_i^{\,2}$ as $L \to \infty$.

The corresponding wetted perimeter, defined as:

$$\text{Perimeter} = \sum \frac{\text{Area exposed}}{\text{Path length along area}} \tag{104}$$

is given by:

$$\text{Perimeter} = \frac{2\,\pi\, R_i\, R_i L}{R_i\, (4\,\pi^2 + L^2)^{1/2}} + 2\,(2\, R_i) \tag{105}$$

or

$$\text{Perimeter} = 2\, R_i \left[2 + \frac{\pi\, L}{(4\,\pi^2 + L^2)^{1/2}}\right] \tag{106}$$

$$L = 4\, y \tag{107}$$

$$\therefore\ \text{Perimeter} = 4\, R_i \left[1 + \frac{\pi\, y}{(\pi^2 + 4\, y^2)^{1/2}}\right]. \tag{108}$$

The equivalent diameter, now defined as:

$$(D_e)_{true} = \frac{4\, A_f'}{\text{Perimeter}} \tag{109}$$

becomes, after simplification:

$$(D_e)_{true} = \frac{8\ R_i\ y^2}{\pi}\ \frac{X - 2\ y\ X^{1/2}}{2\ y\ (\pi y + X^{1/2})} \tag{110}$$

where

$$X = \pi^2 + 4\ y^2\ . \tag{111}$$

A comparison of $(D_e)_{nom.}$ and $(D_e)_{true}$ is shown in Table 6 for t (tape thickness) = 0. For the practical range of $1.25 < y < \infty$, the difference is negligible.

Table 6. Comparison of "Nominal" and "True" Equivalent Diameters for Zero Tape Thickness

y	$(D_e)_{nom.}/D_i$	$(D_e)_{true}/D_i$
0.25	0.611	0.343
0.50	↓	0.495
1.25	↓	0.610
2.00	↓	0.619
2.50	↓	0.618
3.75	↓	0.616
5.00	↓	0.614
∞	↓	0.611

The integrated mean swirl-flow path length may similarly be obtained from:

$$(L_s)_{mean} = \frac{\text{Volume}}{A_f'} = \frac{\pi^2\ L_a}{8\ y^2}\ \frac{1}{\left[\left(1 + \frac{\pi^2}{4\ y^2}\right)^{1/2} - 1\right]}\ . \tag{112}$$

The integrated mean resultant fluid velocity may be obtained from:

$$(V_r)_{mean} = \frac{(L_s)_{mean}\, V_a}{L_a} \tag{113}$$

giving:

$$(V_r)_{mean} = \frac{\pi^2\, V_a}{8\, y^2 \left[\left(1 + \frac{\pi^2}{4\, y^2} \right)^{1/2} - 1 \right]} \quad . \tag{114}$$

APPENDIX 2

Further Evaluation of Inlet-Swirl-Generator Burnout Data

The burnout data of reference 1, obtained with test sections fitted with inlet spiral-ramp or tangential-slot vortex generators, have been recorrelated as shown in Fig. 37, which follows the form developed by Lowdermilk et al.,[14] for burnout with bulk boiling of water in straight flow. The term G_a is the axial mass velocity – i.e., G evaluated from the flow rate and tube cross-sectional flow area. The average and maximum deviations from the 23 data points of curves 3 and 4 taken together are 8.0% and 18.9%, respectively. Two of the 23 points were obtained after publication of reference 1. The data representation is significantly better than in the original correlations.[1]

Six additional tests were made with stainless steel tubes tangentially slotted at the inlet; for four of these runs ϕ_{bo} was greater than 30×10^6 Btu/hr·ft^2, but all six have been designated "melters" and none have been plotted on Fig. 37.* Outside wall temperatures in these tests, as determined by optical pyrometer measurements, reached the 2500 to 2600°F range. Tube failure was initiated by gross external metal fusion rather than thermal burnout arising from bubble coverage of the inner wall. A photograph of the outside of such a tube after test is shown in Fig. 38-a; where B denotes the final burnout location. Axial velocity through the tube (304 stainless steel, 0.240-in. ID, 0.310-in. OD) was 91 fps. Estimated maximum inside and outside wall temperatures were 500°F and 2520°F, respectively. Fig. 38-b is a photomicrograph which shows the five distinct zones produced by a temperature

*The average curve for these 6 points is parallel to curve 3 of Fig. 37 and 62% as high.

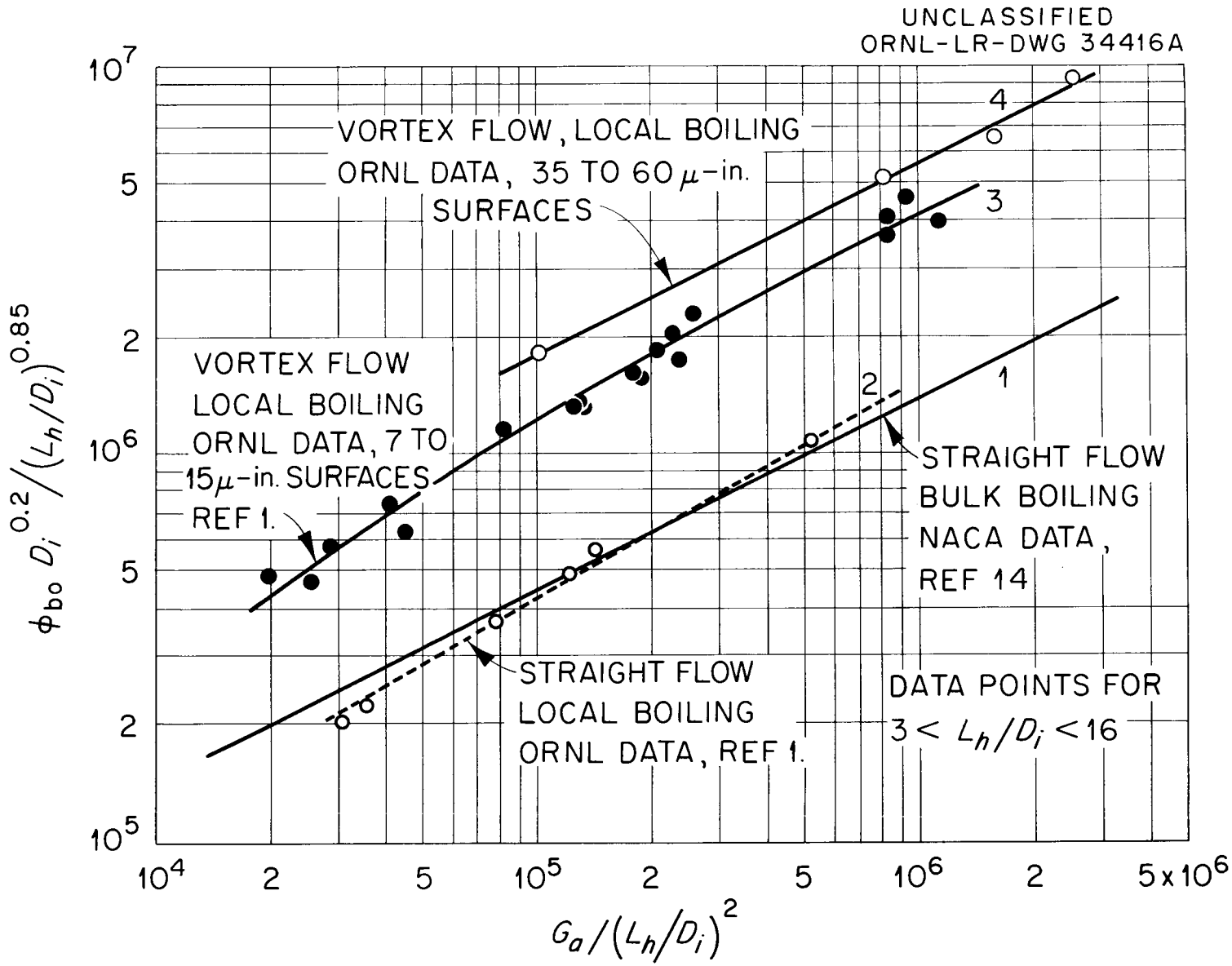

Fig. 37. Recorrelation of Inlet-Swirl-Generator Burnout Data.

UNCLASSIFIED
ORNL PHOTO 49101

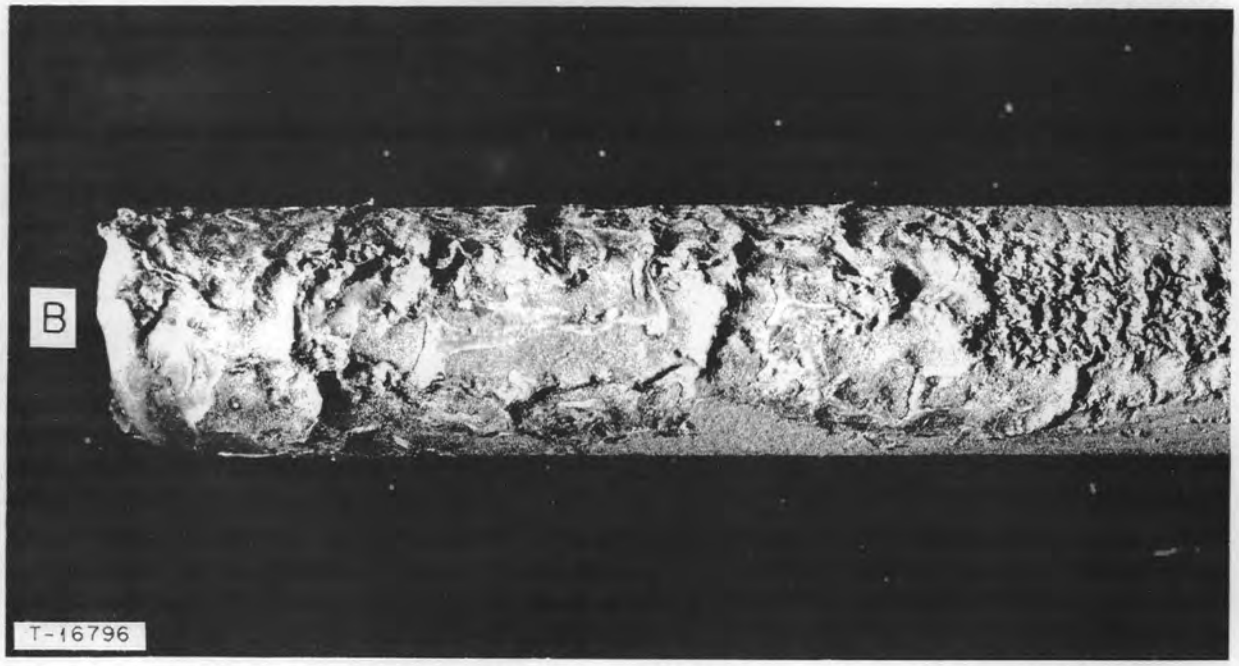

(*a*) Front View of Exterior of Partially Melted Stainless Steel Vortex Tube.

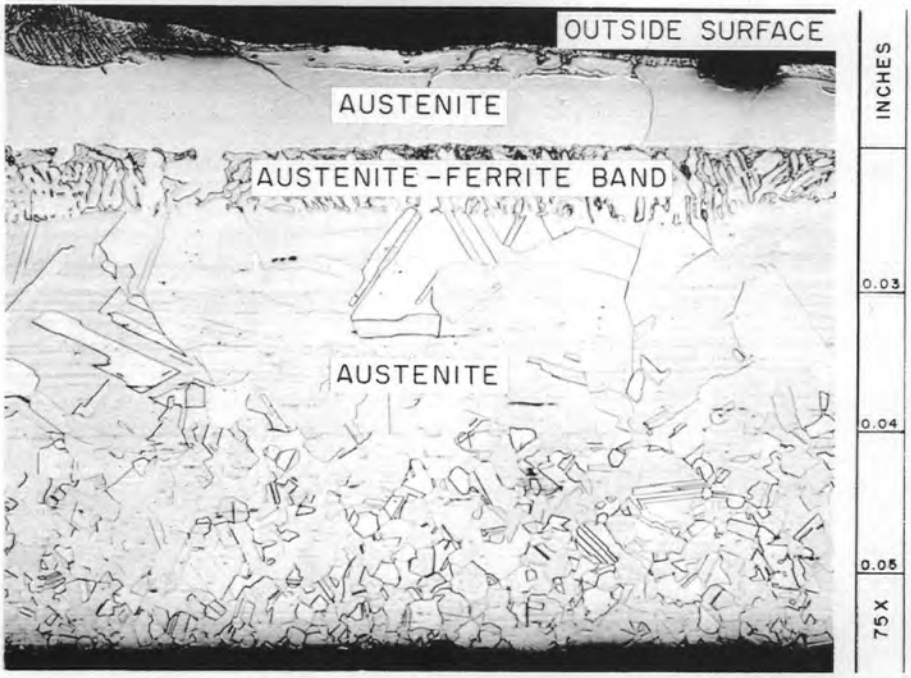

(*b*) Longitudinal Section Taken Through Front Wall of Vortex Tube Above.

Fig. 38

difference of ~ 2000°F across only 0.035 in. of metal. High flux vortex cooling of such tubes might be helpful in studies of very large thermal stresses and of plastic yielding of metals.

In order to obtain some degree of comparison between the inlet-generator vortex data and the newer twisted-tape data, the effective twist ratios for the older data were calculated from:

$$\phi_{bo} = \frac{403{,}000\ V_a \left[1 + (\pi/2\ y)^2\right]^{1/2}}{(L_h/D_i)^{1/3}} \tag{115}$$

which was solved for y to yield:

$$y = \frac{(6.322 \times 10^5)\ V_a}{\left[\phi_{bo}^{\ 2}\ (L_h/D_i)^{2/3} - (16.22 \times 10^{10})\ V_a^{\ 2}\right]^{1/2}} . \tag{116}$$

* Eq. ~~114~~ 116, taken from Fig. 16, is one of the better representations of minimum burnout heat flux for the twisted-tape data and was chosen for its relative simplicity for purposes of the present calculation. The results are given in Fig. 39 as effective y vs L_h/D_i.

The effective y values obtained in this fashion are evidently considerably smaller than those of the tightest twisted tapes used in the more recent studies (2.1 minimum). The fact that the curves are flat, or nearly so, indicates that burnout heat flux varies with L/D in the same fashion with inlet swirl generators as with twisted tapes. Inlet generator data over a larger range of L/D would be necessary to confirm this tentative indication; it is probable that at greater values of L/D the curves of Fig. 39 would assume a positive slope.

* See errata

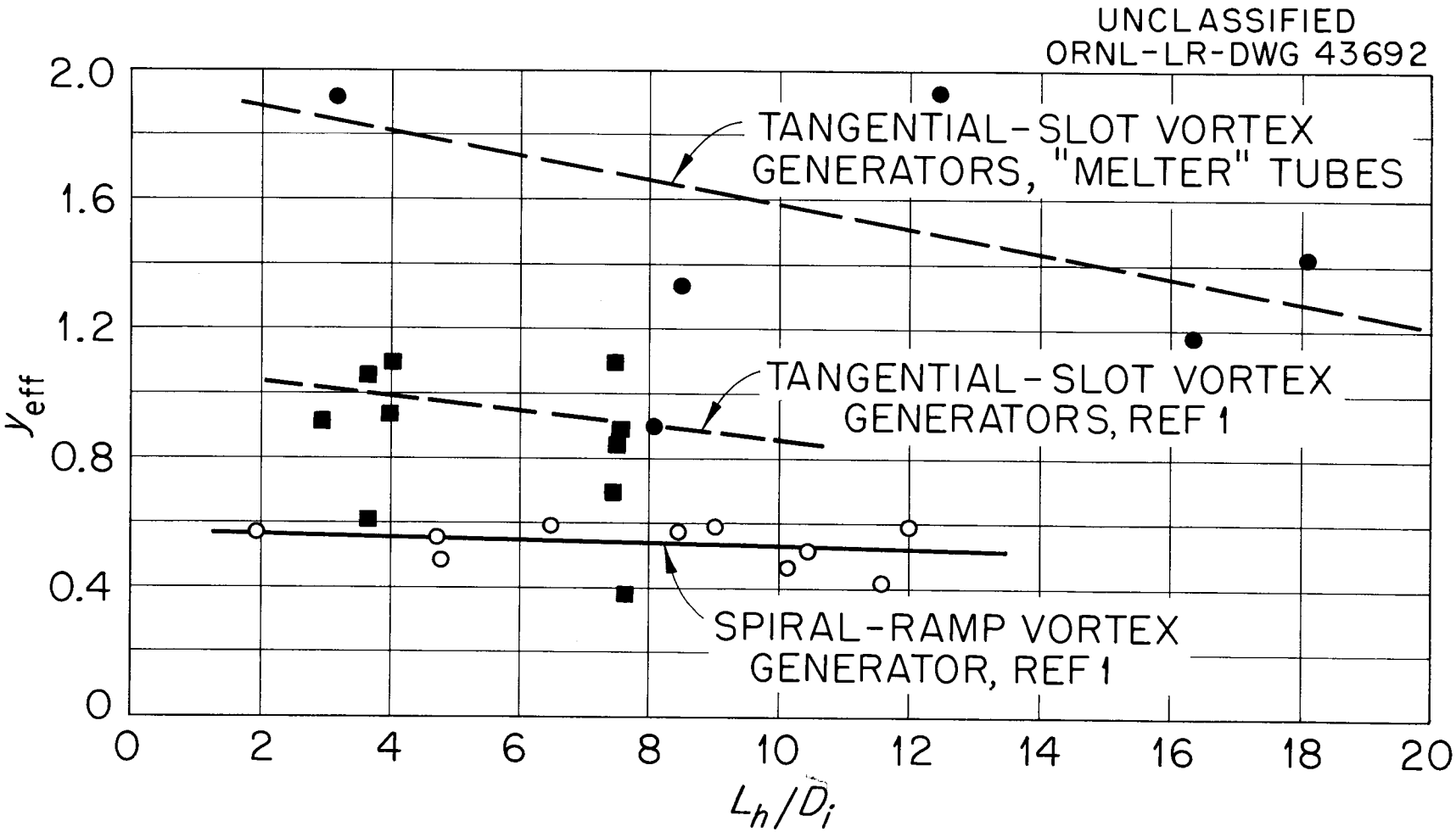

Fig. 39. Effective Twist Ratios of Inlet-Swirl-Generator Vortex Tests, as Calculated from Burnout Data, vs L/D.

NOTATION

(Listed units are used except where otherwise noted)

a	acceleration, ft/sec^2
A_f'	true cross-sectional flow area for swirl flow, ft^2
A_h	internal surface area for heat transfer, ft^2
c	volumetric heat capacity of tube wall, $Btu/ft^3 \cdot °F$
C_p	coolant constant-pressure specific heat, $Btu/lb \cdot °F$
D_e	equivalent diameter, 4 times flow area divided by wetted perimeter, ft
D_i	test section inside diameter, ft
D_o	test section outside diameter, ft
(dE/dx)	potential gradient along test section, volts/ft
f	friction factor, dimensionless; also a-c current frequency, cps
f_a	axial friction factor (see Eq. 48), dimensionless
f_e	empirical friction factor (see Eq. 52), $ft^{1.2}$
f_r	rotational friction factor (see Eq. 50), dimensionless
F	force, lb_f
Fr	Froude number, $V^2/g\ D_i$, dimensionless
g	gravitational acceleration, ft/sec^2
g_c	conversion constant, $32.17\ lb_m \cdot ft/lb_f \cdot sec^2$
G	coolant mass velocity, $lb/hr \cdot ft^2$ of flow area
G_a	G based on V_a, $lb/hr \cdot ft^2$
Gr	Grashof number, $D^3\ \rho^2\ g\ \beta\ (\Delta t)_f/\mu^2$, dimensionless; also resultant coolant mass velocity, $lb/hr \cdot ft^2$
h	surface heat-transfer coefficient, $Btu/hr \cdot ft^2 \cdot °F$ (per sec in Eq. 23)
h_{am}	mean axial-flow heat-transfer coefficient based on t_{bm}, $Btu/hr \cdot ft^2 \cdot °F$

NOTATION (continued)

h_{vm}	mean vortex-flow heat-transfer coefficient based on t_{bm}, Btu/hr.ft^2.°F
j	Colburn heat-transfer factor, St $(Pr)^{2/3}$
k	thermal conductivity, Btu/hr·ft^2·°F/ft
L	tape twist ratio, internal radii/360-deg twist
L_a	axial tube length, ft
L_h	test section heated length, ft
L_{si}	swirl-flow path length at inner tube wall, ft
m	mass, lb_m
Nu	Nusselt number, hD/k, dimensionless
P	absolute static pressure, psia
P_f	total pumping power across test section, fluid hp
ΔP	pressure drop, psi (psf in Eqs. 55 – 59 and Eq. 64, and in Appendix 1)
ΔP_e	pressure drop caused by swirl formation at tube entrance, psf
Pr	Prandtl number, $C_p\mu/k$, dimensionless
q	rate of heat transfer, Btu/hr
R	radius, ft
Re	Reynolds number, $D\rho V/\mu$, dimensionless
$(Re)_a$	axial Reynolds number, $D_i\ \rho_b\ V_a/\mu_b$, dimensionless
$(Re)_r$	rotational Reynolds number, $D_e\ \rho_b V_{ri}/\mu_b$, dimensionless
R_i	test section inside radius, ft
R_o	test section outside radius, ft
s	cooled surface area per unit length, ft^2/ft
St	Stanton number, h/C_pG, dimensionless
t	temperature, °F
t_b	bulk coolant temperature, °F

NOTATION (continued)

t_f	film temperature, $(t_i + t_b)/2$, °F
t_i	inside tube temperature, °F
t_o	outside tube temperature, °F
t_t	thickness of twisted tape, ft
Δt_f	over-all film temperature drop, $(t_i - t_b)$, °F
Δt_{sat}	liquid-film superheat, $(t_i - t_{sat})$, °F
Δt_{sub}	degree of subcooling, $(t_{sat} - t_b)$, °F
v	volume of tube wall per unit length, ft^3/ft; also volume, ft^3
V_a	superficial axial coolant velocity, ft/sec
V_{ri}	resultant coolant velocity at inner tube wall, ft/sec
V_t	tangential coolant velocity, ft/sec
W	coolant weight flow rate, lb/hr
y	tape twist ratio, internal diameters/180-deg twist
$y_{eff.}$	effective twist ratio for flow through vortex tubes with inlet swirl generators, internal diameters/180-deg flow rotation
α	temperature coefficient of thermal conductivity
β	volumetric coefficient of thermal expansion, $(°F)^{-1}$
β'	temperature coefficient of electrical resistivity
ρ	electrical resistivity, ohm-ft; also coolant density, lb/ft^3
ϕ	heat flux based on internal surface area, $Btu/hr \cdot ft^2$
ω	a-c current frequency, radians/sec
τ	thermal time constant of test section, sec
μ	dynamic viscosity of coolant, $lb_m/ft \cdot sec$

NOTATION (continued)

Subscripts

a	for axial flow
a-c	with alternating-current heating
b	bulk (coolant mixed mean) value
bo	at burnout
℄	at tube centerline
crit.	critical
d-c	with direct-current heating
e	equivalent; at entrance; empirical
f	film value (evaluated at t_f)
h	heated
i	at inside tube surface
iso	isothermal
LB	with local boiling
m	mean
max	maximum
min	minimum
nom.	nominal
o	at outside tube surface; reference temperature in Eqs. 1-b to 1-d
r	resultant
s	swirl
sat	saturation
t	tangential
v	for vortex flow
1	at test-section inlet
2	at test-section exit

ORNL-2911
UC-34 Physics and Mathematics
TID-4500 (15th ed.)

INTERNAL DISTRIBUTION

1. L. G. Alexander
2. C. F. Allen (K-25)
3. R. B. Briggs
4-14. R. D. Bundy
15. C. A. Burchsted
16. C. E. Center
17. T. G. Chapman
18. R. A. Charpie
19. A. Chetham-Strode
20. R. D. Cheverton
21. H. C. Claiborne
22. R. S. Cockreham
23. T. E. Cole
24. C. W. Collins
25. J. W. Cooke
26. F. L. Culler
27. J. E. Cunningham
28. L. B. Emlet (K-25)
29. E. P. Epler
30. W. K. Ergen
31. W. R. Gall
32-61. W. R. Gambill
62. W. F. Gauster
63. J. P. Gill
64. J. C. Griess
65. L. A. Haack
66. D. C. Hamilton
67. R. J. Hefner
68. R. L. Higgins (K-25)
69. N. Hilvety
70. H. W. Hoffman
71. L. B. Holland
72. T. N. Jones
73. W. H. Jordan
74. P. R. Kasten
75. C. P. Keim
76. M. T. Kelley
77. J. J. Keyes, Jr.
78. G. J. Kidd, Jr.
79. W. Kofink
80. A. I. Krakoviak
81. J. A. Lane
82. C. G. Lawson
83. J. S. Lewin
84. R. S. Livingston
85. J. Lones
86. M. I. Lundin
87. J. N. Luton
88. F. E. Lynch
89. R. N. Lyon
90. E. R. Mann
91. H. A. McLain
92. J. R. McWherter
93. J. W. Michel
94. C. S. Morgan
95. K. Z. Morgan
96. J. P. Murray (Y-12)
97. M. L. Nelson
98. R. H. Nimmo
99. L. C. Oakes
100. F. N. Peebles
101. D. Phillips
102. C. A. Preskitt
103. P. M. Reyling
104. M. W. Rosenthal
105. H. E. Seagren
106. E. D. Shipley
107. M. J. Skinner
108. A. H. Snell
109. W. J. Stelzman
110. R. S. Stone
111. J. A. Swartout
112. E. H. Taylor
113. M. Tobias
114. D. G. Thomas
115. J. N. Turpin (Y-12)
116. D. H. Wallace
117. J. L. Wantland
118. A. M. Weinberg
119. M. E. Whatley
120. C. E. Winters
121. M. M. Yarosh
122-123. Central Research Library
124-190. Laboratory Records Department
191. Laboratory Records, ORNL-RC
192-194. ORNL Y-12 Technical Library Document Reference Section
195. Reactor Experimental Engineering Library

EXTERNAL DISTRIBUTION

196. D. H. Groelsema, AEC, Washington
197. Division of Research and Development, AEC, ORO
198-807. Given distribution as shown in TID-4500 (15th ed.) under Physics and Mathematics category (75 copies - OTS)